



UNIVERSIDAD  
**NACIONAL**  
DE COLOMBIA

# **Experimental assessment of rutting in permeable asphalt mixtures**

**Vanessa Senior Arrieta**

Universidad Nacional de Colombia  
Facultad de Minas - Departamento de Ingeniería Civil  
Medellín, Colombia  
2020



# **Experimental assessment of rutting in permeable asphalt mixtures**

**Vanessa Senior Arrieta**

Dissertation for the degree of:  
**Doctor of Civil Engineering**

Advisor:  
PhD. Carlos Alberto Graciano Gallego

Co-Advisor:  
PhD. Carlos Alberto Vega Posada

Research line:  
**Pavements – Asphalt Mixes**

Research Group:  
**VITRA – Vías y Transportes**

Universidad Nacional de Colombia  
Facultad de Minas, Departamento de Ingeniería Civil  
Medellín, Colombia  
2020



*To God and my treasured family, Gertrudis, and Jannina.*

*Thank you for always being there in my life and  
always looking out for me.*

*In memory of my beloved father Herman.*



## Acknowledgements

Accomplishing my major academic goal is a huge attainment that I would not have been able to achieve on my own without my family's endless support. So, the first great thank is dedicated to my mother. If I made it this far, it's just because of her.

I would like to recognize my advisor, Professor Carlos Graciano, for his valuable guidance, the confidence placed from the beginning, and his permanent motivation to develop this research. I whole-heartedly appreciate his testimonial talks which proved significant towards the success of this process of doctoral learning. Much of his personal and academic experience is also printed in this study.

To my very dear friend Claudia Helena, I wish to show my gratitude. Her permanent enthusiasm and support to endure those difficult moments of this beautiful academic journey proved to be very valuable.

The financial support provided by Colciencias was hugely significant to carry out my doctoral study. My gratitude goes to this institution.

To the University of Texas A&M, and especially to Dr. Robert Lytton, for his lectures during the course named "Micromechanical properties of materials", his worthful suggestions, and collaboration in the development of this experimental work while my annual staying at this Institution. Few times in life, you have the opportunity to meet priceless characters who show you a daily passion for work, kindness, a sense of discipline, and interesting conversations beyond academic life. That is all I found in you, Professor Lytton and I am so grateful.

I would also like to extend my thanks to the Technical personnel of the Materials Laboratory at the University of Texas A&M: Rick Canatella and Tony Barbosa, for their

training in the execution of many test procedures for the characterization of the properties of the asphalt mixture.

To Adriana Lammardo for her support in the continuous training for the reconstruction of 2D images with the Mimics software.

In writing this thesis, I received guidance and style corrections in English from my love, Guillermo. Thank you for your great understanding and support. Love you.



## Abstract

This study presents an experimental investigation on the rutting resistance of permeable asphalt mixes (PAM). In practice, PAM, also referred to as Open-graded friction courses (OGFC) or permeable friction courses (PFC), are prone to permanent deformation due to heavy vehicle traffic loads and a weak mineral skeleton caused by their high air void contents. Consequently, the draining capacity of the PAM is diminished making the roads unsafe particularly in wet conditions. Hence, the rutting mechanism of PAM is evaluated through three laboratory tests: dynamic modulus, flow number, and Hamburg wheel tracking test (HWTT).

The laboratory samples were prepared and compacted considering four air voids (AV) contents: 18%, 20%, 22% and 25%. From the HWTT, a comparative analysis was conducted using X-ray computer tomography (X-ray CT) images obtained before and after the tests in order to investigate AV distribution due to rutting. Results from the tests indicated that an increase in AV content reduced the rutting performance of PAM, as well as higher AV content led to larger mix densification and thus a deeper rut was achieved.

Similar results were attained from the analysis of the X-ray CT images, nevertheless, a larger AV densification was observed in the upper part of the samples beneath the developed rut, which can lead to further weakening the mineral skeleton and progress of other several distress that typically develop for PAM.

**Keywords:** permeable asphalt mixes; rutting resistance; air voids content; moisture damage; flow number; dynamic modulus, X-ray CT.



## Resumen

Este estudio presenta una investigación experimental sobre la resistencia al ahuellamiento en las mezclas asfálticas permeables (PAM). En la práctica, estas mezclas también conocidas como *OGFC*, (capas asfálticas de gradación abierta), o *PFC* (capas de desgaste permeables); son propensas a desarrollar deformación permanente debido a las altas cargas de tráfico vehicular y a un esqueleto mineral débil causado por su alto contenido de vacíos de aire. En consecuencia, la capacidad de drenaje de las PAM disminuye, lo que hace que las superficies de rodadura asfálticas sean inseguras, especialmente en condiciones de humedad. Por esta razón, el mecanismo de ahuellamiento en PAM es evaluado a través de tres pruebas de laboratorio: módulo dinámico, número de flujo y el ensayo en la rueda de Hamburgo (HWTT).

Los especímenes fueron preparados y compactados considerando cuatro contenidos de vacíos de aire (AV): 18%, 20%, 22% y 25%. Se realizó un análisis comparativo empleando imágenes de tomografía computarizada de rayos X, obtenidas antes y después de realizar las pruebas en HWTT para determinar el perfil de distribución de AV debido al ahuellamiento. Los resultados indicaron que un aumento en el contenido AV redujo la resistencia al ahuellamiento de las PAM, así como un mayor contenido de vacíos condujo a una mayor densificación de la mezcla y por lo tanto se logró una huella más profunda.

Resultados similares se obtuvieron del análisis de imágenes de CT de rayos X, sin embargo, se observó una mayor densificación AV en la parte superior de las muestras debajo de la huella desarrollada, lo que puede conducir a un mayor debilitamiento del esqueleto mineral y al progreso de otros tipos de deterioro típicos en este tipo de mezclas.

**Palabras clave:** mezclas asfálticas permeables; resistencia al ahuellamiento; contenido de vacíos de aire; daño por humedad; número de flujo; módulo dinámico, tomografía computarizada de rayos X.

**TÍTULO EN ESPAÑOL:** Evaluación experimental de ahuellamiento en mezclas asfálticas permeables.

# Content

	Pag.
Acknowledgements.....	3
Abstract.....	5
Resumen.....	7
Content.....	9
List of Figures.....	11
List of Tables.....	15
List of Abbreviations and Acronyms.....	17
Chapter 1. Introduction.....	19
1.1 Background.....	19
1.2 Scope.....	20
1.3 Research Aim and objectives.....	22
1.4 Dissertation structure.....	22
Chapter 2. Literature Review in Permeable Asphalt Mixtures.....	25
2.1 Introduction.....	26
2.2 An overview of the mix design for PAM in Colombia.....	28
2.2.1 Materials selection.....	29
2.2.2 Selection of design gradation.....	29
2.2.3 Mixture Design procedure.....	30
2.2.4 Determination of OAC.....	31
2.3 Colombian experience using PAMs.....	33
2.4 Urban pavement in Medellín (Antioquia).....	36
2.4.1 Materials selection and mix design.....	36
2.4.2 Performance and lifecycle.....	37
2.5 Autopistas del Café (Coffee Highways).....	37
2.5.1 Materials selection and mix design.....	38
2.5.2 Performance and lifecycle.....	38
2.6 Transversal de las Américas (Trans-Americas' Highway).....	40
2.6.1 Materials selection and mix design.....	40
2.6.2 Performance and lifecycle.....	41

2.7 Comparative analysis.....	44
2.8 Performance criteria of PAM in rainy countries .....	46
2.8.1 Functionality .....	46
2.8.2 Durability.....	49
2.9 Summary and conclusions.....	50
 Chapter 3. Rutting mechanism assessment in PAM .....	 63
3.1 Introduction .....	64
3.2 Materials characterization.....	66
3.3 Performance tests of rutting resistance .....	69
3.3.1 Dynamic Modulus (DM) tests – Testing protocol .....	69
3.3.2 DM test results.....	73
3.3.3 Flow Number (FN) test protocol .....	77
3.3.4 FN test results.....	78
3.3.5 Hamburg wheel-tracking test (HWTT) – Testing setup.....	81
3.3.6 HWTT results .....	83
3.4 Comparison of the laboratory test methods.....	86
3.5 Comparative analysis using X-ray computer tomography.....	89
3.5.1 Experimental program .....	89
3.5.2 Stepwise procedure for X-Ray CT image data acquisition .....	90
3.5.3 AV distribution profiles measured by X-ray CT imaging .....	91
3.5.4 Scanned samples after performing HWTT - dry.....	92
3.5.5 Scanned samples after performing HWTT - wet.....	93
3.6 Summary and conclusions.....	95
 Chapter 4. Permeability rate in PAM.....	 105
4.1 Introduction .....	106
4.2 Materials and methods.....	107
4.3 X-ray Rotational Computed Tomography Angiography and contrast-agent enhanced.....	108
4.4 Measurements of permeability.....	109
4.4.1 Measurement of AV content by means of Dimensional Analysis.....	109
4.4.2 X-ray Rotational CT Angiography and image-analysis techniques..	110
4.5 Results and discussion .....	110
4.6 Summary and conclusions.....	114
 Chapter 5. Conclusions and future research .....	 117
5.1 Conclusions.....	117
5.2 Recommendations for Further Research.....	118

## List of Figures

<b>Fig. 2-1.</b> Sieve size particle distribution for PAM in Colombian standards [52].....	30
<b>Fig. 2-2.</b> Flowchart of the current laboratory-design procedure of PAM according to Item 453 (Adapted from [52]) .....	32
<b>Fig. 2-3.</b> List of rainiest countries worldwide using PAM, per continent extracted from [61]. Annual average precipitation (mm/year).....	33
<b>Fig. 2-4.</b> (a) Departments in Colombia implementing PAM. (b) Average precipitation per year (mm/year).....	34
<b>Fig. 2-5.</b> Measurement of rutting over PAM section placed in the Trans-Americas' Highway (Dept. of Córdoba).....	42
<b>Fig. 2-6.</b> Measurement of macrotexture for PAM and dense-graded HMA sections placed in Trans-Americas' Highway (Dept. of Córdoba).....	43
<b>Fig. 2-7.</b> Measurement of friction ( $\mu$ ) for PAM and dense-graded HMA sections installed in Trans-Americas' Highway (Dept. of Córdoba).....	44
<b>Fig. 2-8.</b> Flowchart of an improved laboratory-design procedure of PAM.....	48
<b>Fig. 3-1.</b> Particle size distribution for combination of aggregates for PFC samples. ....	67
<b>Fig. 3-2.</b> DM test setup: (a) Sample preconditioned at test temperature; (b) LVDT fixed to hexagonal studs; and (c) test cell setup at the target temperature.....	70
<b>Fig. 3-3.</b> Typical master curve.....	71
<b>Fig. 3-4.</b> Dynamic moduli $E^*$ master curves at $T_{ref} = 20\text{ }^{\circ}\text{C}$ . ....	73

<b>Fig. 3-5.</b> $E^*$ in terms of the AV Content, for $T = 37.8^\circ\text{C}$ and $54.4^\circ\text{C}$ and various frequencies. .....	75
<b>Fig. 3-6.</b> FN test protocol: (a) Loading process in FN test, (b) Strain rate versus loading cycles.....	78
<b>Fig. 3-7.</b> FN vs AV Content. ....	79
<b>Fig. 3-8.</b> FN index vs AV Content.....	79
<b>Fig. 3-9.</b> FN index vs $t(F)$ for various AV contents.....	80
<b>Fig. 3-10.</b> (a) Schematic view with the wheel-tracking path; (b) sample-mold fitting and locations for 11 rut-measurements, units in [mm]; and (c) paired samples setup. ....	82
<b>Fig. 3-11.</b> Rut depth vs Pass number for.....	83
<b>Fig. 3-12.</b> Rut depth vs Pass number for.....	83
<b>Fig. 3-13.</b> $R_d$ vs AV content. ....	83
<b>Fig. 3-14.</b> Rut depth measured in PFC samples. (a) HWTT-dry. (b) HWTT-wet.....	85
<b>Fig. 3-15.</b> Correlation between FN and $E^*$ for $T=37.8^\circ\text{C}$ . ....	88
<b>Fig. 3-16.</b> Location of 50mm diameter cores from HWTT samples. ....	90
<b>Fig. 3-17.</b> Grayscale ranges for 3D masks. (a) mastic (b) coarse aggregates (c) air voids.....	91
<b>Fig. 3-18.</b> 3D Masks from X-ray CT images for 18% AV, HWTT under dry conditions (air voids-aggregates-mastic): (a) before testing; (b) after testing; (c) AV distribution.....	92
<b>Fig. 3-19.</b> 3D Masks from X-ray CT images for 25% AV, HWTT under dry conditions (air voids-aggregates-mastic): (a) before testing; (b) after testing; (c) AV distribution.....	93
<b>Fig. 3-20.</b> 3D Masks from X-ray CT images for 25% AV, HWTT under wet conditions (air voids-aggregates-mastic): (a) before testing; (b) after testing; (c) AV distribution.....	94
<b>Fig. 3-21.</b> 3D Masks from X-ray CT images for 25% AV, HWTT under wet conditions (air voids-aggregates-mastic): (a) before testing; (b) after testing; (c) AV distribution.....	95
<b>Fig. 4-1.</b> Sieve size particle distribution for PAM. ....	107



**Fig. 4-2.** Rotational Angiography equipment with X-ray detector and work place with a sample disposed to be scanned..... 108

**Fig. 4-3.** Total AV content versus Water-accessible AV content..... 111

**Fig. 4-4.** [a] Sample compacted of PAM. [b] Sample PAM-115 including contrast (orange path). [c] Sample PAM-112 including contrast (orange path - plane view)..... 113



## List of Tables

<b>Table 2-1.</b> Summary version of the current practice of PAMs in Colombia _____	35
<b>Table 2-2.</b> Mixture design parameters in countries using PAM _____	39
<b>Table 2-3.</b> Particle size gradations. PAM (Trans-Americas' Highway) and MD (Coffee highways), [52] _____	41
<b>Table 3-1.</b> Asphaltic material mixing temperature by Grade and Type [50] _____	68
<b>Table 3-2.</b> STOA and Compaction Temperatures by Grade. Adapted from [51]._____	68
<b>Table 3-3.</b> Summary of experimental plan to asses rutting in PFC_____	69
<b>Table 3-4.</b> Parameters used in sigmoidal function by AV content % _____	72
<b>Table 3-5.</b> Summary of Dynamic Modulus tests result at T =54.4°C and T =37.8°C.____	74
<b>Table 3-6.</b> ANOVA and Tukey's HSD test analysis for $E^*$ (37.8 °C, 5 Hz). _____	76
<b>Table 3-7.</b> FN test results_____	79
<b>Table 3-8.</b> ANOVA and Tukey's HSD test analysis for FN (50 °C)._____	81
<b>Table 3-9.</b> HWTT test results. _____	84
<b>Table 3-10.</b> Comparison of test results: $E^*$ (37.8 °C), FN, <i>FN index</i> and $\phi R$ . _____	87
<b>Table 3-11.</b> Limitations and challenges from FN and DM tests. Adapted from [11]____	89
<b>Table 4-1.</b> %AV by $G_{mm}$ and $G_{mb}$ (Dimensional Analysis) and K [cm/s] _____	112



## List of Abbreviations and Acronyms

<b>AASHTO</b>	<i>American Association of State Highway and Transportation Officials</i>
<b>AC</b>	<i>Asphalt Content – Contenido de asfalto</i>
<b>ANOVA</b>	<i>Analysis of variance</i>
<b>ASTM</b>	<i>American Society for Testing and Materials</i>
<b>AV</b>	<i>Air voids</i>
<b>DSR</b>	<i>Dynamic Shear Rheometer</i>
<b>ESAL</b>	<i>Equivalent single axle load</i>
<b>FDOT</b>	<i>Florida Department of Transportation</i>
<b>FHWA</b>	<i>Federal Highway Administration</i>
<b>FN</b>	<i>Flow number</i>
<b>GDOT</b>	<i>Georgia Department of Transportation</i>
<b>HMA</b>	<i>Hot mix asphalt</i>
<b>HWTT</b>	<i>Hamburg Wheel Tracking Test</i>
<b>IDT</b>	<i>Indirect Tensile</i>
<b>IRI</b>	<i>International Roughness Index</i>
<b>JMF</b>	<i>Job Mix Formula</i>
<b>LTOA</b>	<i>Long-Term Oven Aging</i>
<b>MDOT</b>	<i>Mississippi Department of Transportation</i>
<b>MEPDG</b>	<i>Mechanistic-Empirical Pavement Design Guide</i>
<b>MIST</b>	<i>Moisture Induced Stress Tester</i>
<b>NAPA</b>	<i>National Asphalt Pavement Association</i>
<b>NCAT</b>	<i>National Center for Asphalt Technology</i>
<b>NCHRP</b>	<i>National Cooperative Highway Research Program</i>
<b>NLT</b>	<i>Normas de ensayos redactadas por el Laboratorio de Transporte y Mecánica Del Suelo del Centro de Estudios y Experimentación Del Ministerio de Obras Públicas. - Cedex- España</i>
<b>NMAS</b>	<i>Nominal Maximum Aggregate Size</i>
<b>OBC</b>	<i>Optimum Binder Content</i>

<b>OGFC</b>	<i>Open Graded Friction Course</i>
<b>PA</b>	<i>Porous asphalt</i>
<b>PAM</b>	<i>Porous/permeable asphalt mixture</i>
<b>PAV</b>	<i>Pressure Aging Vessel</i>
<b>PCS</b>	<i>Pavement Condition Survey</i>
<b>PEM</b>	<i>Porous European mixes</i>
<b>PFC</b>	<i>Permeable Friction Course</i>
<b>PG</b>	<i>Performance Grade</i>
<b>PMA</b>	<i>Polymer Modified Asphalt</i>
<b>RH</b>	<i>Relative Humidity</i>
<b>RTFO</b>	<i>Rolling Thin Film Oven</i>
<b>SBR</b>	<i>Styrene-Butadiene-Rubber</i>
<b>SBS</b>	<i>Styrene-Butadiene-Styrene</i>
<b>SCDOT</b>	<i>South Carolina Department of Transportation</i>
<b>SGC</b>	<i>Superpave Gyrotory Compactor</i>
<b>SHRP</b>	<i>Strategic Highway Research Program</i>
<b>SN</b>	<i>Stripping Number</i>
<b>SPT</b>	<i>Simple Performance tests</i>
<b>STOA</b>	<i>Short-Term Oven Aging</i>
<b>SUPERPAVE</b>	<i>Superior performance asphalt pavement</i>
<b>TAV</b>	<i>Total air voids</i>
<b>TxDOT</b>	<i>Texas Department of Transportation</i>
<b>TSR</b>	<i>Tensile Strength Ratio</i>
<b>VMA</b>	<i>Voids in mineral aggregates</i>
<b>WMA</b>	<i>Warm asphalt mixture</i>
<b>X-RAY CT</b>	<i>X-Ray Computed Tomography</i>

# Chapter 1. Introduction

## 1.1 Background

In pavement engineering practice, permeable asphalt mixes (PAM) represent a feasible alternative to evacuate runoff water from the surface mainly due to its high content of air voids (AV) within 18% and 25%, provided by a discontinuously distributed mineral skeleton, which allows a surface macro-texture and high hydraulic conductivity. As for its many advantages, the potential to occur splash and spray effects, hydroplaning, and traffic accidents owed to scarce nocturn visibility are considered fundamental parameters in order to attain safer and quieter roads.

During the period when PAM is performing, raveling, clogging, and stripping are common types of distress that may occur, leading to decreased functionality and durability. With respect to its high AV content and low thickness, these particular conditions are often attributed as the main reasons to have a limited serviceability life as compared to conventional hot asphalt mixes (HMA). Over the years, in-depth knowledge has been gathered through various numerical or experimental studies accomplished to assess damage after exhibiting either the above-mentioned distress.

Regarding the development of rutting in PAM, it has barely been investigated so far. The reasons behind this are generally attributed to its coarser mineral composition, its placement in thinner layers, or likely after being discarded as truly structural layers. However, it does not necessarily mean that it is a minor contributor to the concern about the performance of these mixtures, but rather the opposite. In fact, since importance within the pavement has been emerging and its performance gradually understood, there has been an increasing interest in investigating the resistance to rutting of PAM.

Rutting in asphalt mixes is mainly caused by a combination of densification (volume

change) and shear deformation produced by the repetitive application of traffic loads. Factors affecting rutting resistance may vary due to its complex nature associated with weak mineral skeletons, an inadequate binder stiffness, and adhesion or moisture damage issues. In the case of PAM, rutting is primarily influenced by the air voids (AV) densification.

The permanent deformation (rutting formation) is a functionality concern that arises from the rearrangement of the internal structure of air voids as a consequence of the accumulation of vehicle traffic loads which progress to severe damage in terms of permeability loss as well as durability issues (raveling), which can aggravate if the content of air voids increases.

Therefore, the rutting resistance is experimentally addressed in this study by performing a set of laboratory tests including those recommended in NCHRP Project 9-19 [1], which are referred to as Simple Performance Tests (SPT) and currently conducted for field validation of permanent deformation: (i) dynamic modulus (DM) test; and (ii) the flow number (FN) test. These performance tests were suitably complemented with an analysis of X-ray CT images obtained before and after scan samples undergone to HWT tests.

The main contribution of this experimental investigation entails the evaluation of the rutting mechanism in Permeable Asphalt mixes (PAM) and the effect of AV content on their rutting resistance. A set of laboratory test methods were comparatively evaluated for quantifying and screening rutting resistance potential of four PAM with different AV contents. The corresponding results are presented, and evaluated, to screen the rutting potential of PAM in terms of the AV contents. Additionally, from the HWTT, a comparative analysis was conducted using X-ray CT images obtained before and after the tests in order to investigate AV distribution due to rutting.

## **1.2 Scope**

The scope of the study is limited to the experimental assessment of the rutting mechanism in permeable asphalt mixes (PAM). Despite the fact that several distresses affect the functionality and durability of these mixes, the rutting potential was selected to



be investigated since its high AV content seemed strong evidence to affect their performance and thus exhibit permanent deformation. Interestingly, there was an evident lack of literature available or research conducted specifically related to it, which only started to be widely reported in early 2010.

In order to achieve the intended goal, many tasks that were originally defined had to be adjusted to overcome inconveniences as they came out throughout the research process.

A comprehensive literature review was accomplished in order to get a thorough understanding of the field of study and figure out how it had been addressed earlier.

The experimental plan was scheduled to last one year and was entirely conducted in the Materials Laboratory at Texas A&M University (College Station, Texas). Accordingly, the mixture prepared was selected to be a permeable friction course (PFC) designed in accordance with the Texas Department Texas of Transportation -TxDOT- requirements (Item 342). This PFC is similar to mixture standardized in Colombia as PAM or *Mezcla drenante* whose mix design is outlined in (Artículo 453-13 INVÍAS). The rutting mechanism potential was evaluated in samples designed at four AV contents (18%, 20%, 22%, and 25%) by performing specific laboratory tests that will be referred to ahead herein.

As a transitional step in the research, a set of PAM samples was examined employing a medical X-ray scanner for human bodies, but the low image resolution obtained for small objects (Marshall specimens) led to a change to a more powerful machine or a CT scanner specially designed for materials. Results and experiences were documented as seen in Chapter 3.

Finally, the selected X-ray CT non-destructive technique was used to evaluate the internal air voids distribution of PAM specimens before and after to exhibit rutting. The purpose of this evaluation was to determine if there was a difference in the air void distribution among the specimens prepared at two different AV contents (i.e. 18 and 25%) and to analyze the extension of this AV distribution beneath the developed rut.

The research approach followed the abovementioned outline to ensure the accomplishment of delineated goals.

### **1.3 Research Aim and objectives**

This study is aimed at investigating experimentally the rutting mechanism of permeable asphalt mixes through laboratory testing and analysis of two-dimensional X-ray CT images. The objectives of the investigation presented herein are:

- Perform simple performing tests (SPT) such as dynamic modulus (DM) and flow number (FN) and others like Hamburg Wheel Tracking (HWT) on compacted samples in Superpave gyratory compactor (SGC).
- Use the X-ray CT imaging technique to identify changes in air voids (AV) microstructure (content and distribution) in permeable asphalt mixes caused by the rutting test at laboratory-scale (before and after the test), varying the AV content.
- Utilize the experimental data to perform an assessment of the rutting mechanism in permeable asphalt mixes regarding mix design and air voids content. Identify 3D masks for air voids, mastic, and coarse aggregates by employing the X-ray CT imaging technique. Vertical distributions of air voids and interconnectivity are also performed.
- Measure the permeability coefficient by employing an alternative X-ray Rotational Computed Tomography (RCTA) and analyze the flow of anisotropy followed by a contrast solution agent.

### **1.4 Dissertation structure**

This doctoral thesis document is organized into five chapters, which are mainly based on three articles (two of them already published and the last one submitted, to date, in review sent to an international peer-reviewed journal). Specific objectives are accomplished and presented throughout this document. Results, conclusions, and further research are presented herein at the end.

In **Chapter 1**, an introduction to the research problem is presented. It also summarizes the theoretical framework, scope, the research aim, and specific objectives of this thesis.

**Chapter 2** contains a review of the relevant literature in Permeable Asphalt Mixtures. (This chapter is based on the published paper entitled: A review of design, construction, and performance of permeable asphalt mixes in rainy countries: case of Colombia).

A second paper submitted entitled: “Experimental investigation on the rutting resistance of permeable friction courses” which is intended to accomplish specific objectives from the list above is presented in **Chapter 3**. It contains the results of the experimental program conducted and related to the Hamburg Wheel-tracking test and SPTs (dynamic modulus and flow number). It also presents the use of X-ray CT images describing the air voids distribution after the rutting test. The third objective is reached here when describing the distribution of air voids in PAM samples before and after performing a rutting test employing the non-destructive technique of X-ray computed tomography.

An analysis of the permeability rate in OGFC (PAM) is included in **Chapter 4**. This section contains a proceeding paper presented in an International conference in Baveno, Italy (2017). It also presents the results for an exploratory study, linked to this doctoral research, which is conducted on PAM samples employing a medical advanced technique called: X-ray Rotational Computed Tomography Angiography (RCTA).

The last section summarizes the conclusions and presents future work. **Chapter 5** draws the main findings from the previous sections and bring attention to further research to follow in this topic.



## Chapter 2. Literature Review in Permeable Asphalt Mixtures

<https://doi.org/10.1007/s42947-020-0023-2>

**Abstract.** Colombia is located in a tropical region, characterized by a predominant humid rainforest climate. In rainy seasons, traffic accidents are more likely to occur due to the wet condition of the pavement. To overcome this situation, permeable asphalt mixes (PAM) represent a feasible alternative to evacuate runoff water from the surface asphalt layer. PAM are discontinuously-graded asphalt mixes with a high content of air voids (AV) allowing a surface macrotexture and a high hydraulic conductivity attaining safer roads. Over the last decade, road concessionaires -private sector firms that build and operate roads in Colombia for periods consisting of twenty to thirty years- have developed projects employing PAM as top layers over primary-level roads (Inter-state). In consequence, the gained experiences using PAM are varied; some agencies have reported satisfactory behavior, whereas others have reported raveling as the primary distress at the end of their life cycle and then discontinuing its use. This paper aims at providing an overview of the design, construction, and performance of PAM in rainy countries. After explaining the current design practice in Colombia, three case-studies are reported and comprehensively analyzed, considering functionality and durability. From these analyses and compared to abroad experiences, some insights are given to improve the current practice based on performance criteria particularly for rainy countries. At the end, this paper represents a contribution towards the state-of-practice and implementation of PAM in countries with heavy rainfall regimes.

**Keywords:** permeable asphalt mixes, field performance, aggregate gradation, functionality, durability.

## 2.1 Introduction

In the middle of the last century, permeable asphalt mixes (PAM), also known open-graded friction courses (OGFC) or porous friction courses (PFC) [1], were developed in California to improve the surface frictional resistance of asphalt pavements [2,3] due to their characteristic gradation and high air void (AV) contents, usually ranged between 18% and 25%. The permeable nature of PAM is intended to allow water to drain through the surface to an impermeable underlying layer, and then laterally to the edge of the PAM. Furthermore, the reduction of noise levels, splash and spray effects, risk of hydroplaning, and urban heat island effect are additional benefits reported of these mixtures [4-7].

Since its development, the use of PAM has been implemented in the United States, European countries [8-12], a minor group of Asian countries such as Malaysia [13], China, Japan [14] and Korea [15], and Australia [16]. Over the years, the individual experiences each country obtained have led to the improvement of the mix design by adopting their own characteristics (*i.e.* weather, traffic conditions, materials selection, and so on) and construction practices. In 1974, a Federal Highway Administration (FHWA) research program standardized a mixture design procedure for PAM [17] based on the determination of optimum asphalt content without excessive draindown and particle size gradation. The method assembled successful experimental field results attained until then. Later, in 1998, the National Center for Asphalt Technology (NCAT) conducted a survey on the design and construction practices of PAM in the United States [18]. The results indicated that 19 of the 50 states surveyed were using PAM at that time, and 70% of them reported an equal to or above the average performance. Nowadays, 68% from those states continue to use PAM, as stated by Hernández *et al.* [19]. Although Illinois, Ohio, Pennsylvania, and Vermont discontinued their use mainly due to durability issues related to raveling and moisture damage in underlying layers, other states such as Arizona, Nebraska, Louisiana, Mississippi, Tennessee, and Virginia are still implementing these mixes.

In the early 2000s, a new generation of PAM emerged from the experience gained in the United States and European countries. The NCAT implemented substantial modifications

into the mixture design procedure to overcome the difficulties encountered in the performance of PAM [20]. Consequently, changes in the use of coarser gradations, polymer modified binders and fiber stabilizers were promoted, the Superpave gyratory compactor (SGC) technology, Cantabro abrasion loss and draindown tests were included, as well as a method for effectively evaluating total air voids content [21].

Several experimental research projects have focused their attention on evaluating moisture susceptibility [22], rutting [23,24], delamination [25-27] and raveling [28-30], as the primary distresses affecting the durability of PAM [31,32], and the loss of drainage capacity [33,34], and the evolution of clogging [35], issues contributing to decrease its functionality [36-39]. Despite controlling the development of these distresses by conducting demanding laboratory testing and mixture design, the lifespan of PAM is also affected by the combination of critical factors, such as materials, construction techniques, maintenance routines, traffic loading and environmental conditions [31]. However, the performance concerning durability is also dependent on the bonding strength with the underlying layers [27,40-43], but particularly for PAM, since its high air void content creates a significant reduction between areas in contact with fewer contact points among aggregate particles compared to dense-graded mixes, making it prone to delamination or raveling [42].

In Colombia, the research carried out on dense-graded HMA has been emphasized on mix design, the use of neat asphalt cements or polymer-modified binders and aging [44-48], the development of mechanical properties, and environmental effects that diminish its durability [47]. Unlike dense-graded HMA, the design, construction, and performance of PAM in Colombia is reported herein.

Colombia joined a large group of countries worldwide that implemented PAM in 2002, through the development of a mixture design procedure regulated by the National Institute for Roads Network (INVIAS). In order to address the state-of-practice of PAM, the following sequential steps were undertaken to ensure the inclusion of relevant experiences:

1. The online information available in SECOP I [49] -an informative website where Colombian government entities upload a large amount of paperwork regarding public contracts- related to National road projects including placement of PAM was compiled and analyzed.
2. A survey was conducted through road concessionaires and road public institutions to obtain specific information concerning gained experiences in the use of PAM. The questionnaire was intended to inform about mix design, performance, construction technologies, maintenance routines, and difficulties encountered in practice. The outcomes of this survey are summarized in the three case-studies presented herein.
3. An assessment was conducted based on the information gathered in the survey. The mix design and performance of PAM were compared with parameters employed abroad (*e.g.* from American and European specifications [50,51] and particularly with those of countries with similar rainfall regimes).
4. Finally, recommendations and improvements are presented to enhance the current design procedure of PAM for rainy countries.

This paper is divided into three major sections: First, an overview of the current design criteria of the mix is described. Next, the practice of PAM in Colombia is primarily addressed through the analysis of three case-studies. Finally, in the last section, information gathered from the literature review, own and foreign experiences are considered to improve the mixture design in terms of the PAM performance.

## **2.2 An overview of the mix design for PAM in Colombia**

This section contains an overview of the criteria employed to design PAM in Colombia. Similar to other international experiences, the entire process involves four steps: 1) materials selection, 2) selection of design gradation, 3) mixture design, and 4) determination of the optimum asphalt content (OAC). The current mix design method is based on the volumetric properties, and the determination of OAC is intended to meet the allowable disintegration resistance obtained as an output from the Cantabro abrasion test,



as well as its total AV content. Since PAM are prone to ravel as a consequence of cohesion loss, these properties must be attained in order to establish the OAC (%).

Guidelines for the design of PAM were first standardized in Colombia in 2002, and have been modified to the latest version outlined in Item-453 [52]. Over these years, the proportion of natural sand was reduced from 15% to zero for PAM installed on high-trafficked roads. As a result of this modification, the mixture gained texture and strength from the stone-on-stone aggregate skeleton and more adherence since the natural sand is usually unwashed. Similarly, results from experiments conducted in Australia [53] showed that an increase in the content of natural sand may increase voids due to spaces occurring between sand grains.

### **2.2.1 Materials selection**

The first step in the mixture design process is to properly select the materials for PAM (i.e. asphalt binder and coarse aggregates). In general, to select coarse aggregates for PAM, laboratory tests are performed to evaluate mechanical properties such as Micro-Deval abrasion, Los Angeles abrasion, Magnesium sulfate soundness loss, crushed face count, flat and elongated particles, plasticity index, and the sand equivalent.

Regarding asphalt binders, the use of polymer-modified binders (PMB) is highly recommended in Item-453 [52], since these binders enhance the rutting resistance and thermal cracking, and decrease fatigue damage, stripping and temperature susceptibility [54]. Moreover, their viscous properties are suitable to ensure an adequate stone-on-stone contact and to avoid the asphalt draindown. Accordingly, guidelines to design PAM in several states in the U.S. [5,6,50,51,55] implement the additional use of either mineral or cellulose fibers to prevent asphalt draindown.

### **2.2.2 Selection of design gradation**

Fig. 2-1 shows the particle size distribution for PAM according to Colombian standards [52]. A discontinuous gradation curve and a low presence of fine aggregates are required to meet the high AV content (*i.e.* 20-25%) given in Item 453 [52]. To achieve the design

gradation two or three crushed aggregates sources may be proportionally combined in order to fulfill the upper and lower limits displayed in Fig. 2-1. A slight difference is noted between Colombian standards to design PAM outlined in Item 453 [52] and the standard ASTM D7064 [50]. Whereas Item 453 [52] sets a unique gradation design for a range of trial asphalt contents (*e.g.* 4.5% is the initial asphalt content), the guidelines for PAM given in [50] recommend several trial gradations and just one asphalt content (typically between 6.0% and 6.5% for neat liquid asphalts). The variable to adjust in each case is different; in [52] is the asphalt content, and in [50] is the trial gradation.

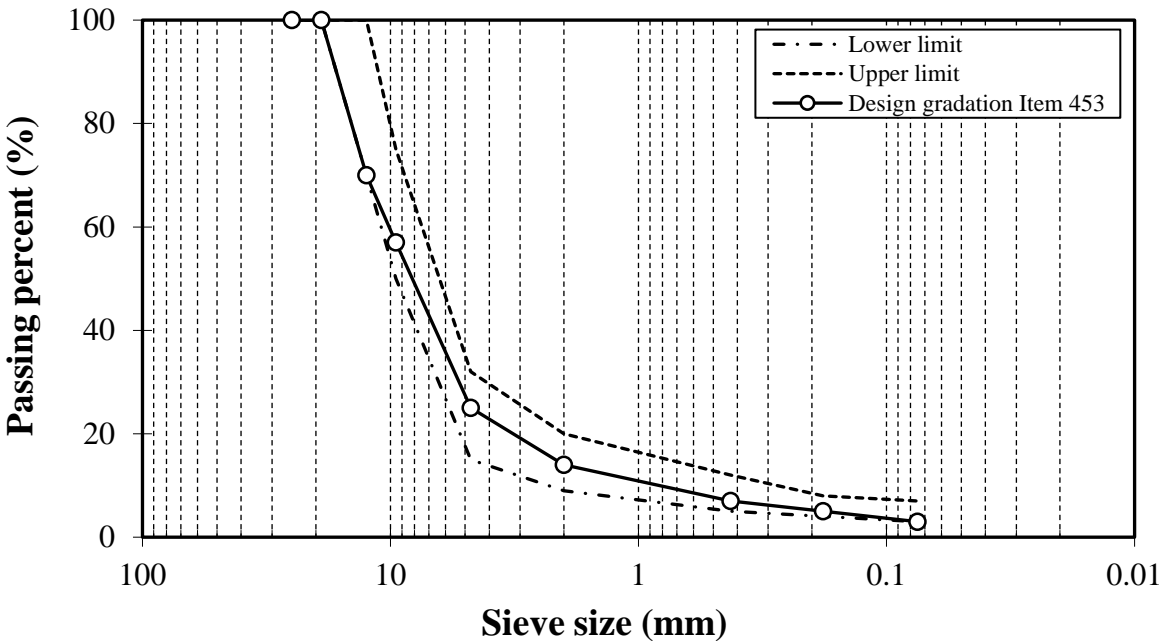


**Fig. 2-1.** Sieve size particle distribution for PAM in Colombian standards [52].

**2.2.3 Mixture Design procedure**

Once the gradation design according to Fig. 2-1, and an initial asphalt content (AC) are selected, the polymer-modified asphalt and aggregates are thoroughly combined at the mixing temperature previously verified, until the latter ones are completely coated by the asphalt binder. As standardized in the Cantabro abrasion test [56], four specimens per each asphalt content are compacted using 50 blows per face of Marshall hammer [57].

Specimens must be 2.5 in (63.5 mm) height, and the diameter must be 4.0 in (101.6 mm). After the trial samples have been compacted and allowed to cool down, they are removed from the molds and tested to determine their bulk specific gravity  $G_{mb}$  through either dimensional analysis outlined in INV E-736 [58], or the vacuum sealing technique given in INV E-802 [59].

Some PAM specimens are moisture-conditioned in a temperature chamber, long enough to ensure a steady temperature of 60 °C for a period of 24 hours. Subsequently, all samples (*i.e.* conditioned and unconditioned) are tested in Los Angeles machine for 300 revolutions at a speed of 30-33 rpm. From the Cantabro abrasion test [56], loss in weight expressed as a percentage is calculated as:

$$\text{Cantabro Loss (\%)} = \frac{P_o - P_f}{P_o} \times 100 \quad (2-1)$$

where  $P_o$  is the specimen mass prior to test, and  $P_f$  is the specimen mass after 300 revolutions. From each trial, a portion of the loose mixture is used to determine the theoretical maximum density  $G_{mm}$  whose value is also known as Rice Specific Gravity, according to test methods provided in INV E-735 [60] or INV E-803 [61].

## 2.2.4 Determination of OAC

Fig. 2-2 depicts a flowchart describing the procedure for designing PAM in Colombia according to Item 453 [52]. Here, the OAC is selected as the minimum content of asphalt binder required to meet the following criteria:

- The average abrasion loss from the Cantabro test for unconditioned samples should be smaller than 25%. For moisture-conditioned samples, the upper limit allowed is 40%. Attaining these values is mandatory in order to ensure stone-on-stone contact.
- Total AV content ranges between 20% and 25%.
- In any case, the selection of OAC is less than 4.5%. In contrast, a range from 6.0-6.5% is proposed in ASTM D7064 [50].
- Drainage capacity is measured by performing a permeability test. The time required for 100 cm<sup>3</sup> of water to flow through the sample should not exceed fifteen seconds (15 s).

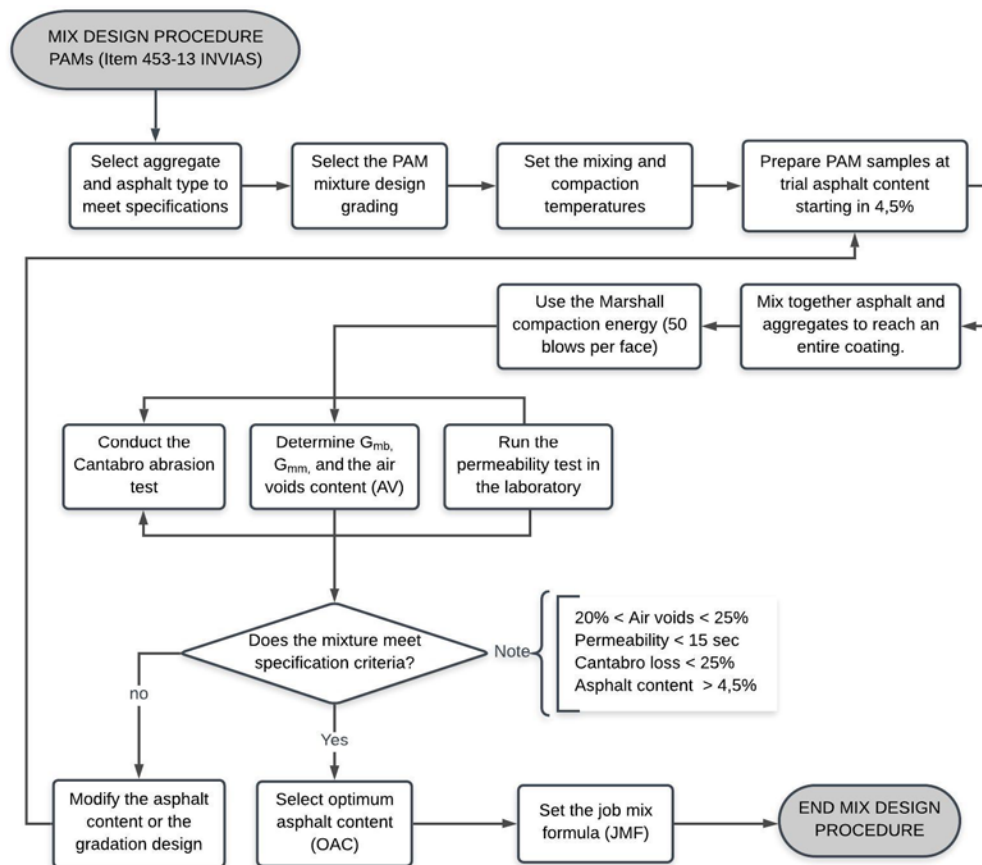


**Fig. 2-2.** Flowchart of the current laboratory-design procedure of PAM according to Item 453 (Adapted from [52])

In connection with previous requirements, the AV content is computed using the procedure outlined in INV E-736 [58]. The bulk specific gravity  $G_{mb}$ , and the theoretical maximum specific gravity  $G_{mm}$  are fundamental volumetric properties influenced by the composition of the mixture in terms of the blend aggregates and asphalt binder. As stated, the dimensional analysis is a useful method to compute  $G_{mb}$ , which is based on the geometrical calculation of total volume (*i.e.* diameter and height) assuming that specimens are regular cylinders (contour pores are negligible). In this regard, Alvarez *et al.* [62] discussed the methods to determine  $G_{mb}$  by comparing vacuum and dimensional analysis techniques. It was concluded that dimensional analysis is the more accurate method to compute  $G_{mb}$  due to the fewer discrepancies in the quantification of AV in contact with the specimen surface, and its capacity to assure consistent evaluations of total AV content.

Finally, once the volumetric parameters  $G_{mb}$  and  $G_{mm}$  are computed, the AV content is expressed as a percentage of the total volume in a compacted PAM as:

$$AV \text{ content } (\%) = \left[ 1 - \frac{G_{mb}}{G_{mm}} \right] \times 100 \quad (2-2)$$

### 2.3 Colombian experience using PAMs

Recently, the World Bank ranked Colombia as the rainiest country worldwide, reaching an average precipitation in depth of 3240 mm/year [63]. Accordingly, the placement of PAM is increasingly promoted by road concessionaires to keep safer roads under this adverse climate conditions. Fig. 2-3 displays the list of rainiest countries worldwide per continent and the precipitation data is provided for those countries implementing indistinctly PAM [8-16]. As also noted in Fig. 2-3, most countries using these mixes present an annual average precipitation data below 2000 mm/year. In this manner, there is a valid reason to assume that the formed thicker runoff film in countries such as Colombia and Malaysia represent a challenge for PAM in terms of functionality.

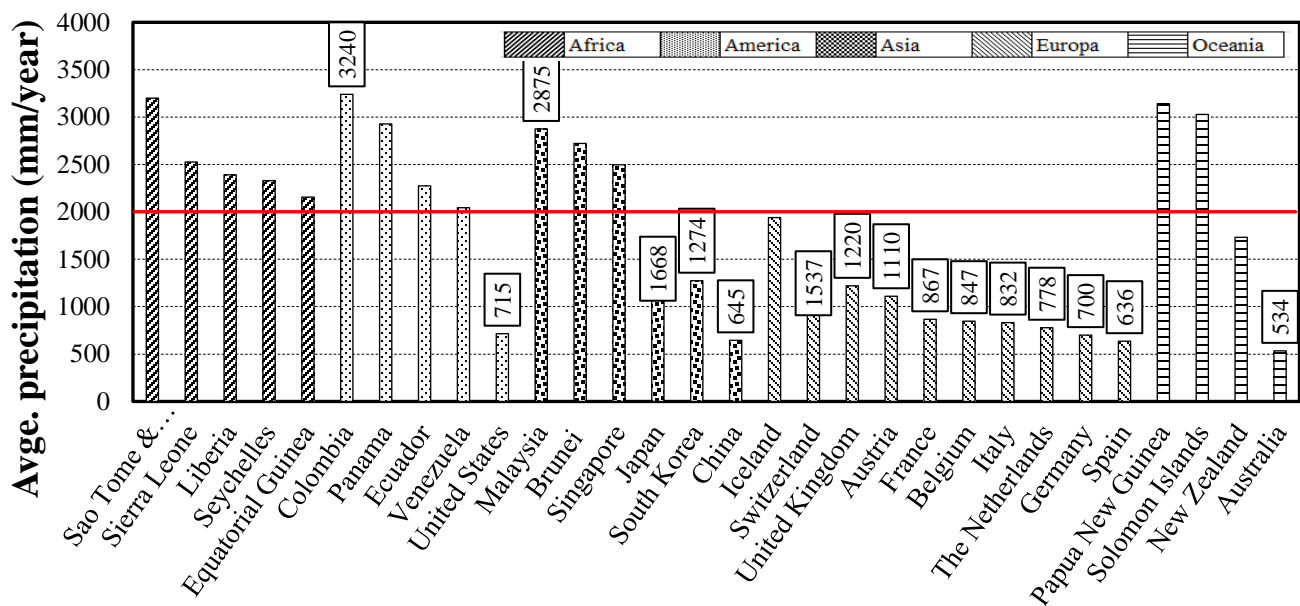
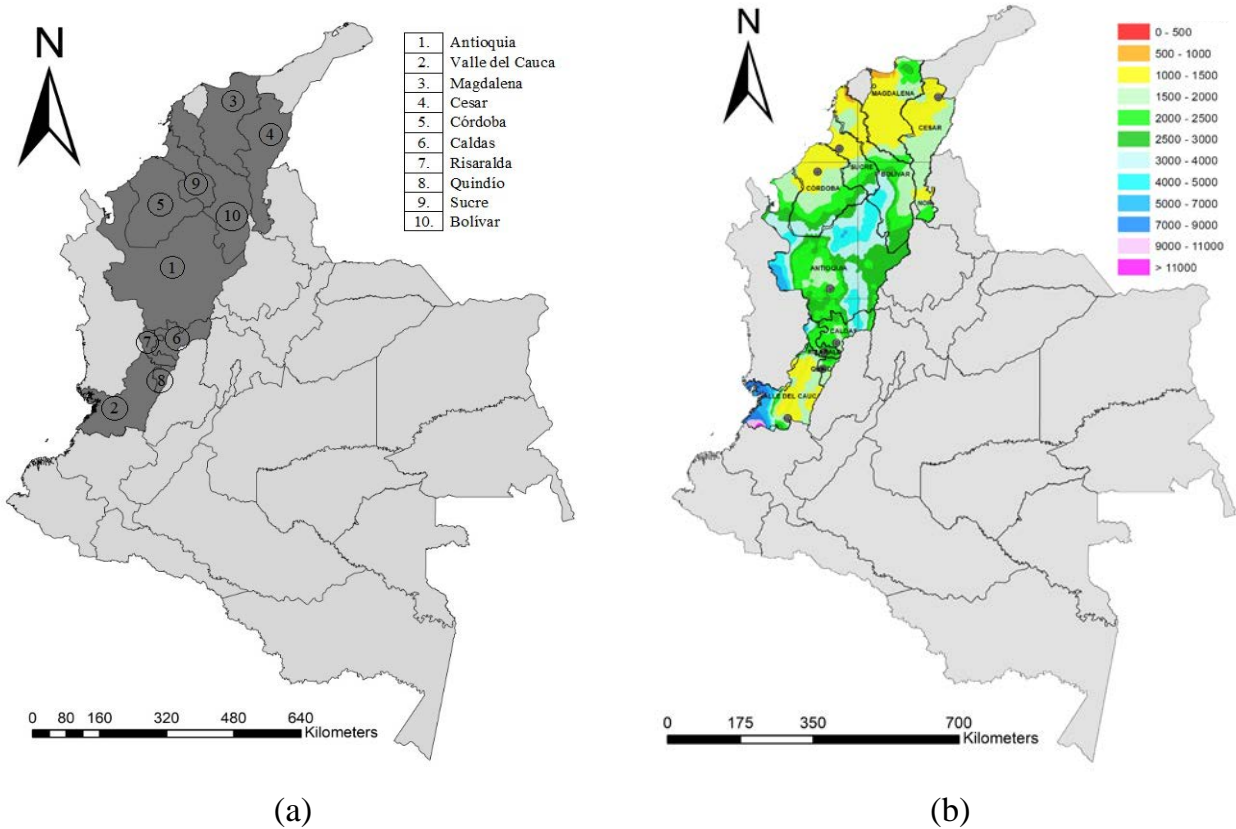





Fig. 2-3. List of rainiest countries worldwide using PAM, per continent extracted from [61]. Annual average precipitation (mm/year).

Table 2-1 summarizes the main features of the mix design and general information of field projects undertaken in Colombia that include PAM. The mix design and placement requirements for PAM are regulated through the Item 453 [52], and it is denoted as *MD*, which in Spanish stands for *Mezcla Drenante*. Since 2010, a group of ten Colombian departments mostly located in the northwestern region (Fig. 2-4a) have made efforts in the use of PAM through the construction of road projects funded by public institutions or road concessionaires. Fig. 2-4a. highlights the Colombian departments in which PAM have been installed as surface layers for primary, and secondary level roads and urban asphalt pavements. Fig. 2-4b depicts the average precipitation (mm/year) for these departments [64]. Even though, the involved regions are quite rainy, the highest levels of precipitation are achieved in the Pacific region in western Colombia.



**Fig. 2-4.** (a) Departments in Colombia implementing PAM. (b) Average precipitation per year (mm/year).

**Table 2-1.** Summary version of the current practice of PAMs in Colombia

ID Project	Urban Pavements	Coffee Highways (Autopistas del Café)	Trans-Americas' Highway (Transversal de las Américas)
<b>Location (Departments)</b>	Antioquia	Caldas, Risaralda, Quindío, and Valle del Cauca	Córdoba, Sucre, Magdalena, Urabá, Bolívar, and Cesar.
<b>Specific Location</b>	Collector Road in Regional <i>Av. Plaza Minorista</i>	National Highway 29 (Various routes)	National Highway 23 between Planeta Rica and Montería
<b>Year of construction</b>	2011	2011	2017
<b>Average Precipitation per project (mm/year)</b>	2000 - 3000	1500 - 3000	1000 - 3000
<b>Illustrations</b>			
<b>Type of mixture</b>	PAM -MD- (INVÍAS)	PAM -MD- (INVÍAS)	PAM -OGFC- (FHWA)
<b>Length (km)</b>	1.4	>20	>50
<b>Thickness (mm)</b>	54	40	23
<b>Type of binder</b>	PMA type III	PMA type II	PMA type II (PG 70-22)
<b>Energy of compaction (method)</b>	Marshall hammer (50 blows per side)	Marshall hammer (50 blows per side)	Marshall hammer (50 blows per side)
<b>Job mix Formula:</b>			
AV content, %	21.2	20	16
VMA, %	25.3	N/A	24.0
VFA, %	15.3	N/A	42.5
OAC, %	3.7	4.5	5.5
Draindown, %	N/A	N/A	0.2 (<0.3)*
Cantabro loss, %			
-Dry samples	12.3	<25	12.0
-Moist. conditioned samples (60 °C)	26.5	<40	14.5
<b>Status in 2020</b>	Removed and replaced	In service	In service

Two design specifications were generally employed for this purpose. PAM (*MD-1*) outlined in [52] for urban pavement in Medellín and *Autopistas del Café* (Coffee Highways), and the FHWA standard [65] for Trans-Americas' Highway. A discrete number of road concessionaires and public institutes were surveyed to collect the mix design and performance data for PAM in Colombia. In the following subsections, these case-studies are presented and discussed. Particularly, the management and performance data for PAM sections owned and operated by road concessionaires is highly reserved, in comparison to other countries where information related to laboratory test results and field performance studies is placed in open-access repositories for screening, for instance, the Long-Term Pavement Performance (LTPP) program [66].

## **2.4 Urban pavement in Medellín (Antioquia)**

In 2011, a search for safer asphalt mixtures led to the placement of PAM in urban pavements of Medellín (Fig. 2-4b). Medellín is the capital of the Department of Antioquia (Fig. 2-4a), and represents the second largest city in Colombia. The average precipitation in this city is within 2000 to 3000 mm/year (Table 2-1), therefore the need of implementing asphalt mixes with high drainage capacity. Since it was the first field project involving the construction of PAM, several problems were faced. Firstly, the mixture design in the laboratory included a new test: the Cantabro test, which had been already a standardized method in Spain since 1986 [67], the sampling and molding procedures were a challenge because of the high AV content (*i.e.* 21.2%) as seen in Table 2-1. Secondly, the on-site compaction process was arduous for workers, since PAM cools down more rapidly compared to the dense-graded HMA.

### **2.4.1 Materials selection and mix design**

A combination of two material sources consisted of 70% of river crushed aggregates, and 30% of crushed sand from a local quarry. These materials were washed, dried and sieved into the select size range according to a PAM gradation in Item 453 [52] and its properties were verified by laboratory tests. Regarding the gradation of the aggregates, the nominal maximum aggregate size (NMAS) was established in 12.5 mm. An OAC of 3.7%



of Styrene-butadiene-styrene (SBS) modified asphalt binder (type III) met the most of requirements given in Section 2.2.4 for PAM installed in this urban road. Neither mineral nor cellulose fibers were used in this project. Results for the Cantabro abrasion test were maintained below the limits (*i.e.* 12.3% and 26.5% for dry and moisture-conditioned, respectively) suggested in Item 453 [52]. The AV content was 21.2%, moreover Table 2-1 summarizes the main features of this project. During the construction phase, a tack coat composed of high-viscosity, cationic rapid-setting emulsion typified as CRS-2 was applied to ensure high shear strength between asphalt layers at a rate within 0.2 and 0.3 kg/m<sup>2</sup>.

#### **2.4.2 Performance and lifecycle**

As reported in Table 2-1, the PAM designed in Medellín comprised a very low OAC of 3.7%, even below the usual content for these mixtures (greater than 4.5%) as described in Item 453 [52]. In the years after 2011, the 54 mm thick PAM withstood the heavy vehicular traffic of more than 20000 vehicles passing daily despite being poorly maintained with anti-clog routines as reported in a public-access repository. In 2019, after eight years in service, this PAM began to ravel and deteriorate progressively until its failure. Finally, it was entirely milled and replaced with a new dense-graded HMA layer. A lesson learned from this experience showed that the placement of PAM in urban pavements brings several challenges since environmental conditions tend to be more adverse due to debris found on the road surface, accelerating clogging distress. In addition, an inadequate OAC reduces adherence, incompletes aggregates coating, and consequently leads to premature raveling.

### **2.5 Autopistas del Café (Coffee Highways)**

*Autopistas del Café* is a road network, managed and operated by a road concessionaire, along the *Eje Cafetero* (Coffee Belt) that goes across four departments namely Caldas, Risaralda, Quindío, and Valle del Cauca (Fig. 2-4a). As seen in Table 2-1, the average precipitation in this area is also between 1500 to 3000 mm/year. Road safety is a main

concern in these highly-trafficked areas, since *Eje Cafetero* is a high-impact economic and tourism sector in Colombia. Nowadays, around 10% of its entire length (256 km) has PAM as the surface layer. Given that the road concessionaire evaluated PAM performance satisfactorily due to all the benefits provided in terms of traffic noise reduction, skid resistance, comfortable driving experience, decreased aquaplaning and improved road safety, the placement of these mixes in other field project sections is increasingly growing.

### **2.5.1 Materials selection and mix design**

PAM used in this field project as surface friction course had a mix design with a NMA of 12.5 mm and an OAC of 4.5% by mass. Crushed stone aggregates were provided from local quarries, and a SBR-modified polymer binder (type II) was supplied by a local company. Sampling and molding were set following the Marshall method, and the mixing and compaction temperatures ranged from 158-166 °C, and 144-152 °C, respectively. Fibers were not used in the mixture. Loss percentages in the Cantabro test were kept below 25% and 40% for each particular testing condition (Table 2-1). The PAM section with an average AV content of 20% was constructed on top of an impermeable layer.

### **2.5.2 Performance and lifecycle**

Currently, these PAM are still in service under high-traffic conditions since they were placed in 2011. The bonding between the 40 mm thick PAM and the dense-graded mixture was guaranteed spreading homogeneously a thin rapid-setting tack coat of polymer-modified binder (PMRS) on the surface of the underlying layer, and the residual amount of asphalt binder ranged from 0.2 to 0.3 kg/m<sup>2</sup>. In the final part of the survey, the respondent was asked about the performance aspects of PAM layers. The question dealt with the estimated average service life of these mixes. As stated by the road concessionaire, PAM is expected to have a lifecycle greater than eight years that can be extended to 15 years according to experiences reported in Spain, (see typical values in Table 2-2). To date, any issues concerning the durability of the installed PAM such as raveling or delamination, have not yet been reported.

**Table 2-2.** Mixture design parameters in countries using PAM

Country	Colombia	Spain	Australia	The Netherlands	Italy	Malaysia	Belgium	Japan	US states using OGFC	Texas (United States)
Ref.	[52]	[10]	[53]	[8]	[12]	[77]	[9][2][2]	[14]	[50][3][3]	[51]
Standards	Item 453-13	Item 543-15	AGPT048 4B-14	N/A	N/A	REAM (type B)	BRRC	N/A	ASTM D7064	TxDOT Item 342
Type of mixture	MD	PA-16 PA-11	OG-10 OG-14 OG-20	PA 0/11 PA 0/16	PA-14 PA-10	PA-14 PA-10	PA 0/14	PA	OGFC	PFC
AV, min., %	20-25	20	20	20	16	18-25	22	20-22	18	18
NMAS (mm)	12.5	16 11.2	9.5 13.2 19	11 16	14 10	14 10	14	13.2	12.5	12.5
Type of Asphalt	PMA	PMA AR	PMA AR	PG asphalt	SBS Modified binder	PMA	PMA AR	MA*	PMA AR	PMA AR
AC, min., %	4.5	4.3	5.5 5.0 4.5	4.5	5	4	4	4	6.0 – 6.5	6.0
Use of fibers	N/A	Optional	mineral fibers	N/A	N/A	N/A	N/A	None	either mineral, cellulose	either mineral, cellulose
Blows in Marshall (b) or gyrations in SGC (gyr)	50 b.	50 b.	80 gyr.	50 b.	50 b.	50 b.	50 b.	50 b.	50 gyr.	50 gyr.
Cantabro loss, Max. %	25* 40**	25* 40**	20* 30**	N/A	25* 30**	15*	20*	20	20* 30**	20*
Moisture damage (TSR test), Min. %	N/A	85	N/A	N/A	N/A	80	N/A	N/A	80	N/A
Draindown, Max., %	N/A	N/A	0.3	N/A	0.2	0.3	N/A	N/A	0,3	0,1
Layer thickness (mm)	20-40	40-50	30	50	40	50	40	25-30	25-30	20-25
Lifecycle (years)	8-10	12-15	8-10	10 - 12	8-10	>8	8-10	7-10	>8	6-8

Note. BRRC: Belgian Road Research Center, REAM: Road Engineering Association of Malaysia. PG: Penetration-graded asphalt. PMA: Polymer-modified asphalt. AR: Asphalt rubber. MA: Type of binder penetration grade 60/70 modified with TPS (Styrenic-Thermoplastic elastomer).

N/A: Information not available

\*Cantabro Abrasion Loss on Unaged/dry Specimens. \*\* Cantabro Abrasion Loss on aged/moisture Specimens

## 2.6 Transversal de las Américas (Trans-Americas' Highway)

*Transversal de Las Américas* is a highway network aimed at integrating Panama, Venezuela, and Colombia, into a single export corridor. This project is operated and managed by the road concessionaire: *Vías de las Américas*. On the Colombian side, the highway is extended through northern departments, namely Magdalena, Antioquia, Córdoba, Bolívar, Sucre, and Cesar (Fig. 2-4a). The average precipitation in this area varies from 1000 to 3000 mm/year (Table 2-1). As part of this network, a 35 km length of PAM mixture was laid on the route from *Planeta Rica* to *Montería* -cities in the Department of Córdoba. Over the last few months, a 22 km length of PAM was installed in the Urabá region in the Department of Antioquia.

### 2.6.1 Materials selection and mix design

Table 2-3 presents the gradation design for the PAM selected according to the upper and lower limits given in the FHWA standard [65]. Details on the mixture design, the selected AV content of 16%, volumetric properties and the job mix formula which were carefully controlled are also provided in Table 2-1. Furthermore, an OAC of 5.5% SBS-modified asphalt binder (Type II) and a workability enhancing additive were used in the design of this mixture. River crushed stone aggregates obtained from local stone-crushing plants were also used in this project. According to the information provided by the road concessionaire, the design of a 23 mm thick asphalt mixture was required to meet the thickness specified in the plans provided by the project owner. However, the NMAAS for PAM that is 12.5 mm as indicated in Item 453 [52] was too coarser to fit that thickness needed to be placed. For this reason, a PAM with a NMAAS of 9.5 mm was designed in this study. A CRS-2 tack coat was applied uniformly covering the dense-graded HMA surface layer. Particularly, for the applied emulsion, the residual amount of asphalt binder was set at 0.32 kg/m<sup>2</sup>.

**Table 2-3.** Particle size gradations. PAM (Trans-Americas' Highway) and MD (Coffee highways), [52]

Sieve size		FHWA Gradation design	FHWA (% passing limits)	MD-1 (PAM) Gradation design	MD-1 (PAM) (% passing limits)
US	SI (mm)				
3/4"	19.0	-	-	100	100
1/2"	12.5	100	100	79	70-100
3/8"	9.5	99.8	95-100	57	50-75
No. 4	4.75	32.6	30-50	25	15-32
No. 8	2.36	13.6	5-15	-	-
No. 10	2.0	-	-	14	9-20
No. 40	0.42	-	-	7	5-12
No. 200	0.075	2.2	2-5	3	3-7

### 2.6.2 Performance and lifecycle

The installed PAM has already been in service for three years since its placement in 2017. Currently, it is still under operation and maintenance, and rehabilitation activities are still considered unnecessary. Above all for this project, results from laboratory testing (*i.e.* rutting, moisture susceptibility and dynamic modulus), were provided for this study. In the case of rutting, a maximum rut depth of 7.32 mm after 20000 passes was attained in the Hamburg Wheel Tracking tester (HWTT), a dynamic modulus of 2969 MPa at 10 Hz was reported, and the moisture susceptibility measured by the Tensile Strength Ratio (TSR) was 86.8% (min. 80%). These measured values agree with those recommended for PAM mixes in several countries (Table 2-2).

At the beginning of 2019, the road concessionaire evaluated the field performance of the installed PAM. A combination of good friction and low levels of roughness is expected for PAM to perform adequately in terms of safety. In this regard, the macrotexture of a pavement surface is the result of large coarse aggregate particles-size in the mixture characterized by a wavelength ranged between 0.5 mm and 50 mm [68-71]. To measure the pavement profile, skid resistance (coefficient of friction), macrotexture condition and

rutting resistance for each lane, a road surface profilometer (RSP) was used. These measurements reported for all parameters are displayed in Fig. 2-5 to Fig. 2-7.

Fig. 2-5 illustrates the rutting performance for a 35 km long PAM mix in a two-way lane. There is a noticeably higher level of rutting in the first 15 km of the left lane, which can be produced by traffic channeled or trucks overloaded in this lane. From this location to the end of the PAM section, the levels of rutting between the lanes remain almost uniform below a 10 mm level, with an average rut depth in the right lane of 3.72 mm, while the left lane achieved a deeper value of 5.0 mm. Excluding measurements at locations K5 and K14, measurements did not exceed the rutting level acceptable for this project (*i.e.* 12.5 mm) which is similar to international standards, for example, the report by the Texas Department of Transportation (TxDOT) [51] uses this value as the criterion for allowable rutting. Rut depths reported herein are closely similar to the outcomes presented in previous studies [20,23,72] for PAM with NMAS 10 mm tested in the laboratory using Hamburg wheel-tracking testers.

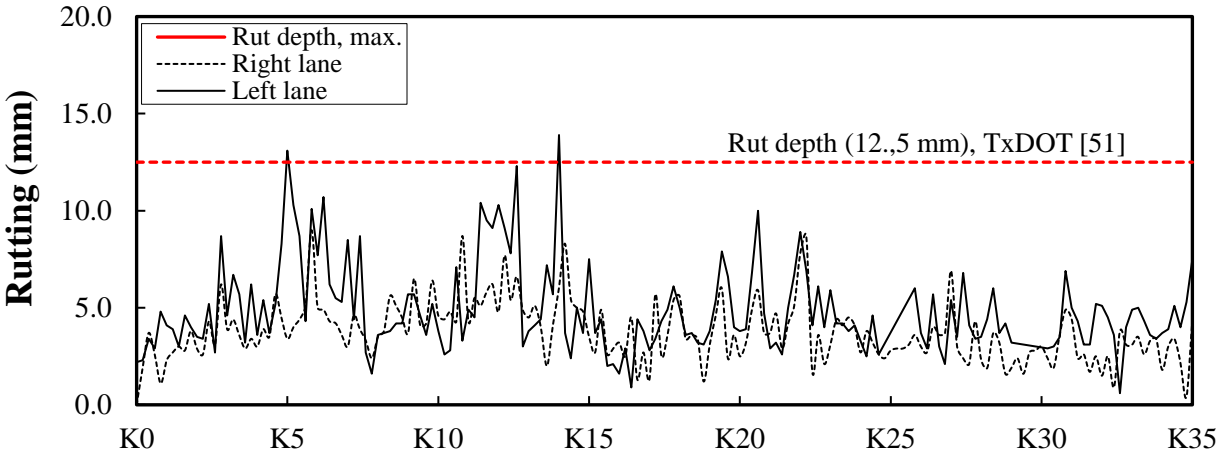


**Fig. 2-5.** Measurement of rutting over PAM section placed in the Trans-Americas' Highway (Dept. of Córdoba)

As seen in Fig. 2-6 and Fig. 2-7, the sections under evaluation were extended over 50 km (K50) in order to include the field section where a dense-graded HMA was placed. The coefficient of friction and macrotexture for the two types of mixture (PAM and dense-graded HMA) were displayed and compared. The end of the PAM section and the beginning

of the dense-graded HMA converge at K35. Fig. 2-6 depicts the mean profile depth (MPD) measured for each lane. The lower limit expected to have the PAM section for the macrotexture condition is set at 0.5 mm. An outstanding performance was achieved by this PAM section with an average MPD of 1.50 mm. A noticeable decrease in texture was observed once the dense-graded HMA section began with an average of 0.94 mm. As expected, the discontinuous gradation of PAM produced greater macrotexture compared to dense-graded HMA mixes. Usually, vehicle users perceive the drop of texture between these two evaluated field sections since the safety condition is reduced due to lower friction while driving, after crossing K35. Similar trends in profile depths are observed for both left and right lanes, along the 50 km section.

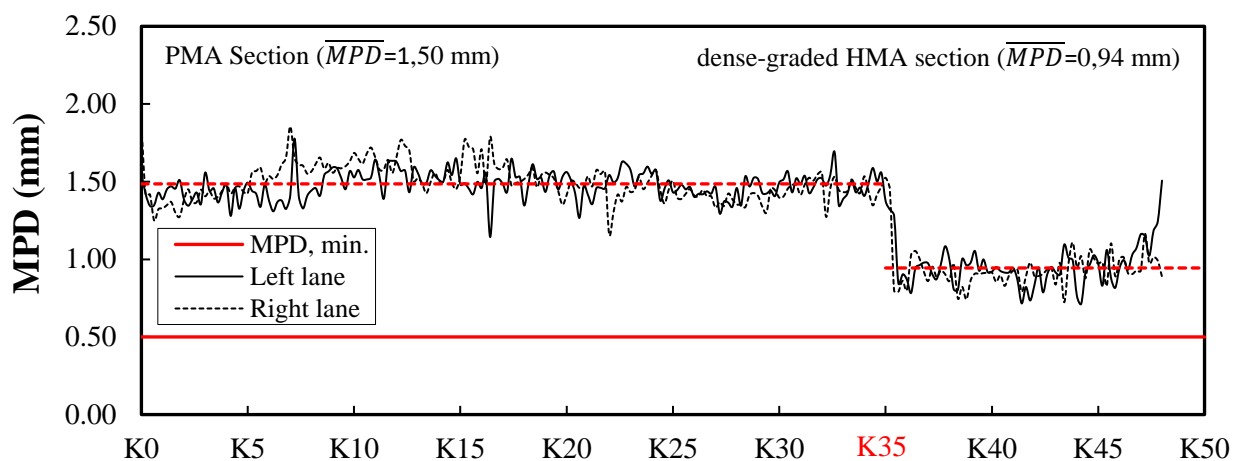


**Fig. 2-6.** Measurement of macrotexture for PAM and dense-graded HMA sections placed in Trans-Americas' Highway (Dept. of Córdoba)

Fig. 2-7 plots the coefficient of friction evaluated for the same field sections, and it was closely associated with the MPD parameter. In general, the rougher the asphalt mixture the greater the friction coefficient. Differences were observed for this parameter between the installed PAM and dense-graded HMA sections. For instance, when comparing the friction coefficient for these two sections, the PAM exhibits an enhancement of 16% in the average from 0.56 to 0.65. It is worth noticing that the dense-graded HMA offers a

smoother vehicular circulation. Despite that, left lanes present a slight variation in the rutting depth as seen in Fig. 5 along the entire section due to a higher traffic volume in this direction, its coefficient of friction shows better results compared to the right lane.

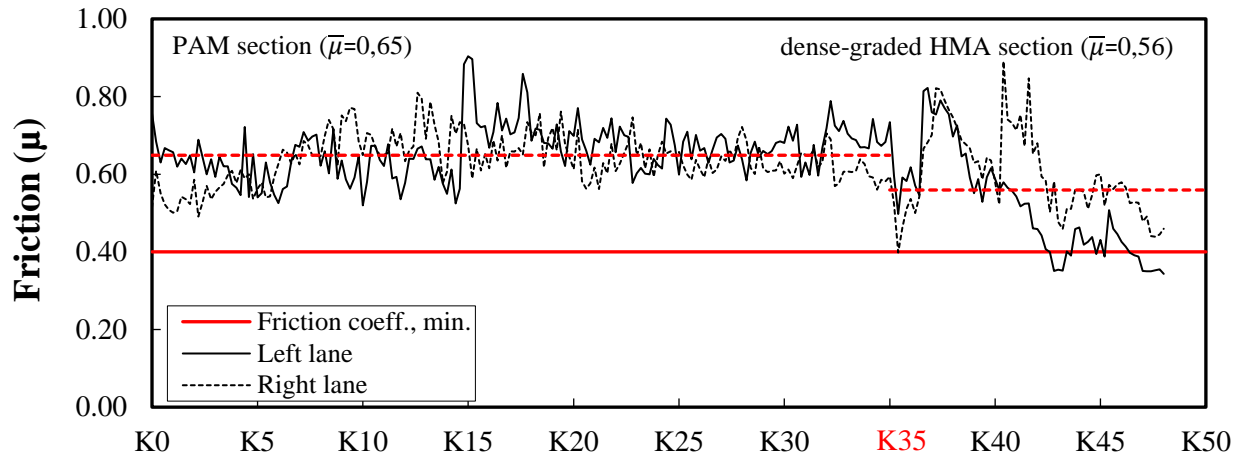


**Fig. 2-7.** Measurement of friction ( $\mu$ ) for PAM and dense-graded HMA sections installed in Trans-Americas' Highway (Dept. of Córdoba)

## 2.7 Comparative analysis

Colombian experience in the use of PAM is evaluated based on the review of the case studies presented herein, and it is also compared to experiences from countries worldwide implementing PAM as reported in Table 2-2. Correspondingly, some remarks are highlighted as follows:

- As previously seen, the Colombian experience in the use of PAM is significant. Nearly 30% of Colombian departments employed PAM as wearing courses for asphalt pavements. However, practice so far has revealed that issues, such as susceptibility to clogging and raveling related to the durability, can be effectively addressed as more PAM mix design controls and maintenance routines are suggested and included in Item 453 [52] and more projects are carried out.
- In general, PAM placed in Colombia has performed adequately. To date, neither stripping nor raveling has been informed as distress, except for PAM placed on the



urban pavement in Medellin that reached its failure by progressive raveling produced by an insufficient OAC. In addition, this experience showed that the use of an  $OAC \leq 4.0\%$  forms a thin binder film coating the coarse aggregates, providing a weak stone-to-stone contact. Moreover, as reported by the road concessionaire, PAM laid in *Autopistas del Café* on steep slopes were prone to clog more rapidly due to extra road dirt and low-speed traffic. However, in the survey this respondent hindered to provide additional informational related to maintenance routines including anti-clog practices and the driven loss of permeability.

- For all case-studies reported herein, differences in NMAAS, OAC, and the AV content were noticeable as registered in Table 2-1. The PAM placed in Trans-Americas' Highway had the finer gradation given its lower NMAAS (9.5 mm) compared to the other two projects (*i.e.* NMAAS 12.5 mm). As reported in [73], since the gradations may vary by adjusting the percent passing the No. 4 (4.75 mm) sieve, the selection of NMAAS has a negligible influence on the performance of PAM. Regarding the as-built thickness, greater values were reported for PAM installed in the urban pavement in Medellin and Coffee Highways (54 and 40 mm, respectively), and a thinner overlay was placed in Trans-Americas' highway (23 mm). As observed in Table 2-2, international experiences confirmed that the thickness affects the durability of PAM, thicker layers are more durable (between 10 and 15 years).
- According to the list of rainiest countries in Fig. 2-3, PAM are mostly implemented in countries where rainfall regimes are not as severe as it occurs in Colombia or Malaysia, reaching annual precipitation levels of 3240 and 2875 mm/year, respectively. For this reason, its high drainage capacity is not fully exploited in many countries. The permeability rate in PAM is influenced by both the AV content and its connectivity in the aggregate packing [74,75]. Consequently, road safety is guaranteed for users while driving in Colombia at high speeds and the surface remains almost dry. Likewise, PAM becomes a suitable alternative to be implemented in other tropical countries such as Rwanda [76], where the precipitation level is a factor contributing to the gradual decreased functional performance of pavements.

- Based on the case studies presented above, it is observed that some mix design parameters included in the design of PAM in Colombia are comparable with successful foreign cases reported in Table 2-2. For instance, the use of SBS-modified polymer asphalts, an average content of 20%, and the loss percentages in the Cantabro test (dry conditions) for urban pavements in Medellin and Trans-Americas' Highway projects that were as low as 12%. Surprisingly, this value for the Cantabro abrasion test is near to 15% (Table 2-2), which is the maximum value allowed by Malaysian guidelines [77], the second rainiest country after Colombia.
- The skid resistance to keep safer roads is one of the major advantages in PAM. In this regard, the performance of the mixture placed in Trans-Americas' Highway attained average values for MPD and coefficient of friction of 1.50 mm and 0.65, respectively (Fig. 2-6 and Fig. 2-7). In comparison, a study related to the performance of field sections of PFC placed in Indianapolis [78] reported values for the coefficient of friction and MPD of 0.42 and 1.37 mm, respectively. These results demonstrate the outstanding performance of these mixes under rainy conditions in Colombia and promises an extended use in future projects.

## **2.8 Performance criteria of PAM in rainy countries**

A comparison made between the successful experience of PAM in the US states [16,19,78] and European and Asian practices [79] to the recent Colombian experience lead to an improved mix design procedure that includes several recommendations cited below. Fig. 2-8 depicts a flowchart summarizing these recommendations, by integrating volumetric properties, performance testing and maintenance routines. To facilitate understanding, the following considerations to be adopted in rainy countries are grouped into criteria of functionality and durability.

### **2.8.1 Functionality**

- The following volumetric parameters namely: voids in coarse aggregate in the dry-rodded condition - a portion of the total aggregate blend retained on the 4.75 mm sieve- ( $VCA_{DRC}$ ) and voids in the coarse aggregate fraction of the compacted mix

( $VCA_{mix}$ ) are convenient to be computed and evaluated in the design of Colombian PAM to ensure the existence of stone-to-stone contact. The  $VCA_{DRC}$  is determined by compacting the stone with the dry-rodded technique according to the test method given in [80] and calculated as:

$$VCA_{DRC} = \left[ \frac{G_{CA}\gamma_W - \gamma_S}{G_{CA}\gamma_W} \right] \times 100 \quad (2-3)$$

where  $G_{CA}$  is the bulk specific gravity of the coarse aggregate,  $\gamma_S$  is the bulk density of the coarse aggregate fraction in the dry-rodded condition ( $\text{kg}/\text{m}^3$ ), and  $\gamma_W$  is the density of water equal to  $998 \text{ kg}/\text{m}^3$ . Therefore, by using the bulk specific gravity of the coarse aggregate fraction and  $G_{mb}$ , the  $VCA_{mix}$  can be calculated with:

$$VCA_{mix} = 100 - \left[ P_{CA} \times \frac{G_{mb}}{G_{CA}} \right] \quad (2-4)$$

where  $P_{CA}$  is the percent coarse aggregate in the total mixture and  $G_{CA}$  is the bulk specific gravity of the coarse aggregate fraction. According to the method proposed by the National Center for Asphalt Technology (NCAT) [5], a PFC mixture achieves stone-on-stone contact when the ratio  $VCA_{mix}/VCA_{DRC} \leq 1.0$ . In contrast, a second study conducted by Alvarez *et al.* [81] reveals that using a maximum ratio  $VCA_{mix}/VCA_{DRC} = 0.9$  is enough to ensure a fully developed stone-on-stone contact in PFC mixtures, this second value may be adopted.

- To ensure the quality in design and placement of PAM, the on-site quality control (QC) tests listed below are required: texture, thermal profile, skid resistance, and ride quality measurement. Nowadays, just a few of these measurements are still controlled by low-tech equipment. For instance, the sand patch test outlined in INV E-791 [82] is proposed to measure the texture for PAM. However, Praticò and Vaiana [83] stated that performing the sand patch test might be not reliable if used in PAM because some material can be poured into the pores. As a suitable substitute to measure texture in PAM, the use of a laser-based tech road profiler is being used.

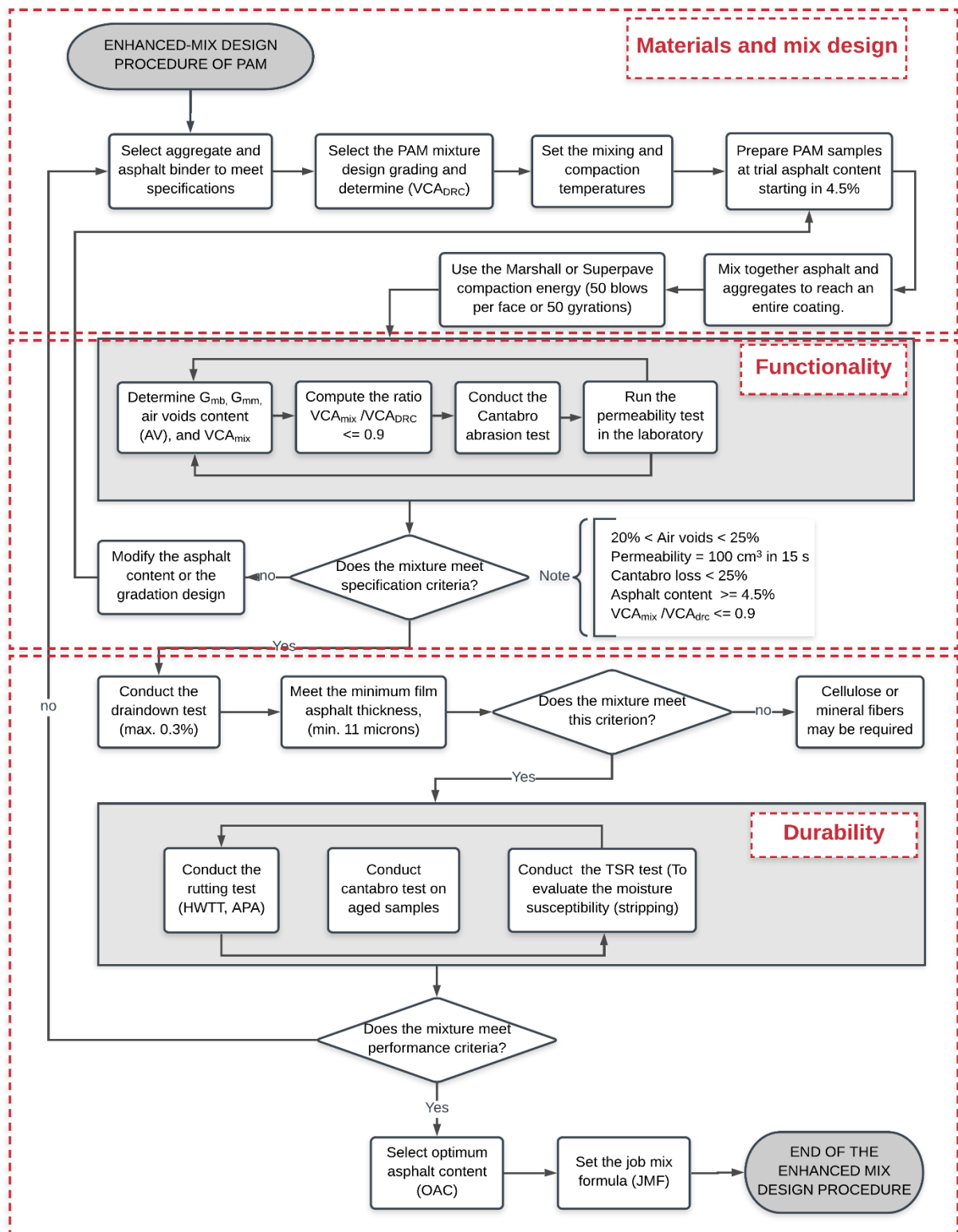


**Fig. 2-8.** Flowchart of an improved laboratory-design procedure of PAM.

- A permeability test should be performed once the PAM has been installed. A field permeameter is currently used to verify the permeability rate. Using a Computed tomography angiography (CTA) technique, Senior *et al.* [84] conducted an exploratory study to measure the permeability flow through the air voids in PAM. In this image study, a contrast dye was injected into the compact PAM sample, while the operator observed the liquid flowing through the thickness of the sample. Results displayed the paths followed by the contrast dye in real-time, the air-voids internal distribution and the permeability rate of PAM. Improvements in the acquisition-time and viscosity of contrast dye should be addressed to standardize the test.
- Maintenance activities focused on cleaning the PAM pore structure should be carried out periodically or as deemed necessary to avoid or delay the clogging as its main functional distress. The causes attributed to the clogging of air voids are divided into two: the accumulation of dust and debris that fill the PAM air voids structure and the high rutting rates and deformation as a result of the effect of heavy traffic loads [85,86]. A progressive clogging can also lead to loss of permeability.

### **2.8.2 Durability**

- Set a minimum value ranged from 8-11 microns for the asphalt film thickness in order to ensure adequate contact from stone-to-stone, reduce the susceptibility for PAM to undergo moisture damage, and diminish the asphalt aging by reducing the oxygen transport rate into the binder. In comparison, conventional dense-graded HMA requires a lower asphalt binder film thickness ranging between 4-6 microns following FHWA standard [65].
- Establish a maximum value of 0.3% for the asphalt draindown in order to adjust the OAC and reduce the potential that excessive binder may draindown in the mix during silo storage or transportation in trucks. Draindown can be prevented by employing stabilizing additives such as cellulose or mineral fibers. These fibers were used in six

field sections constructed in Georgia [20] achieving a rather low percentage in the Cantabro loss abrasion test and a less amount (and severity) of cracking.

- In order to evaluate the potential of moisture damage (stripping) and the development of rutting, two performance tests are recommended to conduct in PAM compacted samples: the tensile strength ratio (TSR) with a minimum value of 80%, and the Hamburg-wheel tracking test (HWTT) or the asphalt pavement analyzer (APA).
- Interface bonding strength between the PAM used in the surface and the next layer is also an important task that should be controlled in field sections to ensure the good overall performance of pavements that include PAM layers. A direct shear test conducted on the interface, comprised of PAM and the underlying layer, provides insights on the type of tack coat and minimum residual rate (*i.e.* residual amount of asphalt on the pavement surface) required to ensure a quality contact between these layers. For PAM, the minimum binder residual rate is usually established in  $0.3 \text{ kg/m}^2$  [87].

## 2.9 Summary and conclusions

This paper aimed at providing an overview of the design, construction, and performance of PAM in rainy countries, with particular emphasis to cases-studies from Colombia. Overall, the results of this study showed the necessity to continue implementing PAM nationwide as well as in rainy countries under similar weather conditions, due to their satisfactory performance and their major contribution to road safety. Finally, from this review, the following conclusions are drawn:

- Colombian experience implementing PAM is useful for other countries with high rainfall regimes. Special considerations in the mixture design of PAM should be made in order to obtain a PAM balanced-performance that ensures the durability and functionality due to thicker films of rainwater to evacuate. Regarding its functionality, the permeability rate plays an important role during its lifespan, to ensure the safety road conditions, even on a wet surface.

- Cationic (CRS) or anionic (ARS) rapid-setting asphalt emulsions are currently employed in the application of tack coats for bonding asphalt layers. The asphalts accepted for emulsions can be conventional or polymer-modified, and its typical composition is 60% residual asphalt and 40% water.
- Additional requirements in laboratory tests to design PAM in Colombia must be adjusted or complemented. The test to control the asphalt draindown and minimum asphalt film thickness are parameters to consider in selecting OAC in the job mix formula. In addition, the use of fibers and some performance tests may be included as minimum compliance to design and produce PAM (*e.g.* moisture susceptibility and rutting tests).
- Similar to other countries, an open access database containing onsite performance, laboratory test results, mix design parameters and quality control (QC) tests conducted periodically should be available for public screening in order to compare later with field measurements.
- Scientifics and practitioners around the world face various challenges regarding the design, placement, and conservation of PAM. In terms of material selection, the use of high-quality crushed stone aggregates and polymer-modified binders is vital to ensure a good performance and also helps to enhance the resistance of raveling. Regarding functionality, it is important to guarantee the effective permeability during its service life. For this reason, maintenance activities including anti-clog routines must be scheduled and the QC tests periodically conducted. Durability related issues that require further attention are raveling and delamination; major controls on construction practices should be conducted to enhance the performance of PAM.

## References

- [1] A. Alvarez, O. Reyes, R. Miró, A review of the characterization and evaluation of permeable friction course mixtures, *Ingeniare* 22 (4) (2014) 469–482.
- [2] H. Smith, Performance Characteristics of Open-Graded Friction Courses. Synthesis No. 180. National Coop. Highway Research Project (NHCRP), Federal Highway Administration (FHWA), Washington, D.C., USA, 1992.
- [3] G. Huber, Performance Survey on Open-Graded Friction Course Mixes. Synthesis No. 284. National Coop. Highway Research Project (NHCRP), Federal Highway Administration (FHWA), Washington, D.C., USA, 2000.
- [4] L. Cooley, J. Brumfield, R. Mallick, W. Mogawer, M. Partl, L. Poulikakos, G. Hicks, Construction and Maintenance Practices for Permeable Friction Courses. National Coop. Report 640. Highway Research Project (NHCRP). Washington, D.C., USA, 2009.
- [5] P.S. Kandhal, Design, Construction and Maintenance of Open-Graded Asphalt Friction Courses, NAPA, Information series 115, Lanham, Maryland, USA, 2002.
- [6] E. Arámbula, C. Estakhri, A. Martin, M. Trevino, A. Smit, J. Prozzi, Performance and Cost Effectiveness of Permeable Friction Course (PFC) Pavements. Report No. FHWA/TX-12/0-5836-2. Texas Transportation Institute. Austin, Texas, USA, 2013.
- [7] P. Weiss, M. Kayhanian, J. Gulliver, L. Khazanovich, Permeable pavement in northern North American urban areas: research review and knowledge gaps, *Inter. J. Pavement Eng.* 20 (2) (2019) 143–162.
- [8] J. Van Der Zwan, T. Goeman, H. Gruis, J. Swart, R. Oldenburger, Porous asphalt wearing courses in the Netherlands: State of the Art Review, *Transp. Res. Rec.* 1265 (1990) 95–110.
- [9] G. Van Heystraeten, C. Moraux, Ten Years' Experience of Porous Asphalt in Belgium, *Transp. Res. Rec.* 1265 (1990) 34–40.



- [10] A. Ruiz, R. Alberola, F. Pérez, B. Sánchez, Porous asphalt mixtures in Spain, *Transp. Res. Rec.* 1265 (1990) 87–94.
- [11] T. Isenring, H. Köster, I. Scazziga, Experiences with Porous Asphalt in Switzerland, *Transp. Res. Rec.* 1265 (1990) 41–53.
- [12] G. Di Mino, M. Giunta, The volumetric mix-design of porous asphalt: An Italian study of N design determination, *Adv. Characterisation Pavement Soil Eng. Mater. Proc. Inter. Conf. Adv. Characterisation Pavement Soil Eng. Mater.* 2 (2007) 1055–1062.
- [13] M. Hamzah, M. Hasan, C. Che, N. Abdullah, A Comparative Study on Performance of Malaysian Porous Asphalt Mixes incorporating Conventional and Modified binders, *J. Appl. Sci.* 10 (20) (2010) 2403–2410.
- [14] H. Nakanishi, M. Hamzah, M. Mohd, P. Karthigeyan, O. Shaur, Mix design and application of porous asphalt pavement using Japanese technology, *Mater. Sci. Eng.* 512 (1) (2019) 012026.
- [15] F. Gu, D. Watson, J. Moore, N. Tran, Evaluation of the benefits of open graded friction course: Case study, *Constr. Build. Mater.* 189 (2018) 131–143.
- [16] A. Alvarez, A. Martin, C. Estakhri, J. Button, C. Glover, S. Jung, Synthesis of Current Practice on the Design, Construction, and Maintenance of Porous Friction Courses. FHWA/TxDOT Report 0-5262-1. Texas Transportation Institute Austin, Texas, USA, 2006.
- [17] R. Smith, J. Rice, S. Spelma, Design of Open-graded Friction Courses. Interim Report FHWA-RD-74-2. Federal Highway Administration (FHWA), Washington, D.C., USA, 1974.
- [18] P.S. Kandhal, R. Mallick, Open-Graded Asphalt Friction Course: State of the Practice. Transportation Research Circular E-C005, National Research Council, Washington, D.C., USA, 1998.

- [19] M. Hernandez, S. Caro, E. Arámbula, A.E. Martin, Mix design, performance and maintenance of Permeable Friction Courses (PFC) in the United States: State of the Art, *Constr. Build. Mater.* 111 (2016) 358–367.
- [20] R.B. Mallick, P.S. Kandhal, L. Cooley, D. Watson, Design, Construction, and Performance of New-Generation Open-Graded Friction Courses. Report 00-01. NCAT, Auburn, Alabama, USA, 2000.
- [21] D. Watson, K. Moore, K. Williams, L. Cooley, Refinement of New-Generation Open-Graded Friction Course Mix Design, *Transp. Res. Rec.* 1832 (2003) 78–85.
- [22] E. Masad, A. Castelblanco, B. Birgisson, Effects of air void size distribution, pore pressure, and bond energy on moisture damage, *J. Test. Eval.* 34 (1) (2006) 15–23.
- [23] K. Jeong, S. Hwang, S. Lee, K. Kim, Investigation of rutting potential of Open Graded Friction Course (OGFC) mixes using asphalt pavement analyzer, *KSCE J. Civ. Eng.* 15 (7) (2011) 1259–1262.
- [24] E. Coleri, J.T. Harvey, K. Yang, J. M. Boone, Micromechanical investigation of open-graded asphalt friction courses' rutting mechanisms, *Constr. Build. Mater.* 44 (2013) 25–34.
- [25] W. Song, X. Shu, B. Huang, M. Woods, Laboratory investigation of interlayer shear fatigue performance between open-graded friction course and underlying layer, *Constr. Build. Mater.* 115 (2016) 381–389.
- [26] W. Song, X. Shu, B. Huang, M. Woods, Factors affecting shear strength between open-graded friction course and underlying layer, *Constr. Build. Mater.* 101 (2015) 527–535.
- [27] W. Song, X. Shu, B. Huang, M. Woods, Influence of interface characteristics on the shear performance between open-graded friction course and underlying layer, *J. Mater. Civ. Eng.* 29 (8) (2017) 1–9.
- [28] L. Mo, M. Huurman, M. Woldekidan, S. Wu, A. Molenaar, Investigation into material optimization and development for improved ravelling resistant porous asphalt

- concrete, *Mater. Des.* 31 (7) (2010) 3194–3206.
- [29] E. Arámbula, R.A. Hill, S. Caro, L. Manrique, E.S. Park, E.G. Fernando, Understanding mechanisms of ravelling to extend open graded friction course (OGFC) service life. Final Report BDR74–977–04. Texas A&M University System, College Station, USA, 2016.
- [30] J. De Visscher, A. Vanelstraete, Ravelling by traffic: Performance testing and field validation, *Inter. J. Pavement Res. Technol.* 10 (2017) 54–61.
- [31] H. Wu, J. Yu, W. Song, J. Zou, Q. Song, L. Zhou, A critical state-of-the-art review of durability and functionality of open-graded friction course mixtures, *Constr. Build. Mater.* 237 (2020) 117759.
- [32] A.E. Alvarez, A.E. Martin, C. Estakhri, R. Izzo, Evaluation of durability tests for permeable friction course mixtures, *Inter. J. Pavement Eng.* 11 (1) (2010) 49–60.
- [33] A. Alvarez, A. Martin, C. Estakhri, Drainability of permeable friction course mixtures, *J. Mater. Civ. Eng.* 22 (6) (2010) 556–564.
- [34] J. Chen, Y. Zhang, H. Li, Y. Gao, Rutting-induced permeability loss of open graded friction course mixtures, *J. Test. Eval.* 44 (2) (2016) 719–724.
- [35] E. Coleri, M. Kayhanian, J.T. Harvey, K. Yang, J.M. Boone, Clogging evaluation of open graded friction course pavements tested under rainfall and heavy vehicle simulators, *J. Environ. Manag.* 129 (2013) 164–172.
- [36] S.N. Suresha, G. Varghese, A. U. Ravi, Effect of aggregate gradations on properties of porous friction course mixes, *Mater. Struct.* 43 (6) (2010) 789–801.
- [37] L.F. Walubita, J. Zhang, A.N. Faruk, A.E. Alvarez, T. Scullion, Laboratory hot-mix asphalt performance testing: asphalt mixture performance tester versus universal testing machine, *Transp. Res. Rec.* 2447 (1) (2014) 61–73.
- [38] L.F. Walubita, L. Fuentes, A. Prakoso, L.M. Rico, J.J. Komba, B. Naik, Correlating the

HWTT laboratory test data to field rutting performance of in-service highway sections, *Constr. Build. Mater.* 236 (2020) 117552.

- [39] L.F. Walubita, L. Fuentes, S.I. Lee, I. Dawd, E. Mahmoud, Comparative evaluation of five HMA rutting-related laboratory test methods relative to field performance data: DM, FN, RLPD, SPST, and HWTT, *Constr. Build. Mater.* 215 (2019) 737–753.
- [40] J. Wang, F. Xiao, Z. Chen, X. Li, S. Amirkhanian, Application of tack coat in pavement engineering, *Constr. Build. Mater.* 152 (2017) 856–871.
- [41] M. Mazumder, M.S. Lee, S.J. Lee, Installation and implementation of proper tack coat application, *J. Korean Asph. Inst.* 9 (1) (2019) 14–39.
- [42] B. Danish, Investigation of bonding between open graded friction courses and underlying asphalt pavement layers. (PhD. Dissertation), Clemson University, South Carolina, USA, 2018.
- [43] W. Zhang, Effect of tack coat application on interlayer shear strength of asphalt pavement: A state-of-the-art review based on application in the United States, *Inter. J. Pavement Res. Technol.* 10 (2017) 434–445.
- [44] F.A. Reyes-Lizcano, C.M. Lizarazo, A.S. Figueroa, M.A. Candia, G.W. Flintsch, Dynamic characterization of hot-mix asphalt mixtures using modified and conventional asphalts in Colombia, *Proc. of the 88th TRB Annual Meeting*, Washington, D.C., USA, 2009.
- [45] S. Caro, L. Coral, B. Caicedo, Modelación del ahuellamiento en mezclas asfálticas de pavimentos [Rutting modeling in asphalt pavement mixtures], *Rev. Ing.* 18 (7) (2003) 41–47 [In Spanish].
- [46] J. Preciado, G. Martínez, M. Dugarte, A. Bonicelli, J. Cantero, D. Vega, Y. Barros, Improving Mechanical Properties of Hot Mix Asphalt using Fibres and Polymers in Developing Countries, *IOP Conference Series Mater. Sci. Eng.* 245 (2) (2017) 022013.
- [47] H. Rondón, F.A. Reyes, G. Flintsch, D.E. Mogrovejo, Environmental effects on hot mix asphalt dynamic mechanical properties: Case study in Bogota, Colombia, *Transp. Res.*

- Rec. 3637 (1) (2012) p.13.
- [48] H. Rondón, F.A. Reyes, A.S. Figueroa, E. Rodriguez, C.M. Real, T.A. Montealegre, Estado del conocimiento del estudio sobre mezclas asfálticas modificadas en Colombia [State-of-knowledge on modified asphalt mixtures in Colombia], *Infraestruct. Vial*, 19 (2008) 10–20 [In Spanish].
- [49] SECOP I, Colombian government entity website. (SECOP I). <https://www.contratos.gov.co/consultas/inicioConsulta.do>. Accessed: 07 September 2019.
- [50] American Society for Testing and Materials, Standard Practice for Open-Graded Friction Course (OGFC) Mix Design. ASTM D 7064, ASTM International, West Conshohocken, PA, USA, 2013.
- [51] Texas Department of Transportation, Standard specification for Permeable friction Courses (PFC). Item 342. TxDOT, USA, 2014.
- [52] Instituto Nacional de Vías, Especificaciones Generales de Construcción de carreteras: Mezcla drenante [Colombian Specifications for Road Construction: Permeable Asphalt Mixes]. Artículo 453 (Item 453-13). Bogotá, Colombia, 2007 [In Spanish].
- [53] Austroads, Austroads. Guide to Pavement Technology Part 4B: asphalt, Sydney, Australia, 2014.
- [54] Y. Yildirim, Polymer modified asphalt binders, *Constr. Build. Mater.* 21 (1) (2007) 66–72.
- [55] C.K. Estakhri, A.E. Alvarez, A.E. Martin, Guidelines on construction and maintenance of porous friction in Texas. Report FHWA/TX-08/0-5262-2. Austin, Texas, USA, 2008.
- [56] Instituto Nacional de Vías, Normas de Ensayo para Materiales de Carreteras. Caracterización de las mezclas bituminosas abiertas por medio del ensayo Cantabro

- de pérdida por desgaste [Colombian Road Standards: Characterization of Permeable Asphalt Mixes by means of Cantabro Loss Test]. INV E-760. In correspondance to AASHTO T-96. Bogotá, Colombia, 2013 [In Spanish].
- [57] Instituto Nacional de Vías, Normas de Ensayo para Materiales de Carreteras. Resistencia de mezclas asfálticas en caliente empleando el aparato Marshall [Colombian Road Standards: Resistance of Hot Asphalt Mixes employing Marshall]. INV E-748. In correspondance to AASHTO T-245. Bogotá, Colombia, 2013 [In Spanish].
- [58] Instituto Nacional de Vías, Normas de Ensayo para Materiales de Carreteras. Porcentaje de vacios con aire en mezclas asfálticas compactadas densas y abiertas [Colombian Road Standards: Air Voids Percent in Compacted Dense- and Permeable Asphalt Mixes]. INV E-736. In correspondance to ASTM D 3203. Bogotá, Colombia, 2013 [In Spanish].
- [59] Instituto Nacional de Vías, Normas de Ensayo para Materiales de Carreteras. Determinación de la gravedad específica bulk y de la densidad de mezclas asfálticas compactadas mediante el método de sellado automático por vacío [Colombian Road Standards: Determination of Bulk Specific Gravity and Density of Compacted Asphalt Mixtures through the Automatic Vacuum Sealing Method]. INV E-802. In correspondance to ASTM D 6752. Bogotá, Colombia, 2013 [In Spanish].
- [60] Instituto Nacional de Vías, Normas de Ensayo para Materiales de Carreteras. Gravedad Específica Máxima Medida ( $G_{mm}$ ) y Densidad de mezclas asfálticas para pavimentos [Colombian Road Standards: Theoretical Maximum Specific Gravity and Density of Asphalt Mixtures]. INV E-735. In correspondance to ASTM D 2041. Bogotá, Colombia, 2013 [In Spanish].
- [61] Instituto Nacional de Vías, Normas de Ensayo para Materiales de Carreteras. Determinación de la gravedad específica máxima y de la densidad máxima de las mezclas asfálticas para pavimentación mediante el método de sellado automático por vacío [Colombian Road Standards: Maximum Specific Gravity and Density of

- Asphalt Mixtures through the Automatic Vacuum Sealing Method]. INV E-803. In correspondance to ASTM D 6857. Bogotá, Colombia, 2013 [In Spanish].
- [62] A. Alvarez, A. Martin, C. Estakhri, R. Izzo, Determination of Volumetric Properties for Permeable Friction Course Mixtures, *J. Test. Eval.* 37 (1) (2008) 1–10.
- [63] The World Bank, Average precipitation in depth (mm per year). (The World Bank, 2014),  
[https://data.worldbank.org/indicator/AG.LND.PRCP.MM?end=2014&most\\_recent\\_value\\_desc=true&start=2014&view=map](https://data.worldbank.org/indicator/AG.LND.PRCP.MM?end=2014&most_recent_value_desc=true&start=2014&view=map). Accessed 11 November 2019.
- [64] IDEAM, Average precipitation in depth (mm per year) for Colombian states. (IDEAM), <http://atlas.ideam.gov.co/visorAtlasClimatologico.html>. Accessed 17 November 2019.
- [65] Federal Highway Administration, Open Graded Friction Courses. Technical Advisory T 5040.31, FHWA, Washington, D.C., USA, 1990.
- [66] Strategic Highway Research Program (SHRP), The Long-Term Pavement Performance (LTPP) program, United States, 1991.  
<https://infopave.fhwa.dot.gov/Data/DataSelection>. Accessed 07 September 2019.
- [67] F. Pérez, M. Calzada, Analysis and Evaluation of the Performance of Porous Asphalt: The Spanish Experience in Surface Characteristics of Roadways: International Research and Technologies, West Conshohocken, PA, USA, 1990.
- [68] G. Flintsch, E. De León, K. McGhee, I. Al-Qadi, Pavement Surface Macrotecture, Measurement and Applications, *Transp. Res. Rec.* 1860 (2003) 168–177.
- [69] P. Georgiou, A. Loizos, Quality assurance of HMA pavement surface macrotecture: empirical models vs experimental approach, *Inter. J. Pavement Res. Technol.* 12 (4) (2019) 356–363.
- [70] R. Justo-Silva, A. Ferreira, Pavement maintenance considering traffic accident costs,

Inter. J. Pavement Res. Technol. 12 (6) (2019) 562–573.

- [71] S. Cafisoa, A. Di Graziano, D.G. Gouliasb, C. D’Agostino, Distress and profile data analysis for condition assessment in pavement management systems, Inter. J. Pavement Res. Technol. 12 (2019) 527–536.
- [72] L. Cooley, E. Brown, D. Watson, Evaluation of OGFC Mixtures containing Cellulose Fibers. NCAT Report 00-05. Auburn, Alabama, USA, 2000.
- [73] H. Nekkanti, B.J. Putman, B. Danish, Influence of Aggregate Gradation and Nominal Maximum Aggregate Size on the Performance Properties of OGFC, Transp. Res. Rec. 2673 (1) (2019) 240-245.
- [74] D.M. Kusumawardani, Y.D. Wong, Evaluation of aggregate gradation on aggregate packing in porous asphalt mixture (PAM) by 3D numerical modelling and laboratory measurements, Constr. Build. Mater. 246 (2020) 118414.
- [75] D.M. Kusumawardani, Y.D. Wong, The influence of aggregate shape properties on aggregate packing in porous asphalt mixture (PAM), Constr. Build. Mater. 255 (2020) 119379.
- [76] L. Bo, M.J. Kundwa, C.Y. Jiao, Z.X. Wei, Pavement performance evaluation and maintenance decision-making in Rwanda, Inter. J. Pavement Res. Technol. 12 (2019) 443–447.
- [77] Public Works Department, Standard Specification for Road Works, Section 4, Flexible Pavement, Kuala Lumpur, Malaysia, 2008.
- [78] R.S. Mc Daniel, W. Thornton, Field Evaluation of a Porous Friction Course for Noise Control, TRB Annual Meeting Transp. Res. Board. Washington, D.C., USA, 2005.
- [79] D. Gibbs, R. Iwasaki, R. Bernhard, J. Bledsoe, D. Carlson, C. Corbisier, K. Fults, T. Hearne, K. McMullen, D. Newcomb, J. Roberts, J. Rochat, L. Scofield, M. Swanlund, Quiet Pavement systems in Europe. Report No. FHWA-9L-05-011. Alexandria, VA, USA, 2005.



- [80] American Society for Testing and Materials, Standard Test Method for Bulk Density (Unit Weight) and Voids in Aggregate. ASTM C 29. ASTM International, West Conshohocken, PA, USA, 2017.
- [81] A. Alvarez, E. Mahmoud, A. Martin, E. Masad, C. Estakhri, Stone-on-Stone Contact of Permeable Friction Course Mixtures, *J. Mater. Civ. Eng.* 22 (11) (2010) 1129–1138.
- [82] Instituto Nacional de Vías, Normas de Ensayo para Materiales de Carreteras. Textura superficial de un pavimento mediante el método del círculo de arena [Colombian Road Standards: Measuring Pavement Macrotexture Depth Using a Volumetric Technique]. INV E-791. In correspondance to ASTM E 965. Bogotá, Colombia, 2013 [In Spanish].
- [83] F. Praticò, R. Vaiana, A study on the relationship between mean texture depth and mean profile depth of asphalt pavements, *Constr. Build. Mater.* 101 (2015) 72–79.
- [84] V. Senior, C. Graciano, C. Vega-Posada, S. Álvarez, N. Ramírez, Permeability flow measurement for open-graded friction courses, in *Pavement and Asset Management – Proc. World Conference on Pavement and Asset Management, WCPAM 2017*, M. Crispino, Ed. London, Taylor & Francis Group, UK, 2019, pp. 585–592.
- [85] S.N. Suresha, G. Varghese, U. Ravi, Laboratory and Theoretical Evaluation of Clogging behaviour of Porous Friction Course Mixes, *Inter. J. Pavement Eng.* 11 (1) (2010) 61–70.
- [86] D. Savio, M.R. Nivitha, J.M. Krishnan, Influence of climate and traffic on the HMA rut-depth for India, *Inter. J. Pavement Res. Technol.* 12 (2019) 595–603.
- [87] CALTRANS, Tack Coat Guidelines, State of California Department of Transportation Division of Construction, Sacramento, USA, 2009.



## Chapter 3. Rutting mechanism assessment in PAM

*(This chapter is based on the paper entitled: Experimental investigation on the rutting resistance of permeable friction courses submitted to Construction and Building Materials – CONBUILDMAT-D-20-03732R1)*

**Abstract.** This paper presents an experimental investigation on the rutting resistance of permeable friction courses (PFC). In practice, PFC are prone to permanent deformation due to heavy traffic loads and a weak mineral skeleton caused by their high air void contents. Consequently, the draining capacity of the PFC is diminished making the roads unsafe in wet conditions. Hence, the rutting mechanism of PFC is evaluated through three laboratory tests: dynamic modulus (DM), flow number (FN), and Hamburg wheel tracking test (HWTT). The samples were prepared and compacted considering four air voids (AV) contents: 18%, 20%, 22% and 25%. From the HWTT, a comparative analysis was conducted using X-ray computer tomography (X-ray CT) images obtained before and after the tests in order to investigate AV distribution due to rutting. The results show that the dynamic modulus, the flow number and the rutting response are severely affected by increasing the AV content in the PFC mixes. After increasing the AV content, the dynamic modulus and the flow number decreases significantly, while the rutting depth increases. From the analysis of the X-ray CT images, a larger AV densification was observed in the upper part of the samples beneath the developed rut, whereas in the bottom part the AV content increased further weakening the mineral skeleton.

**Keywords:** permeable friction courses; rutting resistance; moisture damage; permanent deformation; flow number; dynamic modulus; AV content; X-ray CT.

### 3.1 Introduction

In road engineering practice, rutting in hot-mix asphalts (HMA) is mainly caused by a combination of densification (volume change) and shear deformation produced by the repetitive application of traffic loads, mostly under hot weather conditions. Material properties influencing rutting resistance may vary due to its complex nature associated with weak mineral skeletons, inadequate binder stiffness, and adhesion or moisture damage issues [1]. External factors affecting rutting resistance of asphalt pavement also includes, climatic condition, traffic volumes, speed, and axle types, and construction quality [2]. Moreover, the properties of the asphalt components change over time, depending on loading and temperature conditions [3].

Over the last two decades, rutting in HMA has been the focus of several research projects across the world [2-24]. In spite of being an unavoidable distress in HMA, field rutting failures can be mitigated throughout performing adequately laboratory tests during the HMA mix-design screening stage. In the NCHRP Project 9-19 [3], three Simple Performance Tests (SPT) were recommended for field validation of permanent deformation: (i) dynamic modulus (DM) test; (ii) the flow time; and (iii) the flow number (FN) test. Firstly, these SPT were mainly employed for dense-graded HMA [4-7]. Through time, additional tests have been included to evaluate, characterize, quantify, and screen rutting potential in the laboratory such as the repeated load permanent deformation (RLPD), simple punching shear test (SPST), and Hamburg wheel tracking test (HWTT).

DM testing has demonstrated a great potential for HMA material characterization, and applications for pavement structural design as a research-level test tool to develop mechanistic models [6,8-12]. It is a key parameter that correlates material properties to field fatigue cracking and rutting performance [9]. With FN testing the onset of shear deformation can be identified for asphalt mixtures, and allows to quantify their permanent deformation characteristics [6,9-17]. The RLPD testing setup is similar to the FN test, but using different input load magnitudes. It has been identified as a more comprehensive research-oriented test, for its potential to generate comprehensive HMA material properties for pavement structural design, pavement modeling, and mechanistic-empirical analyses [10-12,14]. HWTT is widely used across the world, and has a proven

history of effectively identifying and screening HMA mixes susceptible to rutting and moisture damage (stripping) [2,10,12,13,16,18-20].

Comparative studies have also been conducted to establish possible correlations between these test methods mentioned above, and to rank their ability to characterize HMA mix rutting resistance potential [6,8,11,12]. Laboratory test results indicated that the FN Index, computed from the FN test data, exhibited a better correlation with results from both the DM and RLPD tests [11]. This FN index has also the ability to statistically differentiate the HMA mixes [16]. When compared to field performance data, most laboratory test predictions correlated well with the actual measured field performance data, with the HWTT and SPST tests exhibiting superiority over the other test methods [12].

Field rutting failures mostly occur in long-steep-slope sections, bus stops, high-temperature environments, heavy truck-trafficked areas, intersection with high shear stress gradients, and curves [2,18]. Among HMA, porous friction courses (PFC) exhibit low rutting resistance due to their high air void (AV) content [12,21]. In critical road areas, PFC deteriorates as densification and shear flow to the sides of the wheel path increase [13]. Irregularities in the deformed surface profile affects the ride quality and bring safety concerns due to:

- reduction in pavement surface friction and skid resistance, during wet weather, at the vehicle-pavement interface [22-25].
- deformation-related clogging can cause a significant rutting-induced permeability loss [26,27] diminishing water drainage from the surface. During rainy events, the possibilities of vehicle hydroplaning increases, splash and spray to drivers and pedestrians also increase, and road sign visibility decreases [28-31].
- clogging can also lead to a loss in environmental benefits by increasing road noise pollution [32-35].

Durability of PFC is also affected by raveling, in which the PFC disaggregate after mechanical and chemical processes that can be accelerated by repetitive trafficking accelerated and moisture [36-38]. Despite their weak mineral skeleton, PFC mixes

contributed to the structural capacity of asphalt pavements, reducing fatigue and permanent deformation damage [39,40]. Under coupled conditions of high temperature and rainfall in rainy summer weather, the presence of water in the pores of PFC creates pore pressure, which facilitates moisture damage and consequently decreases the rutting resistance [41].

Apart from laboratory testing and field measurements, X-ray computer tomography (X-ray CT) techniques have been employed to quantify the structure of air voids in HMA [21,42-48]. This technique has already been used to study the movement of aggregates and changes in AV content occurring through rutting accumulations of HMA [21,47]. From the results, it seems that rutting in PFC is primarily influenced by AV densification, which decreases with an increasing depth [21,27].

As seen above, the rutting resistance potential of PFC is still a challenge for the development of an improved mix design with an enhanced field performance [38]. Therefore, this paper presents an experimental investigation on the effect of AV content on the rutting resistance of permeable friction courses (PFC). Three laboratory test methods were comparatively evaluated for quantifying and screening rutting resistance potential of four PFC with different AV contents. These methods are: DM test, FN test, and HWTT. The samples were prepared and compacted considering four air voids (AV) contents: 18%, 20%, 22% and 25%. The corresponding results are presented, and evaluated, to screen the rutting potential of PFC in terms of the AV contents. Additionally, from the HWTT, a comparative analysis was conducted using X-ray CT images obtained before and after the tests in order to investigate AV distribution due to rutting.

### **3.2 Materials characterization and experimental design plan**

This section presents the material characterization, including testing parameters, AV contents, and the preconditioning setup of the PFC samples employed for the laboratory tests (DM, FN, and HWTT). Fig. 3-1 displays the particle size distribution and master gradation limits used herein according to the required PFC-Coarser mix design given by the Texas Department of Transportation (TxDOT) Specification in Item 342 [49]. A combination of two sources of crushed sandstone aggregates obtained from a local quarry

in Texas, United States, were sieved to prepare the PFC-C laboratory samples. The optimum content of 6% of a PG 76-22 polymer-modified binder was used to ensure an adequate film thickness to coat aggregates and a minimum asphalt draindown according to the (TxDOT) Specification in Item 342 [49].

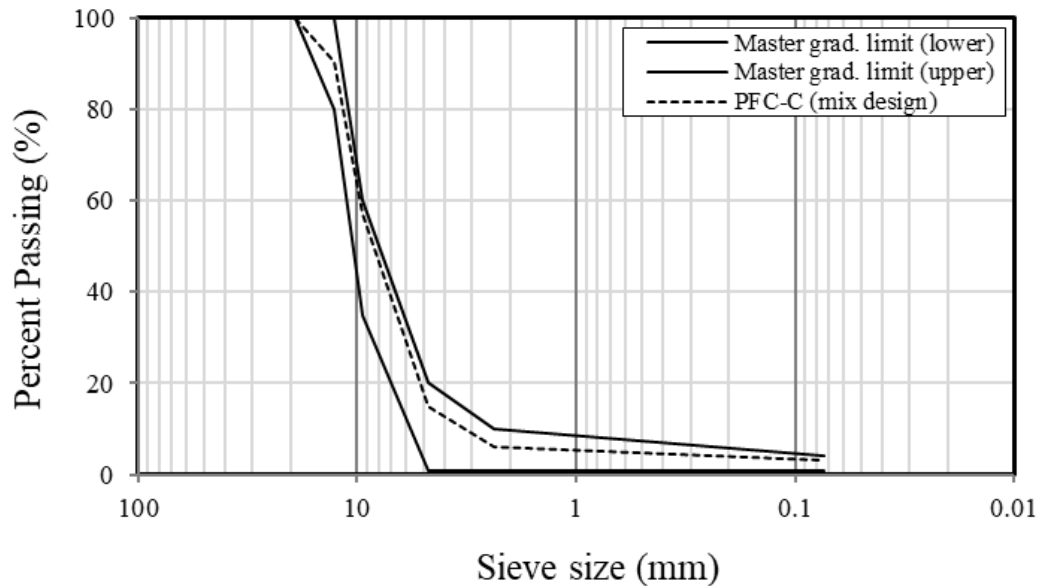


**Fig. 3-1.** Particle size distribution for combination of aggregates for PFC samples.

Table 3-1 presents a list of mixing temperatures by binder grade as described in Tex-205-F [50]. Since a PG 76-22 was used, the corresponding mixing temperature was selected in 163 °C to thoroughly mix the asphalt material and aggregates by means of a mechanical mixer until the materials were completely coated.

Table 3-2 presents the compaction temperatures by type grade. A compaction temperature of 149 °C was selected for a corresponding PG grade mixture, in accordance with the guidelines given in Tex-241-F [51]. Prior to compaction process, PFC samples were placed in oven at the same compaction temperature to characterize for short-term oven aging (STOA) for 2 hr. ± 5 min.

**Table 3-1. Asphaltic material mixing temperature by Grade and Type [50]**

Type Grade	Asphalt Material Temp. (°C)	Mixing Temp. (°C)
PG 70-28, PG 76-22	163	163
PG 64-28, PG 70-22	149	149
PG 64-22, PG 64-16	143	143
AC-3, 5, 10; PG 58-28; PG 58-22	135	135
RC-250	38	74
MC-250	38	74
MC-800	60	88
CMS-2	60	113
AES-300	60	113
Asphalt rubber (A-R) Binder	163	163

**Table 3-2. STOA and Compaction Temperatures by Grade. Adapted from [51].**

Type Grade	Compaction Temp. (°C)
PG 58-28	121
PG 64-22	121
PG 64-28	135
PG 70-22	135
PG 70-28	149
PG 76-22	149
PG 76-28	149
Asphalt rubber (A-R)	149

Once selected mixing and compaction temperatures, cylindrical PFC specimens were fabricated in accordance with AASHTO PP 60 [52], and individually compacted within a superpave gyratory compactor (SGC) to four target compaction densities in the range of  $82 \pm 2\%$  and  $75 \pm 2\%$  (*i.e.* to attain four AV contents: 18%, 20%, 22%, and 25%). Once the PFC samples were removed from the steel molds, they remained on PVC supports at room temperature overnight before testing.



Finally, Table 3-3 presents a summary of experimental design plan used. Volumetric properties, number of replicates and sampling dimensions are also reported in Table 3-3.

**Table 3-3.** Summary of experimental plan to asses rutting in PFC

Test	Height (mm)	Diameter (mm)	Air voids (%)	Replicates	$G_{mm}$	$G_{mb}$
Dynamic modulus	150	100	18	3	2.425	1.976
			20	3		1.919
			22	3		1.897
			25	3		1.824
Flow number	150	100	18	3	2.425	1.976
			20	3		1.919
			22	3		1.897
			25	3		1.824
HWTT	62	150	18	2*	2.425	1.898
			25	2*		1.806

### 3.3 Performance tests of rutting resistance

#### 3.3.1 Dynamic Modulus (DM) tests – Testing protocol

DM tests were conducted following the AASHTO TP-79 Standard [53], using an Asphalt Mixture Performance Tester (AMPT) for the four AV contents. PFC cylindrical samples were cored and trimmed from its original size to approximately 100 mm diameter by 150 mm in height to meet the corresponding testing requirements. Coring and sawing processes reduce the heterogeneity in the internal structure (*e.g.* vertical and horizontal distributions of the AV content, air void size, and connected air void content) [48,54,55].

The DM tests were performed using controlled sinusoidal compressive stress to an unconfined specimen over a range of six loading frequencies: 0.1, 0.5, 1, 5, 10 and 25 Hz, and four temperatures: 6 °C (24h), 20 °C (4h), 25°C (2h) and 45 °C (1h), the numbers within parenthesis correspond to the preconditioning times in hours. Three replicates were tested for each condition, then, a total of 48 tests were performed. DM tests produced

strains smaller than 150 microstrain, thus ensuring that laboratory data measured at these levels attain high precision results.

Fig. 3-2 illustrates the experimental setup for the DM test, after preconditioning the samples, these are placed inside the test cell, and LVDTs are installed using the hexagonal studs previously glued directly to the sample. Then, the upper plate is automatically adjusted to the sample after closing the cell allowing the test to start.

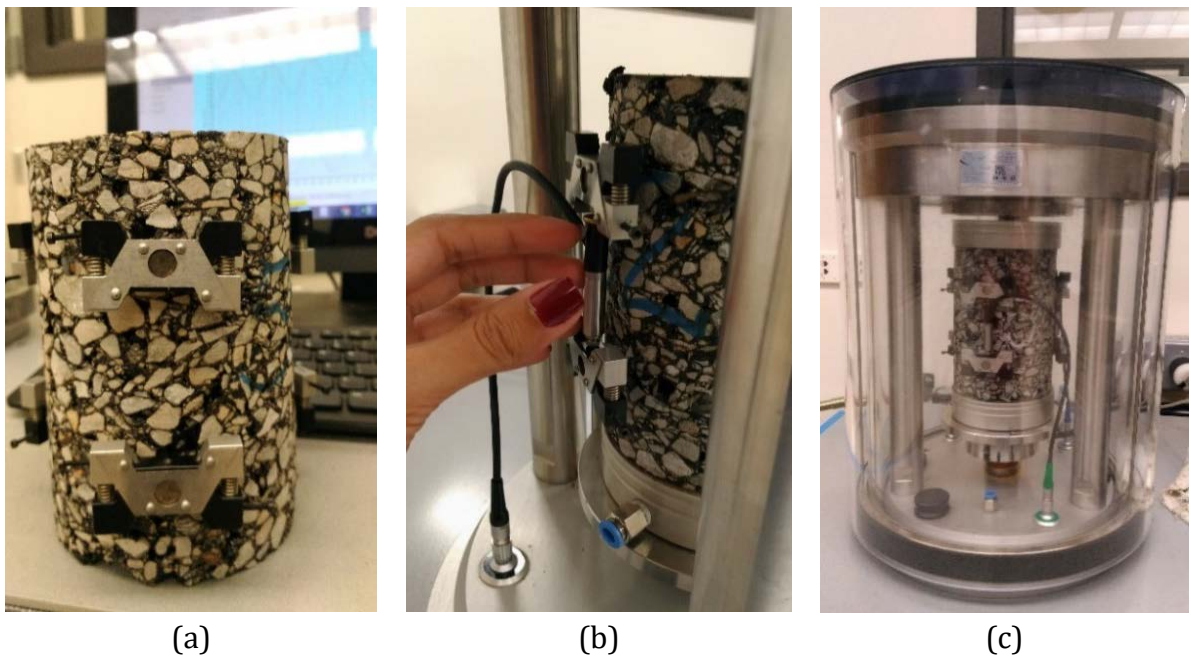


**Fig. 3-2.** DM test setup: (a) Sample preconditioned at test temperature; (b) LVDT fixed to hexagonal studs; and (c) test cell setup at the target temperature

- *Complex modulus*

The complex modulus  $E^*$  is a response developed under sinusoidal dynamic compressive axial load conditions, and represents the stiffness of a viscoelastic material. The real and imaginary portions of the complex modulus are written as

$$E^* = E' + iE'' \quad (3-1)$$

In Eq. (3-1), the first term  $E'$  generally represents the storage modulus, which is the portion of elastic behavior of material, and the second term  $E''$  is referred to as the loss modulus or the viscous behavior of the complex modulus. The phase angle  $\phi$  indicates the

viscous properties of the material being under evaluation. Typically, a viscoelastic material has a phase angle within the range of  $0^\circ$  to  $90^\circ$ . The complex modulus in terms of  $\phi$  is:

$$E^* = E' \cos \phi + iE'' \sin \phi \quad (3-2)$$

The absolute value of the complex modulus  $|E^*|$  corresponds to the dynamic modulus, which is mathematically defined as the maximum dynamic stress  $\sigma_0$  divided by the peak recoverable axial strain  $\varepsilon_0$ , represented in Eq. (3-3):

$$|E^*| = \frac{\sigma_0}{\varepsilon_0} \quad (3-3)$$

- *Master curve characterization*

Fig. 3-3 depicts a typical master curve for an asphalt mixture. The highlighted zones describe two extreme areas after calculating the reduced frequency at a reference temperature (*i.e.* 20 °C).

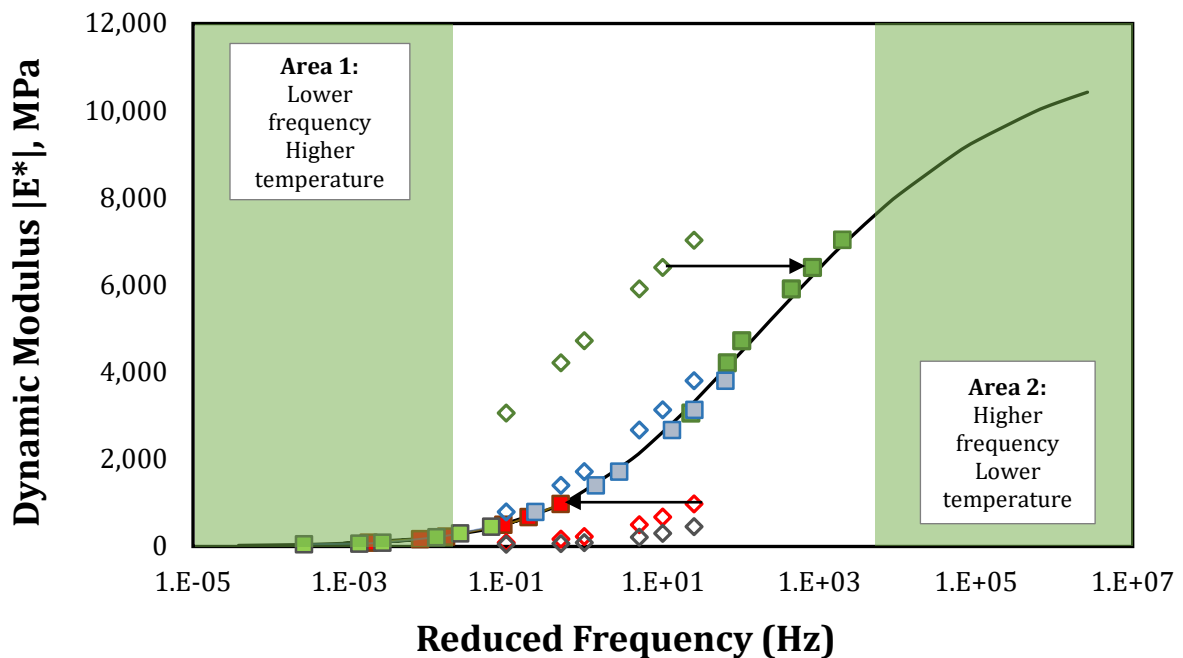


Fig. 3-3. Typical master curve.

Lower dynamic moduli values are obtained in Area 1, characterized by lower loading frequencies and higher temperatures, and higher dynamic moduli values in Area 2 represent higher loading frequencies and lower temperatures. In general, a master curve, as a function of time, can be mathematically represented using a sigmoidal function as follows

$$\text{Log}|E^*| = \delta + \frac{\alpha}{1 + e^{\beta - \gamma \log(F_R)}} \quad (3-4)$$

where  $F_R$  is the reduced frequency at the reference temperature (*i.e.* 20 °C);  $\beta, \gamma$  are parameters describing the shape of the sigmoidal function;  $\delta$  is minimum value of dynamic modulus; and  $\delta + \alpha$  is the maximum value of the dynamic modulus. These parameters are reported in Table 3-4.

**Table 3-4.** Parameters used in sigmoidal function by AV content %

AV, %	Replicate	$\delta$	$\alpha$	$\beta$	$\gamma$
18	1	1.08E-01	4.13E+00	1.13E+00	3.99E-01
	2	3.50E-01	4.01E+00	8.21E-01	4.00E-01
	3	6.66E-01	3.42E+00	9.12E-01	5.10E-01
20	1	-2.84E-01	4.59E+00	1.03E+00	3.53E-01
	2	1.58E-01	3.89E+00	1.11E+00	4.60E-01
	3	3.32E-01	3.81E+00	8.14E-01	4.51E-01
22	1	-1.53E-01	4.44E+00	7.66E-01	3.37E-01
	2	9.14E-01	3.02E+00	8.89E-01	5.70E-01
	3	-2.62E-01	4.43E+00	9.36E-01	3.86E-01
25	1	5.89E-01	3.53E+00	5.33E-01	3.93E-01
	2	8.35E-01	3.20E+00	4.85E-01	4.53E-01
	3	1.09E+00	3.09E+00	3.52E-01	4.24E-01

In Eqs. (3-5) and (3-6), the reduced frequency is computed by merging into a single smooth function, the test loading frequency  $f_t$  multiplied by a shift factor  $a_T$ , which in turn associates the reference temperature with a shift from the test temperature  $T$ . In addition,  $a$ ,  $b$ , and  $c$  are coefficients of the second-order polynomial.

$$F_R = f_t \times a_T \quad (3-5)$$

$$\text{Log } a_T = aT_i^2 + bT_i + c \quad (3-6)$$

### 3.3.2 DM test results

Considering the range of frequencies ( $0.1 \text{ Hz} \leq f \leq 25 \text{ Hz}$ ) and temperatures ( $6 \text{ }^\circ\text{C} \leq T \leq 45 \text{ }^\circ\text{C}$ ) mentioned above, a set of master curves were obtained at the reference temperature  $T_{ref} = 20 \text{ }^\circ\text{C}$  for all tested AV contents, the results are plotted in Fig. 3-4.

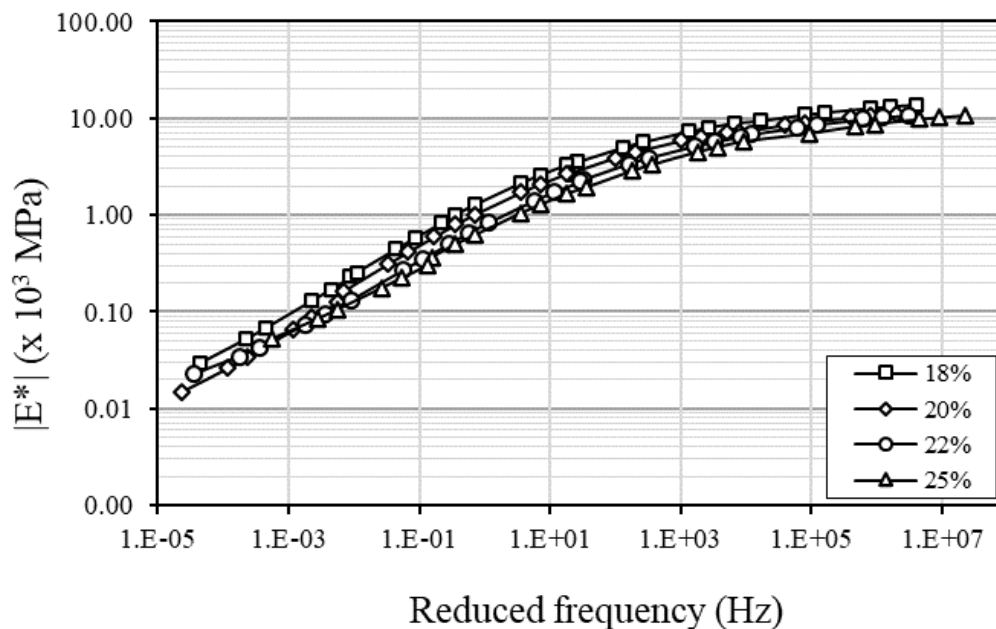


**Fig. 3-4.** Dynamic moduli  $|E^*|$  master curves at  $T_{ref} = 20 \text{ }^\circ\text{C}$ .

From the results plotted in Fig. 3-4, mixtures tested with an AV content of 18% exhibited a higher rutting resistance (the DM magnitude is higher), followed by specimens tested at 20%, 22%. The highest susceptibility to rutting, as expected, was attained for an AV content of 25%. The relationship between the dynamic modulus and the resistance to rutting was conducted by comparing the dynamic modulus observed in master curves for all AV contents at higher temperatures. As a result, in Section 3.4, the rutting potential of

the PFC was screened in terms of AV content, where PFC mixes with 18% AV exhibited the best rutting resistance, and the lowest performance was presented for those with 25% AV content.

As mentioned in the introduction, rutting is a distress mechanism mainly associated with high temperatures (summer), hence DM test results are particularly examined for higher temperatures. Table 3-5 and Fig. 3-5 presents a summary of the DM results for  $T = 37.8\text{ }^{\circ}\text{C}$  and  $54.4\text{ }^{\circ}\text{C}$ . For  $T = 37.8\text{ }^{\circ}\text{C}$ , DM values attained for all AV contents analyzed with frequencies  $f \geq 5\text{ Hz}$  exhibit good repeatability with COV ranging from 4% to 19%. In contrast, for lower frequencies  $f = 0.1\text{ Hz}$  and  $1\text{ Hz}$  the results show a larger variability with COV between 16% and 23%, except for the specimens with 25% AV content. A higher variability in the results is observed for  $T = 54.40\text{ }^{\circ}\text{C}$ , the COV ranged from 20% to 29% for low AV contents (18% and 20%) through all the frequency range. It gets worst for higher AV contents (22% and 25%), in which the COV ranged from 22% to 43%. Some problems related to the inability of the AMPT to remain at the highest test temperature affected the results calculated for  $T = 54.4\text{ }^{\circ}\text{C}$ .

**Table 3-5.** Summary of Dynamic Modulus tests result at  $T = 54.4^{\circ}\text{C}$  and  $T = 37.8^{\circ}\text{C}$ .

AV %	Dynamic Modulus $ E^* $ (MPa)									
	54.4 °C					37.8°C				
	0.1 Hz	1 Hz	5 Hz	10 Hz	25 Hz	0.1 Hz	1 Hz	5 Hz	10 Hz	25 Hz
18	30 (22%)	68 (28%)	129 (29%)	172 (28%)	250 (27%)	91 (23%)	232 (22%)	445 (19%)	584 (17%)	827 (15%)
20	15 (25%)	34 (22%)	65 (20%)	86 (20%)	127 (20%)	61 (22%)	161 (20%)	315 (17%)	418 (15%)	598 (13%)
22	32 (22%)	72 (34%)	132 (39%)	171 (41%)	241 (42%)	62 (21%)	154 (16%)	294 (11%)	386 (10%)	549 (10%)
25	52 (21%)	105 (35%)	178 (41%)	225 (42%)	307 (43%)	80 (6%)	168 (4%)	290 (4%)	367 (5%)	499 (6%)

Note: The values within parenthesis corresponds to the coefficient of variation of 3 replicates.

This observation is more noticeable for the higher AV contents (*i.e.* 22% and 25 %) because of their weaker and more porous mineral skeleton, these specimens were more

likely to exhibit this dispersion while testing at this temperature. Zhang et al. [11] also reported a high variability in the dynamic modulus at high temperatures, which limits the use of DM testing as a screening parameter for rutting potential.

Fig. 3-5 shows the variation of DM in terms of the AV content for various frequencies, for  $T=37.8\text{ }^{\circ}\text{C}$  and frequencies  $f \geq 5\text{ Hz}$  the DM decreases with increasing AV contents. For instance, for  $f = 10\text{ Hz}$  the dynamic modulus decreases 37% from  $|E^*|= 584\text{ MPa}$  (18% AV) to  $|E^*|= 367\text{ MPa}$  (25% AV), the reduction is similar for  $f = 5\text{ Hz}$ , the dynamic modulus decreases 35%. Within the range  $f = 0.1\text{ Hz}$  and  $f = 1\text{ Hz}$  and the AV content varies from 22% to 25% AV, the dynamic modulus increases 29% and 9%, respectively. A different behavior is observed for  $T=54.4\text{ }^{\circ}\text{C}$  throughout the whole range of evaluated frequencies. The dynamic modulus decreases when the AV content goes from 18% and 20%, increasing thereafter for the remaining AV contents. As an example, for  $f = 10\text{ Hz}$  the dynamic modulus decreases 50% from  $|E^*|= 172\text{ MPa}$  (18% AV) to  $|E^*|= 86\text{ MPa}$  (20% AV), after that there is an increase from  $|E^*|= 86\text{ MPa}$  (20% AV) to  $|E^*|= 225\text{ MPa}$  (25% AV), these trends can be clearly observed in Fig. 3-5.

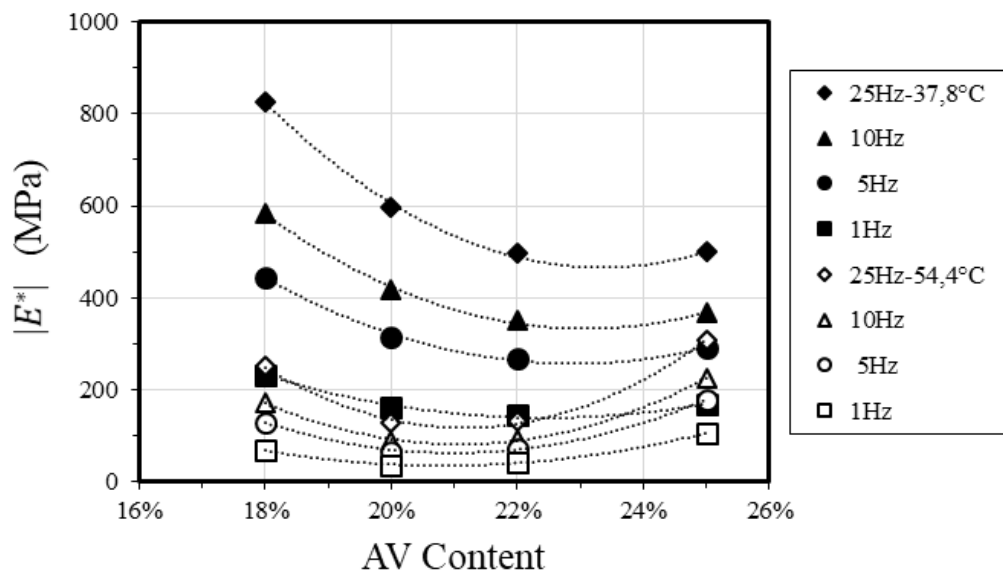


**Fig. 3-5.**  $|E^*|$  in terms of the AV Content, for  $T = 37.8\text{ }^{\circ}\text{C}$  and  $54.4\text{ }^{\circ}\text{C}$  and various frequencies.

Higher values of  $|E^*|$  are expected for lower AV contents (high stiffness mixes), and hence more resistant to rutting. Nevertheless, the results for  $T = 54.4^\circ\text{C}$  exhibit a different trend, for the PFC with 25% AV,  $|E^*|$  values are higher than those for 22% AV. The reliability of these results is compromised by the high variability attained in Table 3-5.

In Fig. 3-5, for a given frequency the largest difference in the dynamic modulus in terms of the temperature was attained for 18% AV, for  $T=37.8^\circ\text{C}$  and  $f = 10\text{Hz}$ ,  $|E^*| = 584\text{ MPa}$ , and for  $T=54.4^\circ\text{C}$  and the same frequency  $|E^*| = 172\text{ MPa}$ , which represents a significant reduction of 70%. In contrast, for 25% AV,  $T=37.8^\circ\text{C}$  and  $f = 10\text{Hz}$ ,  $|E^*| = 367\text{ MPa}$ , and for  $T=54.4^\circ\text{C}$  and the same frequency  $|E^*| = 225\text{ MPa}$ , which represents a reduction of 39%.

Table 3-6 presents the statistical analyses ANOVA and Tukey's HSD for  $|E^*|$  at  $37.8^\circ\text{C}$  (5 Hz). Under these particular conditions of temperature and frequency, the means of the dynamic moduli showed a statistically significant difference through the investigated AV contents determined by one-way ANOVA.

**Table 3-6.** ANOVA and Tukey's HSD test analysis for  $|E^*|$  ( $37.8^\circ\text{C}$ , 5 Hz).

Variables	Sum of Squares	Degrees of freedom	Mean Square	F-value	F critical	Significance
Treatments	56585.67	3	18861.89	7.17	4.07 for $\alpha=0.05$	**
Error	21046.00	8	2630.75			
Total	77631.67	11				
Tukey's HSD						
$\mu_{18} - \mu_{25}$	130.33					*
$\mu_{18} - \mu_{20}$	176.67					**
$\mu_{18} - \mu_{22}$	155.00					**
$\mu_{20} - \mu_{22}$	46.33					
$\mu_{20} - \mu_{25}$	24.67					
$\mu_{22} - \mu_{25}$	21.677					

\*\*Highly significant difference at  $\alpha=0.05$ .

The significance level ( $\alpha$ ) employed in this investigation was 0.05. Since the relationship,  $F\text{-value} = 7.17$  is greater than the critical  $F_{0.05}(3,8)=4.07$ , therefore, the AV



content does have a statistically significant effect on the dynamic module response. For Tukey's HSD, it is established that, the differences between groups of means (*i.e.*  $\mu_{18} - \mu_{25}$ ) larger than  $T_{0.05}(4,8) = 134.15$ , will be declared statistically significant.

According to results from Tukey's HSD reported in Table 3-6, the effect on variation of AV content was highly significant when all pairwise means were compared with the AV content of 18%.

### **3.3.3 Flow Number (FN) test protocol**

The FN test is a repeated load permanent deformation test used to assess the resistance of asphalt mixes to tertiary flow. The FN test is performed following the recommendations given in the NCHRP Project 9-19 [3], in which a haversine compressive load pulse is applied, with a loading time of 0.1 s, followed by a resting time of 0.9 s (Fig. 3-6a), and a deviatoric stress of 206 kPa in PFC samples without confining pressure. As the DM test is non-destructive, the same samples were reused to conduct the FN test. Three replicates were tested for each condition, then, a total of 12 tests were performed. In this study, FN tests were performed at 50 °C (122 °F), this temperature is considered critical during the summer seasons and is consistent with the one used in the HWTT tests.

Fig. 3-6b shows the typical three-stage curve and the flow number (FN) expressed in loading cycles. From this curve, in the primary zone, the permanent deformation accumulates rapidly. The secondary phase gradually outlines as a result of the accumulation of permanent deformation until the PFC reached a constant value. The FN appears as the boundary between the last two stages and is represented as the minimum point on the strain rate curve. Finally, the tertiary stage is characterized by a steeper slope in which the PFC develops a tertiary flow that indicates the onset of shear deformation in asphalt mixtures, which is a significant parameter in the evaluation of resistance to the formation of rutting in the field, as noted by Biligiri *et al.* [56].

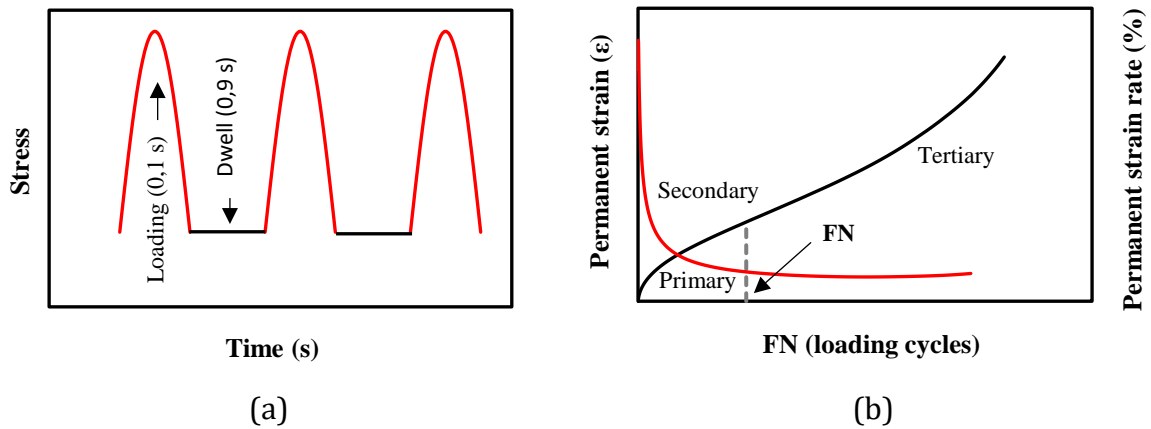


**Fig. 3-6.** FN test protocol: (a) Loading process in FN test, (b) Strain rate versus loading cycles.

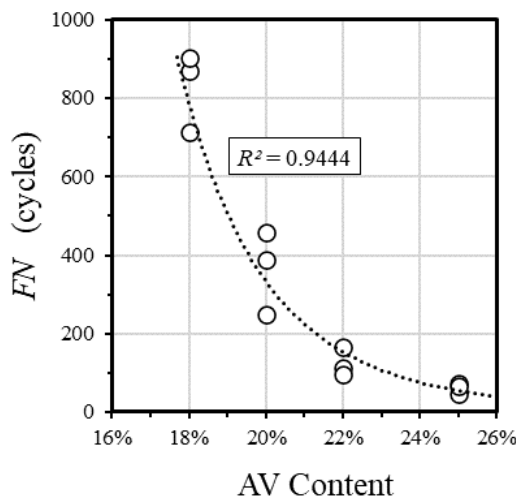
### 3.3.4 FN test results

Table 3-7 presents the results for the FN tests in terms of the AV contents. The measured parameters in this test include: (1) *FN*, in cycles, corresponding to the number of cycles at which tertiary flow begins; (2) accumulated permanent strains at the onset of tertiary flow ( $\epsilon_p(F)$ ), in microns; (3) time to the onset of tertiary flow ( $t(F)$ ), in minutes; and (4) *FN index*, in microns over cycles, defined as the ratio between  $\epsilon_p(F)$  and *FN* [12,16]. Three replicates were tested for each condition, then a total of 12 tests were performed, with an average statistical variability of  $COV = 23\%$  for *FN* (cycles), which are also reported in Table 3-7.

**Table 3-7.** FN test results

Sample ID	FN (cycles)	$\varepsilon_p(F)$	FN index $\varepsilon_p(F)/FN$	t (F) (min)
PFC1801	869	22846	26.29	14.5
PFC1802	715	17179	24.03	11.9
PFC1803	903	11032	12.22	15.1
PFC2001	250	18299	73.20	4.2
PFC2002	389	20362	52.34	6.5
PFC2003	457	15434	33.77	7.6
PFC2201	167	17658	105.74	2.8
PFC2202	114	18958	166.30	1.9
PFC2203	97	18342	189.09	1.6
PFC2501	47	29153	620.28	0.8
PFC2502	72	21470	298.19	1.2
PFC2503	66	16121	244.26	1.1

In Fig. 3-7, the FN is plotted in terms of the AV contents, these results show that the FN decreases significantly with increasing AV contents. On the average, the FN decreases 56% from FN =829 cycles for 18% AV to FN=365 cycles for 20% AV. From 20% AV to 22% AV the decrease is 65%, and from 22% AV to 25% AV decreases 51%. It is also observed that the FN is highly correlated to the AV content with a R-square of 94.44%.



**Fig. 3-7.** FN vs AV Content.

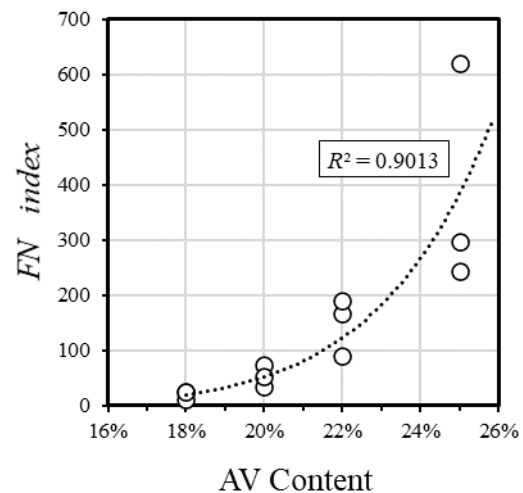


**Fig. 3-8.** FN index vs AV Content

Fig. 3-8 shows the relationship between the *FN index* and the AV content of the samples, it can be observed that the *FN index* increases with the AV content. These two parameters also exhibit a good correlation with a R-square of 90.13%. A large variation is observed for 22% and 25% AV contents. As seen in Table 3-7, accumulated permanent strain  $\epsilon_p(F)$  exhibit a large difference for these two AV contents.

In Fig. 3-9, it is observed that *FN index* and the time to the onset of tertiary flow  $t(F)$  are highly correlated with a R-square of 96.65%. It is clearly observed that for a high AV contents the *FN index* asymptotically increases, hence the large difference attained in the calculated *FN indexes* for 25% AV, which varied from 244.26 to 620.28. For low AV contents, the variability in the measured *FN index* is smaller, for 18% AV the *FN index* varied from 12.22 to 26.29, a large variation in the  $t(F)$  slightly affect the measured *FN index*. In contrast, for increasing AV contents, the variation in  $t(F)$  considerably affects the *FN index*. As pointed out in [12], and from the results presented in Table 3-7 and plotted in Fig. 3-9, it can be noted that the parameters *FN*,  $t(F)$ , and *FN index* are highly correlated. That is, the higher the values of *FN* and  $t(F)$  in magnitude, the lower the value of the *FN index* and vice versa. Lower values of *FN index* evidence a higher rutting resistance for the tested mixes.

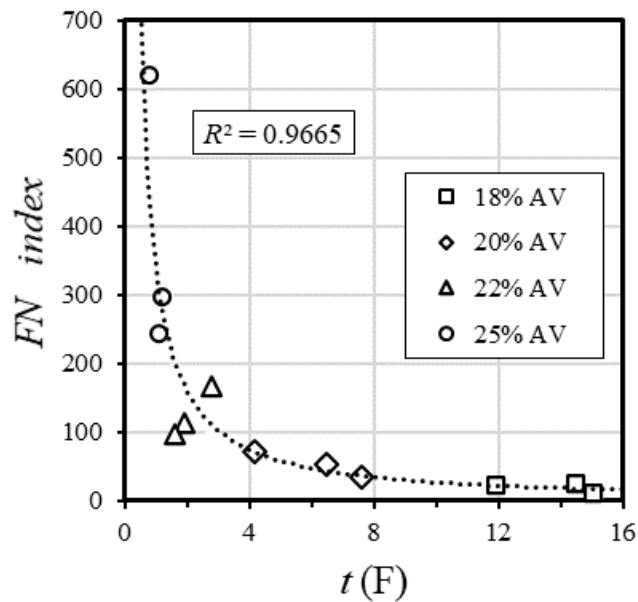


**Fig. 3-9.** *FN index* vs  $t(F)$  for various AV contents.

Regarding the FN results, Table 3-8 presents the statistical analyses ANOVA and Tukey's HSD. Separately, ANOVA for *FN* and *FN index* were analyzed. Results of these analyses revealed statistically significant differences for *FN*. In this case, since  $F$ -value = 64.03 is greater than  $F_{0.05}(3,8) = 4.07$  that represents a significant change in the response of *FN* when varying the AV content. For Tukey's HSD, since  $T_{0.05}(4,8) = 196.96$ , hence, there is a substantial effect on the *FN* response for those pairwise means of AV contents (*i.e.*  $\mu_{18} - \mu_{25}$ ) whose difference is greater than 196.90. It is worth noticing that significant differences were reported for all results pairwise compared for the *FN* test when varying the AV content.

**Table 3-8.** ANOVA and Tukey's HSD test analysis for FN (50 °C).

Variables	Sum of Squares	Degrees of freedom	Mean Square	$F$ -value	$F$ critical	Significance
Treatments	1088721.67	3	362907.22	64.03	4.07 for $\alpha=0.05$	**
Error	45343.33	8	5667.92			
Total	1134065.00	11				
<b>Tukey's HSD</b>						
$\mu_{18} - \mu_{25}$	463.67					*
$\mu_{18} - \mu_{20}$	703.00					**
$\mu_{18} - \mu_{22}$	767.33					**
$\mu_{20} - \mu_{22}$	239.33					*
$\mu_{20} - \mu_{25}$	303.67					**
$\mu_{22} - \mu_{25}$	64.33					

\*\*Highly significant difference at  $\alpha=0.05$ .

### 3.3.5 Hamburg wheel-tracking test (HWTT) – Testing setup

The test procedure to conduct HWTT is outlined in Tex-242-F specification [57]. The device is operated by repeatedly rolling a  $705 \text{ N} \pm 4.5 \text{ N}$ -steel wheel over HMA samples (Fig. 3-10) until reaching 12.5 mm rut depth or 20000 passes based on the PG 76-22 asphalt binder used [57], whichever occurs first. From the DM and FN results previously reported, HWTT tests were only performed using the two extreme AV contents evaluated

herein (*i.e.* 18% AV and 25% AV), the responses to rutting for 20% and 22% AV contents were considered to fall within this range. Eight replicate sets comprised of two 62 mm thick samples each, were tested under environmentally controlled conditions, dry tests (*D*) were performed at  $T=20\text{ }^{\circ}\text{C}$  (dry-empty water bath), and wet tests (*W*) were conducted at  $T=50\text{ }^{\circ}\text{C}$  (heated water bath). Replicate sets were labeled according to their corresponding AV content and moisture condition, for instance sample PFC18D01 has 18% AV and was tested under dry condition.

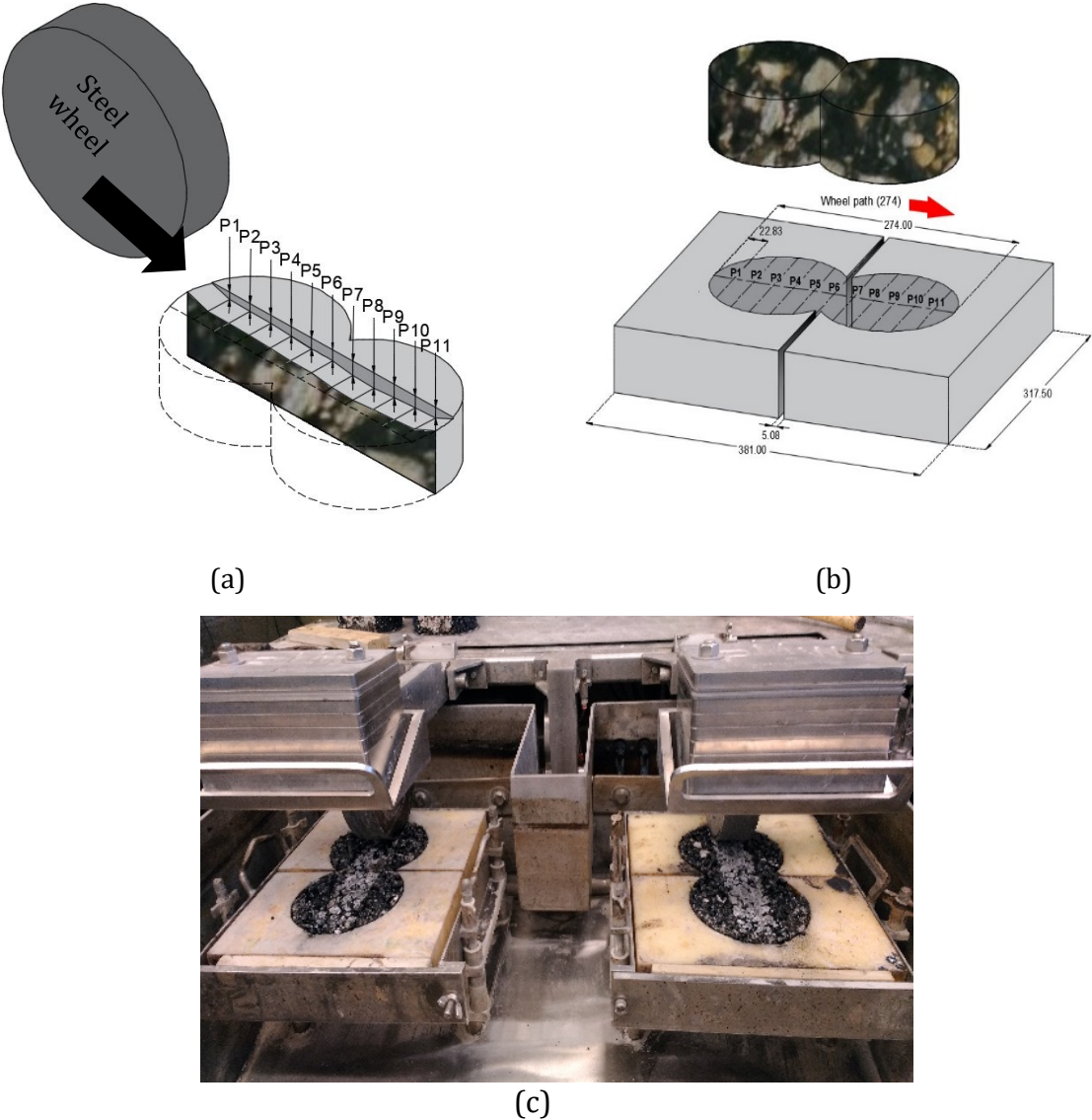


**Fig. 3-10.** (a) Schematic view with the wheel-tracking path; (b) sample-mold fitting and locations for 11 rut-measurements, units in [mm]; and (c) paired samples setup.

### 3.3.6 HWTT results

Table 3-9 shows the results for the HWTT, the rut depth  $R_D$  is computed as the average of six points along the wheel-track. Fig. 3-11 and Fig. 3-12 show the results for the HWTT under dry and wet conditions. Under dry conditions (Fig. 3-11), both PFC exhibit similar behaviors after 20000 passes, for 18% AV the average rut depth for the two replicate sets was  $R_D = 2.68$  mm, and for 25% AV there is slight increase of 23% on this average to  $R_D = 3.32$  mm.

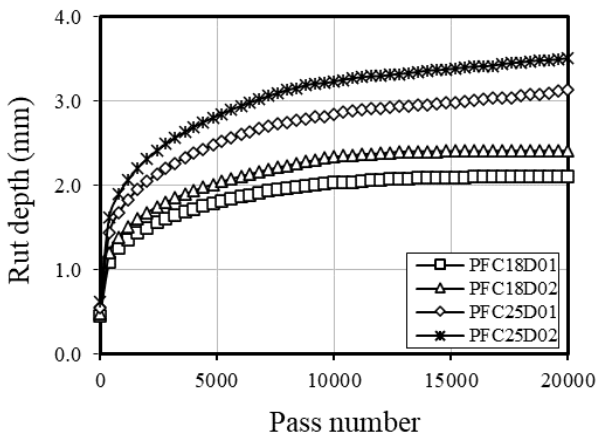


**Fig. 3-11.** Rut depth vs Pass number for HWTT ( $T= 20^\circ\text{C}$ ).

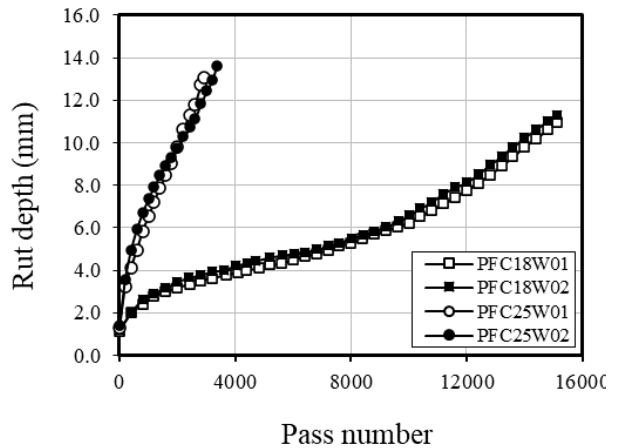


**Fig. 3-12.** Rut depth vs Pass number for HWTT ( $T= 50^\circ\text{C}$ ).

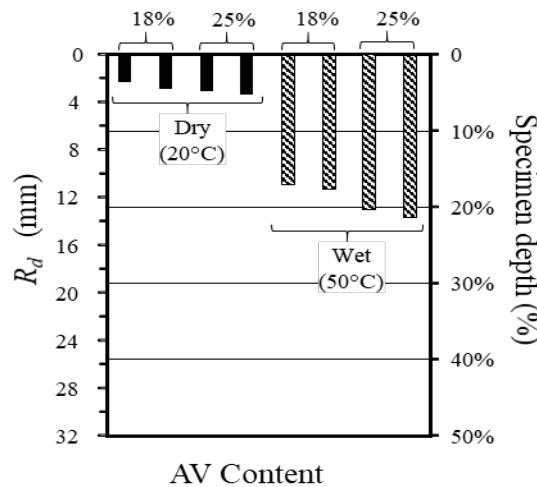


**Fig. 3-13.**  $R_d$  vs AV content.

On the other hand, Fig. 3-12 shows the results obtained under wet conditions, for 18% AV the samples attained a higher number of passes to failure ( $NP_F=15112$  passes) compare to samples with 25% AV ( $NP_F=3127$  passes). Despite the difference in  $NP_F$ , the rut depths are similar,  $R_D=11.16$  mm for 18% AV and  $R_D=13.36$  mm for 25% AV (Fig. 3-13).

In Table 3-9, the rutting depth  $R_D$  was presented as percentage of the sample depth (*i.e.* 62 mm), these results are also plotted in Fig. 3-13. For samples with 25% AV tested under wet conditions, on the average, the rutting depth reaches one-fifth of the depth (21.2%) at a low number of passes (3127 passes).

**Table 3-9.** HWTT test results.

Sample ID	AV (%)	$R_d$ (mm)	$NP_F$	Rutting (%)	$SF$	$\phi_R$ ( $\times 10^{-3}$ )
PFC18D01	18±3	2.41	20000	3.8	1.58	0.11
PFC18D02		2.94	20000	4.7	1.47	0.12
PFC18W01		10.99	15112	17.4	0.99	0.73
PFC18W02		11.32	15112	18.0	0.99	0.75
PFC25D01	25±3	3.13	20000	5.0	1.71	0.16
PFC25D02		3.50	20000	5.6	1.73	0.18
PFC25W01		13.06	2904	20.7	1.22	4.50
PFC25W02		13.65	3350	21.7	1.40	4.07

Fig. 3-14 presents a view of the rut depth measured for specimens tested under dry and wet conditions, respectively. The flat face, which is the part in contact between paired samples is also shown.



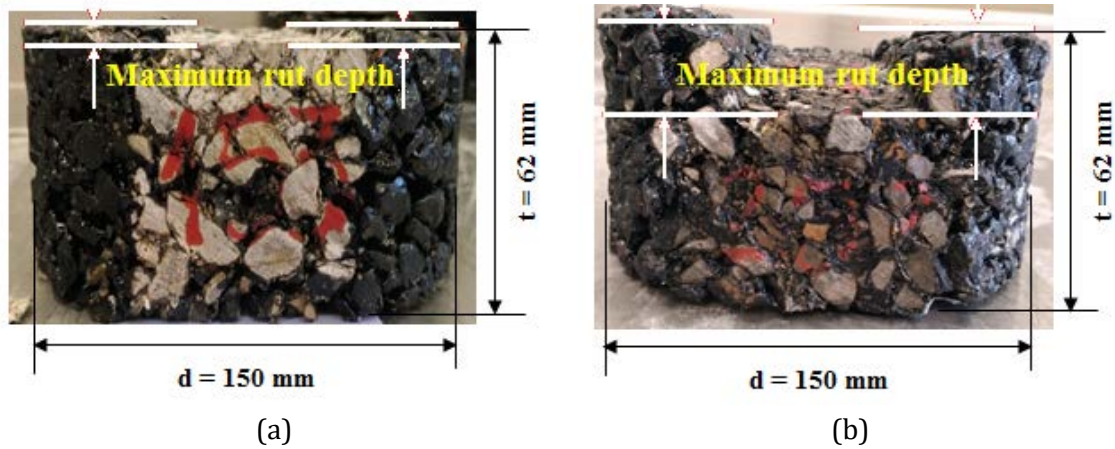


**Fig. 3-14.** Rut depth measured in PFC samples. (a) HWTT-dry. (b) HWTT-wet

Another parameter that can be used to discriminate/screen the rutting potential of the PFC is the shape factor  $SF$  [20], which is defined as the ratio between the area beneath the rutting curve and an equivalent triangular area as follows:

$$SF = \frac{\text{Area under rutting curve}}{\text{Equivalent triangular area}} = \frac{\Delta_A}{(NP_F \cdot R_D)/2} \quad (3-1)$$

The results for  $SF$  calculated with Eq. (3-1) are also reported in Table 3-9. From the analysis of calculated shape factors, it is difficult to determine in an accurate manner the potential to rutting of the evaluated PFC mixes. Walubita *et al.* [10] indicated that a  $SF < 1.00$  is theoretically desirable for high temperature and shear-stress locations, and urban stop-go sections in terms of early-life rutting propensity of surface HMA mixes. In Table 3-9, only the PFC with 18% AV, tested under wet conditions, barely satisfy this screening criterion with a  $SF = 0.99$ . A more suitable parameter to screen the performance of the PFC in the HWTT is the ratio  $\phi_R$  between the rut depth and the number of passes to failures ( $\phi_R = R_D/NP_F$ ). A large  $\phi_R$  indicates a poor response against rutting, in this regard the samples with 25% AV and tested under wet conditions attained the highest  $\phi_R$ .

Summing up, under dry conditions, the resistance of the PFC to rutting can be evaluated separately from moisture effects, for samples tested with 25% AV the suitable

accommodation of aggregates and the driven densification occurred faster than for other samples due to the high AV content. Once again, samples with 25% AV exhibited the worst behavior to withstand permanent deformation (Fig. 3-12) in the presence of water and thus, are more susceptible to rutting/shear failure, due to particles easier to roll over each other when loading is applied [58,59]. Their higher content of air voids, capable to hold more water, are likely to develop an excessive pore pressure allowing PFC mixture to grow the tertiary damage, which subsequently breaks the adhesive bond, between binder and aggregates.

### **3.4 Comparison of the laboratory test methods**

In the previous sections, the rutting potential of PFC was investigated through DM tests, FN tests, and HWTT. As seen in the results, the AV content has a strong influence on the individual responses, nevertheless it is necessary to analyze how all these the parameters are correlated. Table 3-10 presents a comparison between the dynamic modulus  $|E^*|$  (measured at  $T=37.8^\circ\text{C}$  and three frequencies: 5, 10 and 25 Hz), the  $FN$ , the  $FN$  index, and  $\phi_R$  obtained from the HWTT conducted under wet conditions. The ability of these parameters to screen and discriminate the studied PFC mixes can be comparatively evaluated using a discriminatory ratio  $DR$  [12].

This  $DR$  is defined as an arithmetic ratio of two corresponding parametric values comparing a good material (numerator) with a relatively poor of reference material (denominator). As seen in Table 3-10, among all the evaluated parameters the PFC with 18% AV, with the lowest AV content, is consistently identified as the best mix, while the PFC with 25% AV exhibits the poorest performance. It is important to keep in mind that for the  $FN$  index and the ratio  $\phi_R$ , where lower values are indicative of better materials, the  $DR$  was inverted.

**Table 3-10.** Comparison of test results:  $|E^*|$  (37.8 °C),  $FN$ ,  $FN$  index and  $\phi_R$ .

AV %	DM test			FN test		$\phi_R$ ( $\times 10^{-3}$ )
	$ E^* _{37.8^\circ\text{C}.5\text{ Hz}}$	$ E^* _{37.8^\circ\text{C}.10\text{H}}$	$ E^* _{37.8^\circ\text{C}.25\text{Hz}}$	$FN$ (cycles)	$FN$ index	
18	445	584	827	829	20.84	0.74
20	315	416	596	365	53.10	-
22	268	350	496	126	148.29	-
25	290	367	499	62	271.22	4.28
Discrimination Ratios ( $DR$ )						
18 / 25	1.53	1.59	1.66	13.37	13.01	5.78
18 / 20	1.41	1.40	1.39	2.27	2.55	-
18 / 22	1.66	1.67	1.67	6.58	7.12	-
25 / 20	0.92	0.88	0.84	0.17	0.20	-
25 / 22	1.08	1.05	1.01	0.49	0.55	-
22 / 20	0.85	0.84	0.83	0.35	0.36	-
PFC screening-AV Content (%)						
1	18	18	18	18	18	18
2	20	20	20	20	20	-
3	22	25	25	22	22	-
4	25	22	22	25	25	25

In Fig. 3-15, the results reported in Table 3-10 for the dynamic modulus  $|E^*|$  at 37.8 °C and the flow number  $FN$  at 50 °C were normalized for all AV contents with their corresponding values for 18% AV, identified as the PFC with the best rutting potential. Within the range of frequencies analyzed, the ratios  $|E^*|/|E^*|_{18\%}$  and  $FN/FN_{18\%}$  are highly correlated to the AV contents with  $R^2 > 93\%$ . Both parameters are severely affected by the increase in AV contents, the flow number the reduction is approximately 90%, and for the dynamic modulus de reduction is close to 40%.

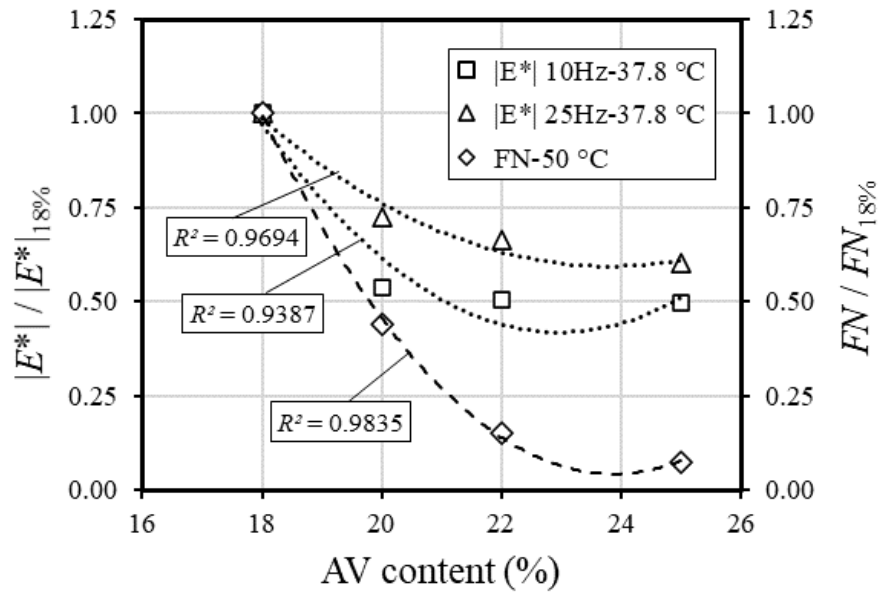


**Fig. 3-15.** Correlation between FN and  $|E^*|$  for  $T=37.8^\circ\text{C}$ .

Comparing laboratory results to field measurements, Walubita et al. [12] proposed the following laboratory pass-fail screening criteria against HMA rutting (excluding PFC mixes) for DM, FN and HWTT tests:  $|E^*| \geq 241$  MPa at  $54.4^\circ\text{C}$  and 5 Hz;  $FN$  index  $\leq 10$  at  $50^\circ\text{C}$ ; and  $R_D \leq 12.5$ mm.

The corresponding values reported in Table 3-5 (Section 3.3.2), Table 3-9 (Section 3.3.5) and Table 3-10 lie mostly outside these criteria. A high variability was observed in the results obtained for DM and FN tests at high temperatures ( $T \geq 50^\circ\text{C}$ ), particularly the DM test method was unable to capture appropriately the mix behavior at  $54.4^\circ\text{C}$  for high AV contents in accordance to limitations described in Table 3-11. It can be attributed to a lack of confinement for the high porous PFC analyzed herein, and during testing it was a challenge to maintain the LVDT studs at high temperatures. Hence, these tests should be performed in a confined mode for comparative purposes.

**Table 3-11.** Limitations and challenges from FN and DM tests. Adapted from [11]

Test	Advantages and applications	Limitations and challenges
FN	<ul style="list-style-type: none"> <li>-Reasonable test time (<math>\leq 3</math> h)</li> <li>-Multiple output data, including FN, <math>\epsilon_p(F)</math>, and <math>t(F)</math>, and FN index.</li> <li>-Reliable FN index to evaluate rutting-resistance response of mixes</li> </ul>	<ul style="list-style-type: none"> <li>-Sample fabrication process is both laborious and long</li> <li>-Cannot readily test field cores</li> <li>-High variability at high test temperatures</li> <li>-Problematic maintaining LVDT studs at high temperatures</li> <li>-Requires experienced operator</li> <li>-Requires UTM equipment</li> </ul>
DM	<ul style="list-style-type: none"> <li>-Rutting performance prediction, especially based on <math> E^* </math> values at 37.8 °C and 54.4 °C</li> <li>-Generation of HMA material properties for pavement structural design, mechanistic-empirical (M-E) models, and performance prediction</li> </ul>	<ul style="list-style-type: none"> <li>-Specimen fabrication process is laborious and long</li> <li>-Cannot readily test field cores</li> <li>-Lengthy test time (minimum 3 days)</li> <li>-High variability at high test temperatures</li> <li>-Problematic getting the temperature to below 0 °C (-10 °C)</li> <li>-Requires experienced operator</li> <li>-Requires UTM or MTS equipment</li> <li>-Not ideal for daily routine mix-design and screening</li> <li>-Needs to be conducted at multiple temperatures</li> </ul>

## 3.5 Comparative analysis using X-ray computer tomography

### 3.5.1 Experimental program

As seen in Fig. 3-11 and Fig. 3-12, HWTT exhibit consistently repeatable test results. In order to scan similar samples for 18% and 25%AV contents, two additional specimens were fabricated from the same batch of the mixture in the laboratory. In addition, two tested specimens in Section 3.3 were chosen, one for each AV content. Then, four cylindrical samples (50 mm in diameter) were cored from the center of those specimens,

as seen in Fig. 3-16, exactly where the deepest rut occurred. Subsequently, these cylindrical samples were scanned before and after conducting HWTT using a ZEISS Xradia 520 Versa 3D X-ray microscope that provided a 160 kV X-ray source.



**Fig. 3-16.** Location of 50mm diameter cores from HWTT samples.

### **3.5.2 Stepwise procedure for X-Ray CT image data acquisition**

An analysis of the internal structure of PFC samples obtained from X-ray CT images was performed through three basic sequential steps, acquisition, processing, and analysis [60], and described briefly as follows. The preliminary step concerns the image acquisition by scanning samples individually. The 160 kV X-ray power source emitted pulses that passed through the PFC sample, then images were taken and amplified on a scintillator and finally detected. During the second phase, the images were reconstructed. Since coarse aggregates have a greater density, a higher number of X-rays can be absorbed, and thus appeared as clearer objects on 2D images. The image processing also covered steps such as smoothing, denoising, and segmentation using the specialized software Materialise Mimics [61]. Finally, in the analysis stage, the segmentation step led to the generation of 3D masks for air voids, mastic, and coarse aggregates with an appropriate grayscale threshold. Fig. 3-17 displays the grayscale ranges which were applied for the domains as follows: 101-150 (for mastic), 151-255 (for coarse aggregates), and 1-100 (for air voids).

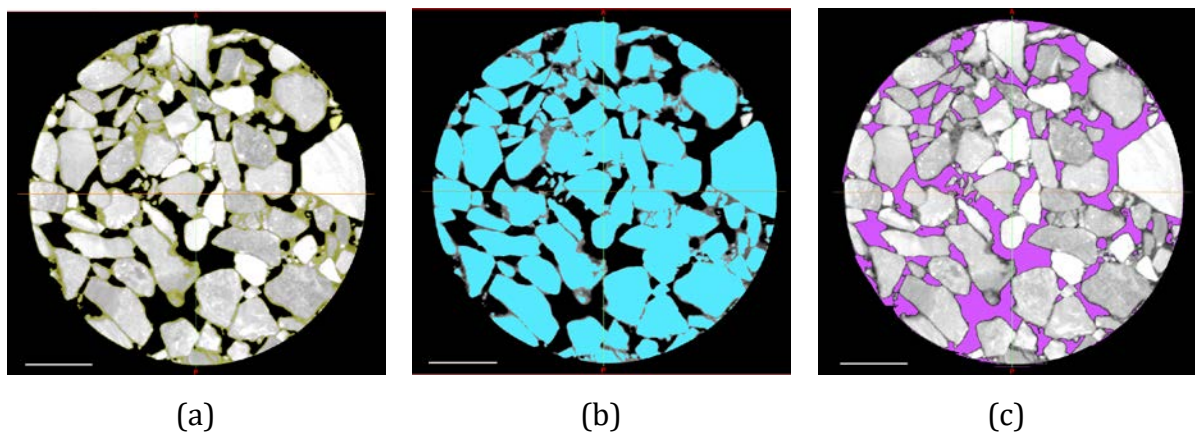


**Fig. 3-17.** Grayscale ranges for 3D masks. (a) mastic (b) coarse aggregates (c) air voids

### 3.5.3 AV distribution profiles measured by X-ray CT imaging

Fig. 3-18 to Fig. 3-21 present the 3D masks generated for the PFC internal structure components: air voids, mastic, and coarse aggregates. AV distributions which were computed from the scan data processed before (red line) and after (blue line) performing the HWTT are also illustrated. The multi-colored AV mask is intended to show various 5mm thick slices generated to compute volumes of voids and its distribution through the sample thickness. In the AV distribution plots, the X-axis represents the variation (%) in AV content, and the Y-axis represents the thickness (mm) of the analyzed samples.

The purple line indicates the  $R_d$  presented in Table 3-9, and the straight black lines represent the theoretical AV content. PFC cores of 25mm cross-section were virtually obtained in order to attain accurate volumetric measurements of the segmented masks. Therefore, the internal structure of the PFC is quantified in terms of the AV characteristics (distribution, areas, and volumes of voids) and coarse aggregates.

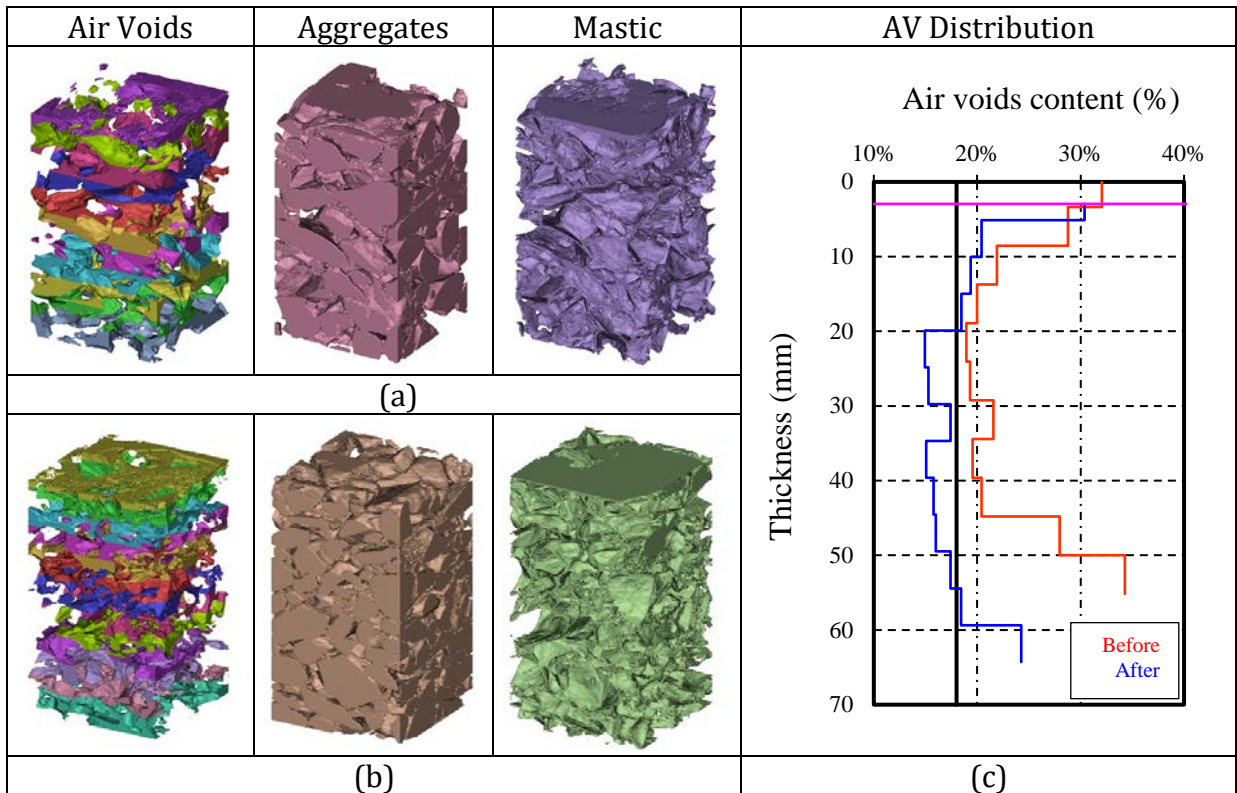


**Fig. 3-18.** 3D Masks from X-ray CT images for 18% AV, HWTT under dry conditions (air voids-aggregates-mastic): (a) before testing; (b) after testing; (c) AV distribution.

### 3.5.4 Scanned samples after performing HWTT - dry

Fig. 3-18 and Fig. 3-19 depict 3D reconstructed masks for PFC samples before and after conducting the HWTT in dry condition. For an AV content of 18% (Fig. 3-18c), the voids are grouped in a C-shaped pattern (red line) where the top and bottom of the samples have a higher AV content compared to their average through the thickness. This AV profile shows close agreement with the results presented in [44,46], where the AV distributions for the PFC mixes were similar. In particular, a 10% reduction in AV content was achieved in the first 10 mm from the developed rut level. Similarly, for samples with a 25% AV content (Fig. 3-19c), air voids are distributed throughout the thickness and gradually decreased to reach approximately one-third of the thickness. In this case, a slight reduction in the AV content before and after the HWTT is observed.



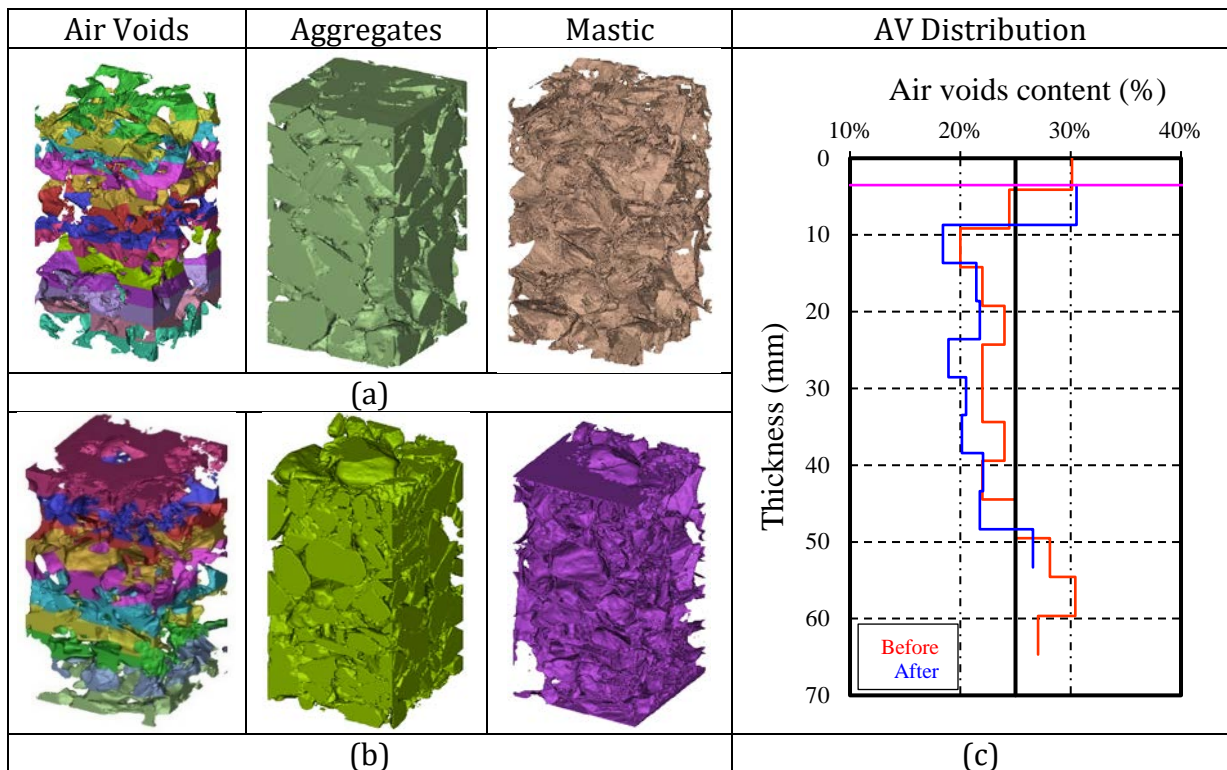


**Fig. 3-19.** 3D Masks from X-ray CT images for 25% AV, HWTT under dry conditions (air voids-aggregates-mastic): (a) before testing; (b) after testing; (c) AV distribution.

### 3.5.5 Scanned samples after performing HWTT - wet

An interesting behavior is observed for scanned samples after performing HWTT in wet conditions. Similar to the dry condition profile, the higher AV content remains above and below the rutted surface by the Hamburg wheel, but in this case, the influence of warm water at  $T = 50\text{ }^{\circ}\text{C}$  accelerated the damage in samples with 18% AV (Fig. 3-20c), and even more for 25% AV (Fig. 3-21c), which increases the air voids content (blue line), and when the wheel pressure is no longer effective to cause higher densification in PFC samples, the AV distribution decreased until aligning to the theoretical AV content.

These AV distribution profiles lead to inferring that there is hidden damage that progresses even below the rut, where the greater AV content (above 30%) observed Fig. 3-20c and Fig. 3-21c, allows the PFC layer to hold more water and is likely to exhibit other distress, such as stripping or raveling due to the binder oxidation rate occurs faster.

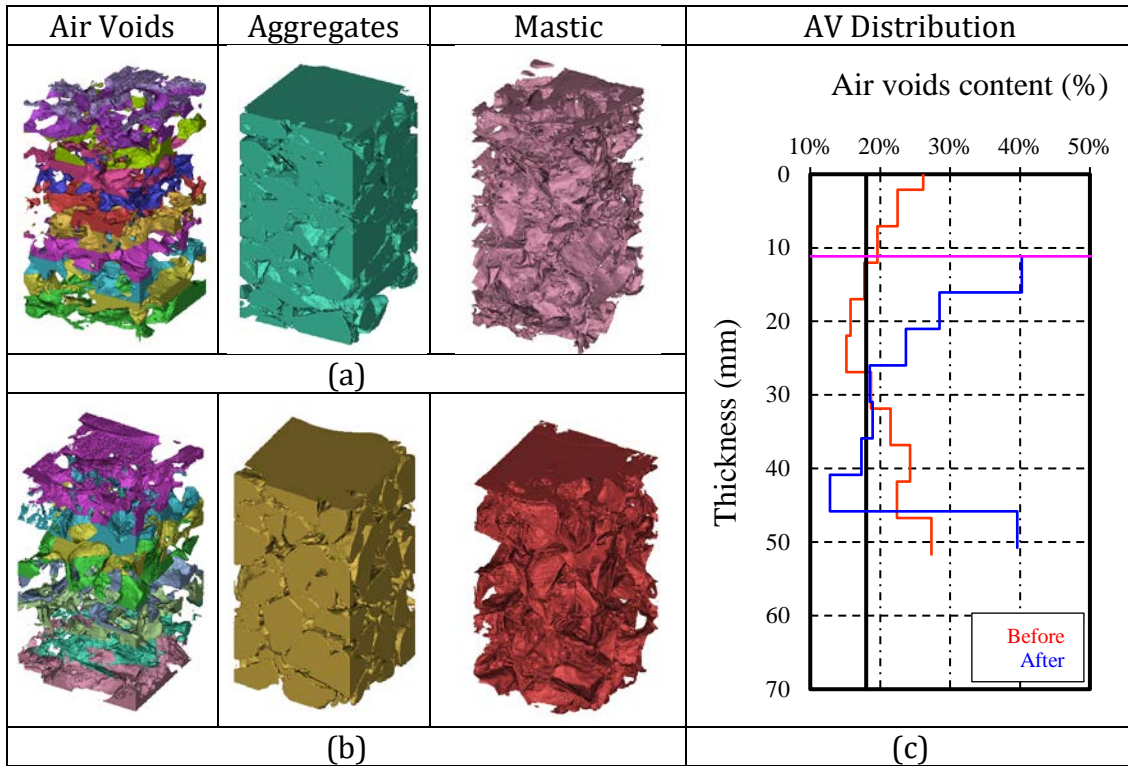


**Fig. 3-20.** 3D Masks from X-ray CT images for 25% AV, HWTT under wet conditions (air voids-aggregates-mastic): (a) before testing; (b) after testing; (c) AV distribution.

HWTT typically assess the rutting resistance in moisture conditions. However, especially for these PFC mixtures, the quantitative consideration in terms of rut depth seemed to be limited regarding the pattern displayed for AV distributions in Fig. 3-20c and Fig. 3-21c. In conclusion, further tests are required for PFC samples withstanding HWTT loading since these may exhibit additional damage once the rut is developed.

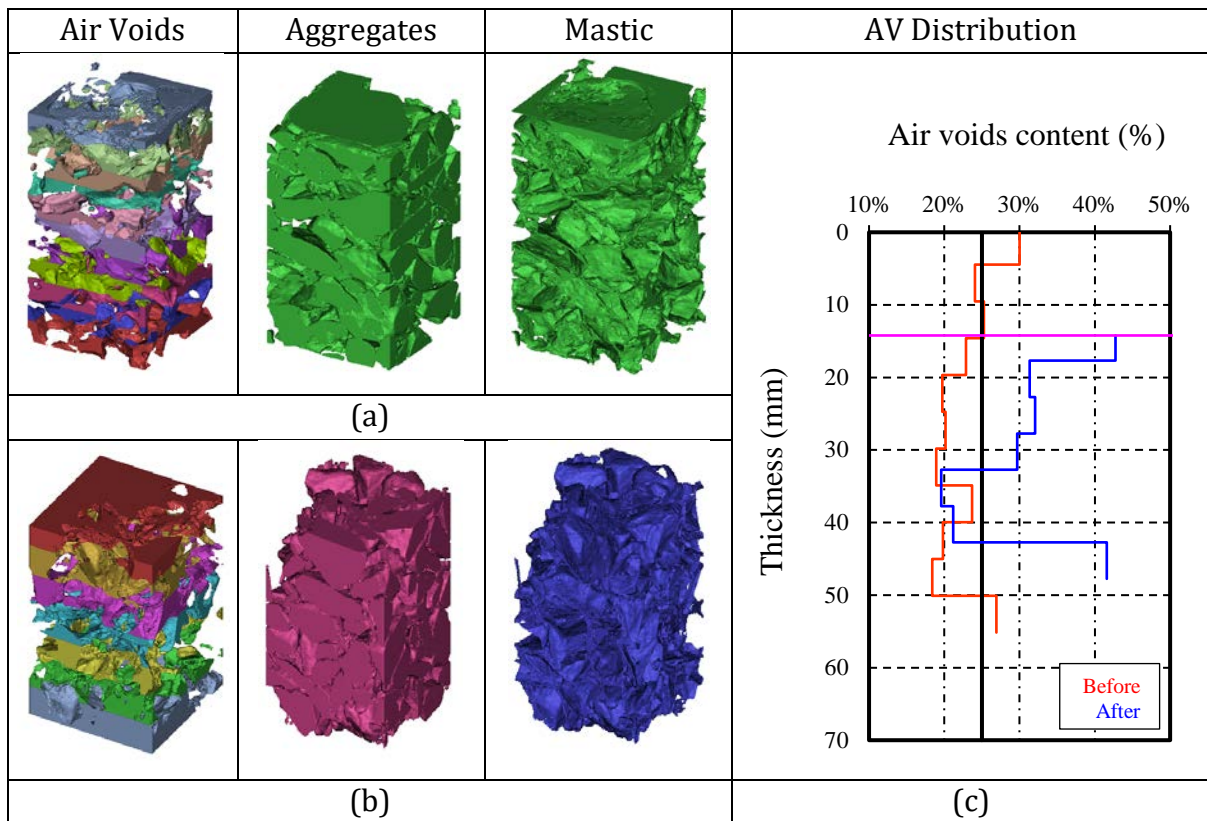


**Fig. 3-21.** 3D Masks from X-ray CT images for 25% AV, HWTT under wet conditions (air voids-aggregates-mastic): (a) before testing; (b) after testing; (c) AV distribution.

### 3.6 Summary and conclusions

An experimental investigation on the rutting resistance of PFC was conducted herein. The rutting potential of PFC was investigated by means of three laboratory tests: DM test, FN test, and HWTT. Additionally, an image-based analysis was performed using X-ray computed tomography (X-ray CT) obtained before and after HWTT. In spite of the simplicity of the experimental plan, the influence of the AV content on the dynamic modulus, flow number, and rutting depth was deeply analyzed.

In PFC, the AV content severely affects the dynamic modulus  $|E^*|$ , flow number  $FN$  ( $FN$  index), and rutting depth  $R_d$  as predictors for rutting potential of PFC. With higher AV content,  $|E^*|$  and  $FN$  values significantly decrease, whereas the developed rut is deeper. In

consequence, PFC with lower AV contents exhibited a higher resistance to rutting. From the results, it was found that for PFC mixes with AV contents between 18% and 22% can exhibit an adequate rutting resistance. The conducted multiple comparison tests by Tukey's HSD revealed a highly significant difference in the response of  $FN$  and  $|E^*|$  when the AV content is varied.

The non-destructive X-ray CT technique was adequate to explore the internal distribution of air voids in PFC mixtures. Differences were clearly identified when the scanned samples underwent the HWTT tests under dry and wet conditions. A higher percentage of air voids (above 30%) was observed for samples analyzed under wet conditions beneath the rut developed. In field conditions, these observations may be extrapolated primarily whether the PFC is in the early-ages of service, the mixture temperature rises above 50 °C and it is poorly compacted (higher AV content). Simultaneous scenarios of overloads and vehicular slow- speeds can also contribute PFC to exhibit deeper ruts, whose damage (greater AV distribution) would extend to approximately the sample's half-thickness.

Further research is required to include the influence of the gradation, binder type, layer thickness, stone-on-stone stiffness, and asphalt content on the rutting resistance of PFC mixtures. It is recommended that DM and FN tests for high porous PFC should be performed in a confined mode. Finally, comparative analysis between laboratory test results and field performance correlating the rutting resistance of PFC mixes should be conducted in order to establish improved screening criteria in terms of the allowed range for AV contents.

## References

- [1] C.L. Monismith, Analytically based asphalt pavement design and rehabilitation: theory to practice, 1962-1992, *J. Transp. Res. Rec.* 1354 (1992) 5–26.
- [2] G. Zou, J. Xu, C. Wu, Evaluation of factors that affect rutting resistance of asphalt mixes by orthogonal experiment design. *Int. J. Pavement Res. Technol.* 10 (3) (2017) 282–288.
- [3] M.W. Witczak, Simple performance tests: summary of recommended methods and database. NCHRP, Project 9-19 Report No. 547, 2006.
- [4] K.E. Kaloush, Simple performance test for permanent deformation evaluation of asphalt mixtures. PhD. Dissertation, Arizona State University, Tempe, Arizona, May 2001.
- [5] A. Bhasin, J.W. Button, A. Chowdhury, Evaluation of simple performance tests on HMA mixtures from the South-Central United States, Report No. FHWA/TX-03/9-558-1, Texas Transportation Institute, 2003.
- [6] A. Apeageyi, Rutting as a function of dynamic modulus and gradation, *J. Mater. Civil Eng.* 23 (9) (2011) 1302–1310.
- [7] R. Bonaquist, Evaluation of Flow Number (FN) as a discriminating HMA mixture property, Technical Report No. WHRP 12-01, Advanced Asphalt Technologies, 2012.
- [8] L.F. Walubita, J. Zhang, G. Das, X. Hu, Ch. Mushota, A.E. Alvarez, T. Scullion, Hot-mix asphalt permanent deformation evaluated by Hamburg wheel tracking, dynamic modulus, and repeated load tests, *J. Transp. Res. Rec.* 2296 (1) (2012) 46–56.
- [9] H. Yu, S. Shen, An investigation of dynamic modulus and flow number properties of asphalt mixtures in Washington State. Final Report No. TNW2012-02, Transportation Northwest (TransNow), 2012.

- [10] L.F. Walubita, J. Zhang, A.N. Faruk, A.E. Alvarez, T. Scullion, Laboratory Hot-Mix Asphalt Performance Testing - Asphalt Mixture Performance Tester Versus Universal Testing Machine, *J. Transp. Res. Rec.* 2447 (1) (2014) 61–73.
- [11] J. Zhang, A.E. Alvarez, S.I. Lee, A. Torres, L.F. Walubita, Comparison of flow number, dynamic modulus, and repeated load tests for evaluation of HMA permanent deformation, *Constr. Build. Mater.* 44 (2013) 391–398.
- [12] L.F. Walubita, L. Fuentes, S.I. Lee, I. Dawd, E. Mahmoud, Comparative evaluation of five HMA rutting-related laboratory test methods relative to field performance data: DM, FN, RLPD, SPST, and HWTT, *Constr. Build. Mater.* 215 (2019) 737–753.
- [13] P. Chaturabong, H.U. Bahia, Mechanisms of asphalt mixture rutting in the dry Hamburg Wheel Tracking test and the potential to be alternative test in measuring rutting resistance, *Constr. Build. Mater.* 146 (2017) 175–182.
- [14] K.P. Biligiri, K.E. Kaloush, M.S. Mamlouk, M.W. Witczak, Rational modeling of tertiary flow for asphalt mixtures, *J. Transp. Res. Rec.* 2001 (1) (2007) 63–72.
- [15] N. Roy, A. Veeraragavan, J.M. Krishnan, Interpretation of flow number test data for asphalt mixtures, *P. I. Civil Eng.-Transp* 168 (3) (2015) 191–199.
- [16] L.F. Walubita, J. Zhang, A.E. Alvarez, X. Hu, Exploring the flow number (FN) index as a means to characterize the HMA permanent deformation response under FN testing, *J. S. Afr. Inst. Civ. Eng.* 55 (3) (2013) 103–112.
- [17] M.C. Rodezno, R. West, A. Taylor, Flow Number test and assessment of AASHTO TP 79-13 Rutting Criteria: Comparison of rutting performance of Hot-Mix and Warm-Mix asphalt Mixtures, *J. Transp. Res. Rec.* 2507 (1) (2015) 100–107.
- [18] L.F. Walubita, L. Fuentes, A. Prakoso, L.M. Rico, J.J. Komba, B. Naik, Correlating the HWTT laboratory test data to field rutting performance of in-service highway sections, *Constr. Build. Mater.* 236 (2020) 117552.
- [19] L.F. Walubita, A.N. Faruk, J. Zhang, X. Hu, S.I. Lee, The Hamburg rutting test-Effects of HMA sample sitting time and test temperature variation, *Constr. Build. Mater.* 108 (2016) 22–28.

- [20] L.F. Walubita, A.N. Faruk, J. Zhang, J.J. Komba, E.I. Alrashyidah, G.S. Simate, The Hamburg Rutting Test (HWTT) alternative data analysis methods and HMA screening criteria, *Int. J. Pavement Res. Technol.* 12 (1) (2019) 110–116.
- [21] E. Coleri, J.T. Harvey, K. Yang, J.M. Boone, Micromechanical investigation of open-graded asphalt friction courses' rutting mechanisms, *Constr. Build. Mater.* 44 (2013) 25–34.
- [22] V. Adam, S.C. Shah, Evaluation of open-graded plant mix seal surfaces for correction of slippery pavements, *J. Transp. Res. Rec.* 523 (1974) 88–96.
- [23] I.J. Huddleston, H. Zhou, R.G. Hicks, Performance evaluation of open-graded Asphalt concrete mixtures used in Oregon, *J. Assoc. Asphalt Pav.* 60 (1991) 19–42.
- [24] B.J. Putman, L.C. Kline, Comparison of Mix Design Methods for Porous Asphalt Mixtures, *J. Mater. Civil. Eng.* 24 (11) (2012) 1359–1367.
- [25] F. Gu, D. Watson, J. Moore, N. Tran, Evaluation of the benefits of open graded friction course: Case study, *Constr. Build. Mater.* 189 (20) (2018) 131–143.
- [26] E. Coleri, M. Kayhanian, J.T. Harvey, K. Yang, J.M. Boone, Clogging evaluation of open graded friction course pavements tested under rainfall and heavy vehicle simulators, *J. Environ. Manage.* 129 (2013) 164–172.
- [27] J. Chen, Y. Zhang, H. Li, Y. Gao, Rutting-induced permeability loss of open graded friction course mixtures, *J. Test. Eval.* 44 (2) (2016) 719–724.
- [28] P. S. Kandhal, *Design, Construction and Maintenance of Open-Graded Asphalt Friction Courses*, NAPA, Information series 115, Lanham, Maryland, 2002.
- [29] J.C. Nicholls, *Review of UK Porous Asphalt Trials*, *Transp. Res. Lab. Report No. 264*, 1997.
- [30] P. Rungruangvirojn, K. Kanitpong, Measurement of visibility loss due to splash and spray: Porous, SMA and conventional asphalt pavements, *Int. J. Pavement Eng.* 11 (6) (2010) 499–510.

- [31] G. Dell'Acqua, M. De Luca, R. Lamberti, Indirect skid resistance measurement for porous asphalt pavement management, *J. Transp. Res. Rec.* 2205 (1) (2011) 147–154.
- [32] H. Bendtsen, B. Andersen, Noise-Reducing Pavements for Urban Roads, Danish Road Directorate (DRD), *Nordic Road and Transport Research*. 3 (1999) 6–14.
- [33] E. Freitas, P. Pereira, L. de Picado-Santos, A. Santos, Traffic noise changes due to water on porous and dense asphalt surfaces, *Road Mater. Pavement*. 10 (3) (2009) 587–607.
- [34] L.A. Cooley, J. Brumfield, R. Mallick, W. Mogawer, M. Partl, L. Pulikakos, G. Hicks, Construction and Maintenance Practices for Permeable Friction Courses. NCHRP, Report No. 640, 2009. <https://doi.org/10.17226/14310>.
- [35] S.N. Suresha, G. Varghese, A.U. Ravi-Shankar, Laboratory and theoretical evaluation of clogging behaviour of porous friction course mixes, *Int. J. Pavement Eng.* 11 (1) (2010) 61–70.
- [36] L. Manrique-Sanchez, S. Caro, E. Arámbula-Mercado, Numerical modelling of ravelling in porous friction courses (PFC), *Road Mater. Pavement*. 19 (3) (2018) 668–689.
- [37] E. Arámbula-Mercado, R.A. Hill, S. Caro, L. Manrique, E.S. Park, E.G. Fernando, Understanding mechanisms of ravelling to extend open graded friction course (OGFC) service life, Final Report BDR74–977–04, 2016.
- [38] H. Wu, J. Yu, W. Song, J. Zou, Q. Song, L. Zhou, A critical state-of-the-art review of durability and functionality of open-graded friction course mixtures, *Constr. Build. Mater.* 237 (2020) 117759.
- [39] Y. Wang, Z. Leng, G. Wang, Structural contribution of open-graded friction course mixes in mechanistic–empirical pavement design, *Int. J. Pavement Eng.* 15 (8) (2014) 731–741.
- [40] L. Manrique-Sánchez, S. Caro, Numerical assessment of the structural contribution of porous friction courses (PFC), *Constr. Build. Mater.* 225 (2019) 754–764.



- [41] X. Wang, X. Gu, F. Ni, H. Deng, Q. Dong, Rutting resistance of porous asphalt mixture under coupled conditions of high temperature and rainfall, *Constr. Build. Mater.* 174 (2018) 293–301.
- [42] E. Masad, V.K. Jandhyala, N. Dasgupta, N. Somadevan, N. Shashidhar, Characterization of air void distribution in asphalt mixes using X-ray Computed Tomography, *J. Mater. Civil Eng.* 14 (2) (2002) 122–129.
- [43] E. Masad, S. Saadeh, T. Al-Rousan, E. Garboczi, D. Little, Computations of particle surface characteristics using optical and X-ray CT images, *Comp. Mater. Sci.* 34 (4) (2005) 406–424.
- [44] A.E. Alvarez, A.E. Martin, C. Estakhri, Internal structure of compacted permeable friction course mixtures, *Constr. Build. Mater.* 24 (6) (2010) 1027–1035.
- [45] L. Tashman, E. Masad, J. D’Angelo, J. Bukowski, T. Harman, X-ray Tomography to characterize air void distribution in Superpave Gyrotory Compacted specimens, *Int. J. Pavement Eng.* 3 (1) (2012) 19–28.
- [46] A.E. Alvarez, E.M. Fernández, A.E. Martin, O.J. Reyes, G.S. Simate, L.F. Walubita, Comparison of permeable friction course mixtures fabricated using asphalt rubber and performance-grade asphalt binders, *Constr. Build. Mater.* 28 (1) (2012) 427–436.
- [47] E. Coleri, J.T. Harvey, K. Yang, J.M. Boone, A micromechanical approach to investigate asphalt concrete rutting mechanisms, *Constr. Build. Mater.* 30 (2012) 36–49.
- [48] A.E. Alvarez, J.S. Carvajal, Practical lessons learnt from the application of X-ray computed tomography to evaluate the internal structure of asphalt mixtures, *DYNA* 81 (188) (2014) 52–59.
- [49] TxDOT–Texas Department of Transportation. Standard Specifications for Construction and Maintenance of Highways, Streets, and Bridges. Permeable Friction Course (PFC) (Item 342) Austin, Texas, 2004.

- [50] TxDOT–Texas Department of Transportation. Test Procedure for Laboratory method of mixing bituminous mixtures, TxDOT Designation: Tex-205-F, TxDOT, Austin, Texas, 2019.
- [51] TxDOT–Texas Department of Transportation. Test Procedure for Compacting bituminous specimens using the superpave gyratory compactor (SGC)., TxDOT Designation: Tex-241-F, TxDOT, Austin, Texas, 2019.
- [52] AASHTO (2013). Standard Specifications for Transportation Materials and Methods of Sampling and Testing. Standard AASHTO PP-60, Standard Practice for preparation of cylindrical performance test specimens using the Superpave gyratory compactor (SGC), Washington D.C., 2013.
- [53] AASHTO (2013). Standard Specifications for Transportation Materials and Methods of Sampling and Testing. Standard AASHTO TP-79, Standard Method of Test for determining the dynamic modulus and flow number for asphalt mixtures using the Asphalt Mixture Performance Tester (AMPT), Washington D.C., 2013.
- [54] A.E. Alvarez, J.S. Carvajal, O.J. Reyes, C. Estakhri, L.F. Walubita, Image analysis of the internal structure of warm mix asphalt (WMA) mixtures, Proceedings of TRB 91st Annual Meeting, pp. 1-17, 2012.
- [55] A.E. Alvarez, A.E. Martin, C. Estakhri, Internal structure of compacted permeable friction course mixtures, Constr. Build. Mater. 24 (6) (2010) 1027–1035.
- [56] K.P. Biligiri, K.E. Kaloush, M. Mamlouk, M.W. Witczak, Rational modeling of tertiary flow for asphalt mixtures, Transp. Res. Rec. J. Transp. Res. Board No. 2001 (1) (2007) 63–72.
- [57] TxDOT–Texas Department of Transportation. Test Procedure for the Hamburg Wheel-Tracking Test., TxDOT Designation: Tex-242-F, TxDOT, Austin, Texas, 2019.
- [58] D.M. Kusumawardani, Y.D. Wong, Evaluation of aggregate gradation on aggregate packing in porous asphalt mixture (PAM) by 3D numerical modelling and laboratory measurements, Constr. Build. Mater. 246 (2020) 118414.
- [59] D.M. Kusumawardani, Y.D. Wong, The influence of aggregate shape properties on

- aggregate packing in porous asphalt mixture (PAM), *Constr. Build. Mater.* 255 (2020) 119379.
- [60] B. Mahanta, P.G. Ranjith, T.N. Singh, V. Vishal, W. Duan, M. Sazid, Digital Rock Physics and application of high-resolution micro-CT techniques for geomaterials in: *Deep Rock Mechanics: From Research to Engineering, Proceedings of the International Conf. on Geo-Mechanics, Geo-Energy and Geo-Resources*, p. 92, 2018.
- [61] Materialise Innovation Suite, Mimics Innovation suite V22.0 released in 2019. Belgium.



## Chapter 4. Permeability rate in PAM

*(This chapter is based on the published conference paper entitled: "Permeability Flow Measurement for Open-Graded Friction Courses" Pavement and Asset Management: Proceedings of the World Conference on Pavement and Asset Management, WCPAM - 2017. ISBN: 97800367209896 ed: CRC Press Taylor & Francis Group, v., p.585 - 595, 2019.)*

**Abstract.** Permeable asphalt mixes (PAM) have gained a wider acceptance in road construction practices in comparison to conventional dense-graded courses (HMA), due to their high air void contents that allow water to be removed from the pavement through the asphalt layer. This capability is directly related to the air voids (AV) content and its connectivity. Nevertheless, both functionality and durability progressively might suffer changes as soon as the pavement is on service. Problems related with clogging, raveling and even rutting, are considered the primary distresses affecting permeability of PAM. The experimental research conducted herein is performed through conventional laboratory tests, X-ray Rotational Computed Tomography Angiography contrast-enhanced (RCTA) and image analyses are conducted on OGFC samples. This paper aims at measuring permeability flow in PAM by means of total air voids content and water-accessible AV, along with geometrical data obtained from X-ray Rotational Computed Tomography Angiography. Finally, the results demonstrate the reliability of this technique to measure permeability in OGFC.

**Keywords:** permeable asphalt mixes, permeability flow, open-graded friction courses, X-ray CT rotational angiography, internal structure analysis.

## 4.1 Introduction

Permeable asphalt mixes (PAM) are widely used in areas susceptible to rain flooding events that are commonly laid over impervious asphalt mixes widely. Its high draining capacity and its particular aggregates size gradation improve the wet skid resistance, ride quality, as well as reduce splashing and spraying in wet climates in order to provide safer roads in places where it's implemented [1,2].

Regarding its draining capacity, permeability is an important property that involves parameters such as AV content, size, and shape of the aggregates and mastic film distribution (*i.e.* combination of binder and fine aggregates smaller than 2 mm). In this sense, Huang *et al.* [3] investigated the permeability in various asphalt mixtures, including OGFC, and established it as a function of aggregates and air void (AV) connectivity. Mallick *et al.* [4] experimentally demonstrated that its performance and durability depend on the gradation of the particle size as well as the type of binder. By means of dimensional analysis [5,6], it was established that the draining capacity strongly depends on the volume of the connected AV.

As the internal structure of the mixtures also influences the permeability rate, the use of X-ray CT, an image-based non-destructive technique has become a revolutionary method to access the characterization of materials. Cnudde *et al.* [7,8] used the X-ray Computed Tomography (CT) to investigate the microstructure of building materials or even porous materials, such as rocks, soils, bones, and asphalt mixtures, and established that the pore-size distribution influences permeability. Álvarez *et al.* [9,10] found it useful to evaluate the internal structure of asphalt mixes, as well as to investigate the permeability in asphalt concrete using CT X-ray images [11]. In recent studies [12,13], an equation was proposed to approximate the permeability of asphalt mixtures considering the AV content and the surface area of the aggregates.

This study conducted aims to investigate the permeability rate in OGFC by using the X-ray Rotational Computed Tomography Angiography (RCTA). In this technique, a contrast agent runs through the interconnected air voids-path in real-time, while scanning the sample and obtaining 2D images. In this paper, RCTA and useful geometrical data obtained from the internal structure were used to determine the permeability in samples

compacted in the laboratory. The results showed the permeability flow in PAM and the AV distribution along with the vertical and horizontal directions.

## 4.2 Materials and methods

The samples were prepared according to a PAM gradation in Item 453 [14]. The nominal maximum aggregate size (NMAS) was established in 12.5 mm. Fig. 4-1 shows the particle size gradation used to prepare PAM specimens in laboratory. Within 20 samples, 16 were scanned using X-ray RCTA, 2 were used as control specimens, and the remaining 2 samples to compute the theoretical maximum specific gravity ( $G_{mm}$ ).

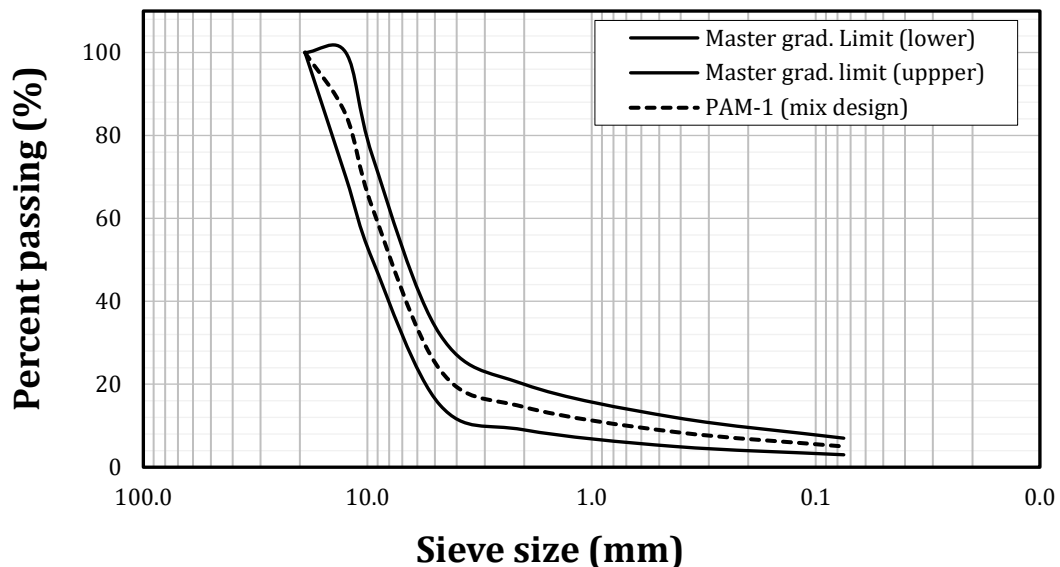


**Fig. 4-1.** Sieve size particle distribution for PAM.

A percentage of 5.5% polymer modified asphalt (PMA-type III) was used as a binder, and the range for mixing and compaction temperatures varied from 150 °C - 157 °C and 137 °C - 142 °C, respectively. Samples were individually placed inside the oven to stabilize the temperature set at 140 °C, and then compacted using 50 Marshall Hammer blows per face. After compaction, these specimens held for 30 min approximately in molds to keep cylindrical shape. Dimensions of diameter and height were measured after allowing the specimens to cool overnight. Using these measurements, the  $G_{mb}$  and  $G_{mm}$  were calculated.

### 4.3 X-ray Rotational Computed Tomography Angiography and contrast-agent enhanced

The following procedure complied in order to obtain the 2D images and reconstruction in 3D images using X-ray RCTA. Firstly, samples were scanned one at a time. Then, while they were held at the same initial position, the contrast-agent containing 50% water and 50% iodine-based solution, was injected on the sample surface with the contrast-agent solution. As long as they were injected, the scanning process was repeated. As a result, a group of 2D grayscale images was acquired and recorded. Each image pixel has an intensity between 0 -zero- for air voids (lowest density) and 255 for aggregates (highest density).

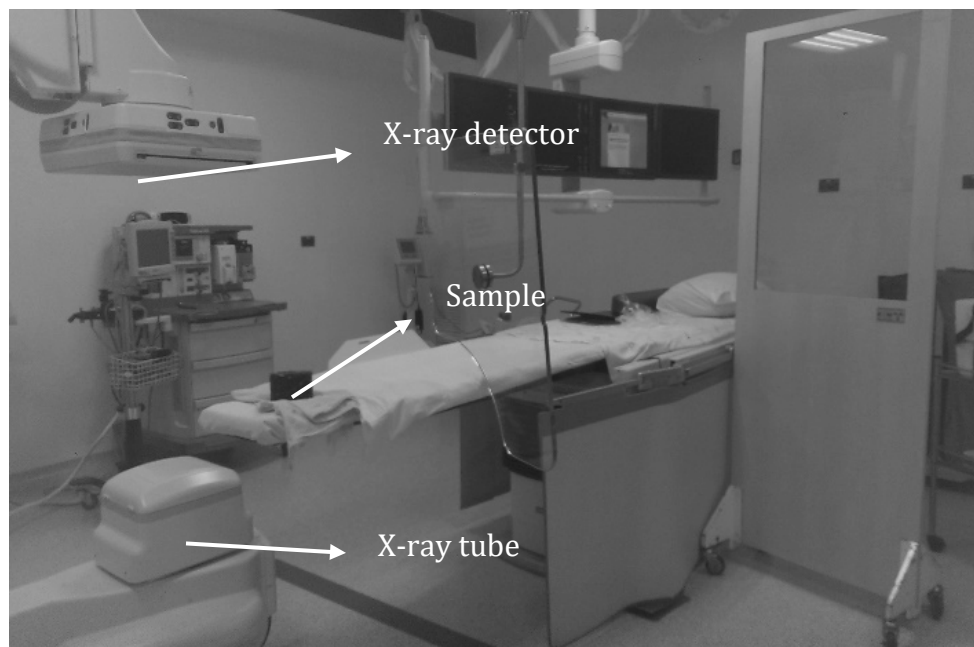


**Fig. 4-2.** Rotational Angiography equipment with X-ray detector and work place with a sample disposed to be scanned.

Fig. 4-2 shows the Siemens® Artis Zee Angiography equipment which was employed to obtain the images. The acquisition time employed was eight seconds per sample and 397 images were captured per sample.

In real-time, the path followed by the contrast-agent through interconnected AVs top-down along the samples' internal structure was observed on a screen. Since the



acquisition time (contrast-agent flowing top-down into the sample) and the volume injected of the solution are known, the permeability rate can be computed. Furthermore, it is possible to obtain significant data concerning the flow-path directions. The 2D images were acquired using Software Syngo VC14J by means of complex reconstruction algorithms. Each slice had a thickness of 0.90 mm and a voxel size of 0.43 mm. 3D objects were reconstructed for each sample by merging the group of corresponding 2D images.

## 4.4 Measurements of permeability

### 4.4.1 Measurement of AV content by means of Dimensional Analysis

The mix design of PAM is based on the volumetric properties and the presence of stone-on-stone contact [15]. AV content is expressed as a percent of the total volume of the compacted specimen and it is computed as:

$$Total\ AV\ content(\%) = \frac{G_{mm} - G_{mb}}{G_{mm}} \times 100 \quad (4-1)$$

$$G_{mb} = \frac{\frac{W_d}{V}}{\rho_{water}} \quad (4-2)$$

$G_{mm}$  is the theoretical maximum specific gravity of the mixture and  $G_{mb}$  is the bulk specific gravity of the compacted mixture. The water-accessible AV content (*i.e.* the proportion of the total volume of a compacted mixture that is accessible to water) is an alternative parameter computed in [5] as follows:

$$Water - accessible\ AV = \frac{V - \frac{(W_d - W_s)}{\rho_{water}}}{V} \times 100 \quad (4-3)$$

The dimensional analysis involves the following parameters:  $V$  is the total volume of the regular cylinders from an average height and diameter,  $W_d$  is the air-dry mass of the compacted sample, and  $W_s$  is the sample saturated mass in water, determined without the application of vacuum.

#### **4.4.2 X-ray Rotational CT Angiography and image-analysis techniques**

X-ray Computed Tomography is an effective non-destructive technique to study the microstructure of porous materials, providing the analysis of fluid flow paths and identification of three regions particularly in asphalt mixes: coarse aggregates, mastic, and the air voids. Meanwhile, the sample is still intact and can be used for other tests, such as rutting or fatigue tests.

The X-ray absorption level varies across materials, and it is a direct function of the density. In this sense, thicker materials are capable to absorb more X-rays than lighter allowing the limited pass to some of them, thus decreasing their intensity. Solely, those X-rays crossing the material are finally detected and subsequently, 2D images are generated with an intensity level within a grayscale threshold. These sectional images are used to reconstruct the 3D-microstructure of a sample by means of computer simulation of the performance of the material under several loading and environmental conditions.

The complementary X-ray RCTA contrast-enhanced technique used herein is frequently used for medical diagnosis and its main purpose aims to analyze how blood flows through the thin arteries in the heart. By applying the same principle, the X-Ray RCTA technique is extended to permeable asphalt mixes. In this particular case, the contrast-agent continuously runs through the internal structure of PAM and stops at clogged, or disrupted air voids. The 2D images are acquired in real-time along the entire process.

### **4.5 Results and discussion**

Fig. 4-3 presents the AV and water-accessible AV contents. The water-accessible AV content represents about 50% of total AV content, which is consistent with the fact that just some air voids are connected allowing the water-flow. Consequently, it is not suitable to determine the PAM permeability considering the total AV content, but water-accessible AV content or effective porosity.

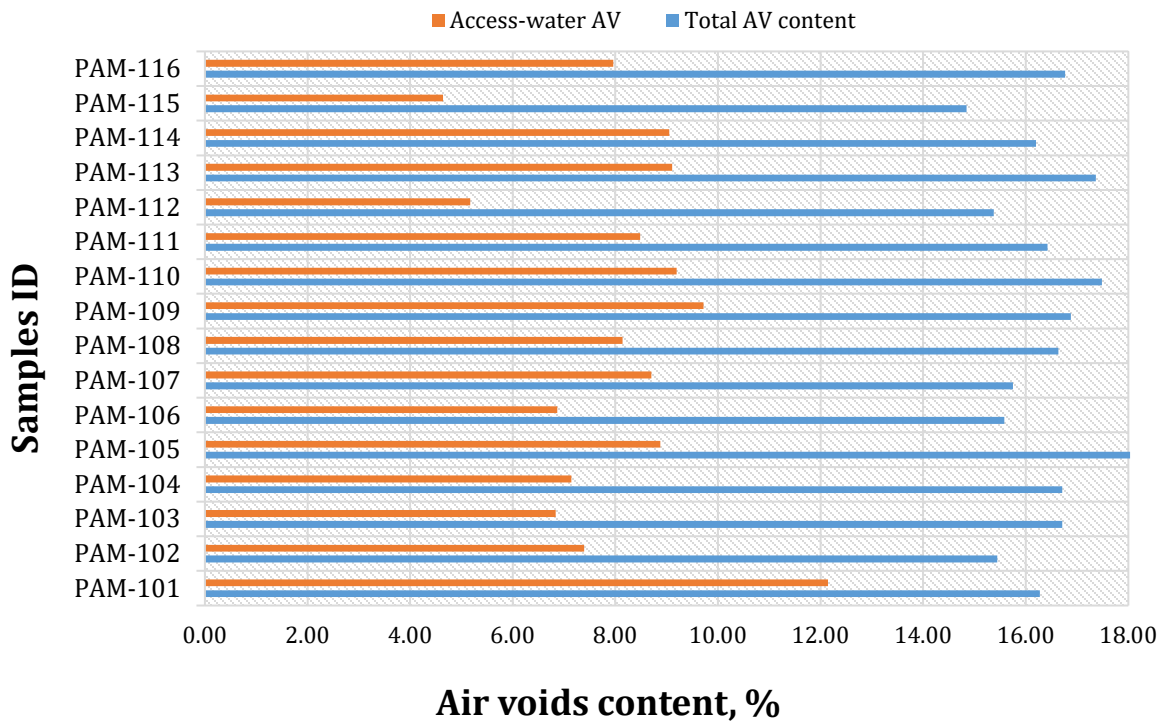


**Fig. 4-3.** Total AV content versus Water-accessible AV content

Despite of all samples were designed and prepared from the same batch, both computed AV and water-accessible AV contents were different among them. Most of the samples had an AV content within 14% and 16%, whereas, water-accessible AV content ranged from 6% to 8%. It is mainly due to that total AV content includes air voids located at the sample's boundaries considered as a smooth-contour cylinder.

Several studies have presented similar results as reported herein. For instance, [3] found that the hydraulic conductivity ranged from 0.27 to 1.47 cm/s after conducting experimental tests on OGFC samples in a dual-mode flexible wall permeameter. Another study [16], conducted laboratory-scale research employing a falling-head permeameter, a similar gradation, and a binder content of 5.0%; and found that the hydraulic conductivity for PAM samples was  $5.78 \times 10^{-2}$  cm/s.

**Table 4-1.** %AV by  $G_{mm}$  and  $G_{mb}$  (Dimensional Analysis) and  $K$  [cm/s]

Sample ID	Height (mm)	Diameter (mm)	Mass (g)	$G_{mb}$	Total AV %	Water- accessible AV %	Length max. [mm]	$K$ [ $\times 10^{-1}$ cm/s]
PAM-101	68.3	102	1184	2.13	16	12.2	23.7	3.0
PAM-102	67.6	102	1184	2.15	15	7.4	31.3	3.9
PAM-103	67.7	102	1169	2.12	17	6.8	43.7	5.5
PAM-104	67.5	102	1166	2.12	17	7.1	38.6	4.8
PAM-105	69.3	102	1177	2.08	18	8.9	47.4	5.9
PAM-106	66.6	102	1165	2.14	16	6.9	38.9	4.9
PAM-107	68.2	102	1191	2.14	16	8.7	20.6	2.6
PAM-108	67.4	102	1164	2.12	17	8.1	35.7	4.5
PAM-109	66.8	102	1151	2.11	17	9.7	41.4	5.2
PAM-110	67.7	102	1158	2.10	18	9.2	25.8	3.2
PAM-111	66.8	102	1158	2.12	16	8.5	42.2	5.3
PAM-112	67.2	102	1178	2.15	15	5.2	40.1	5.0
PAM-113	68.6	102	1175	2.10	17	9.1	41.4	5.2
PAM-114	67.5	102	1173	2.13	16	9.1	22.9	2.9
PAM-115	68.2	102	1204	2.16	15	4.6	43.3	5.4
PAM-116	68.5	102	1181	2.11	17	7.9	63.1	7.9

.presents the total AV and water-accessible AV contents, and the results for hydraulic conductivity,  $K$  [cm/s]. Former parameters were computed according to Eqs. (5-1) and (5-3) and it was used a  $G_{mm} = 2.54$  computed following the procedure outlined in ASTM D2041 [17]. Additional geometrical data are also shown in Table 4-1. Hydraulic conductivity,  $K$  was computed measuring the longest straight distance ran by the contrast in [cm], divided by the time in which the contrast agent was liberated on the sample surface and crossed their internal structure till the 2D image was acquired.

Based on previous experiences in the United States, the National Center for Asphalt Technology (NCAT) [4] established that a permeability magnitude greater than 100 m/day (*i.e.* 0.12 cm/s) for OGFC is adequate to ensure a good performance. Similarly, [18] stated

that permeability values around  $10^{-2}$  [cm/s] or higher are appropriated in order to obtain good drainage.

Basically, Fig. 4-4 shows the contrast-agent distribution once it has been injected and crossed throughout the sample. As presented in Table 4-1 the AV distribution was slightly different as shown in Fig. 4-4.

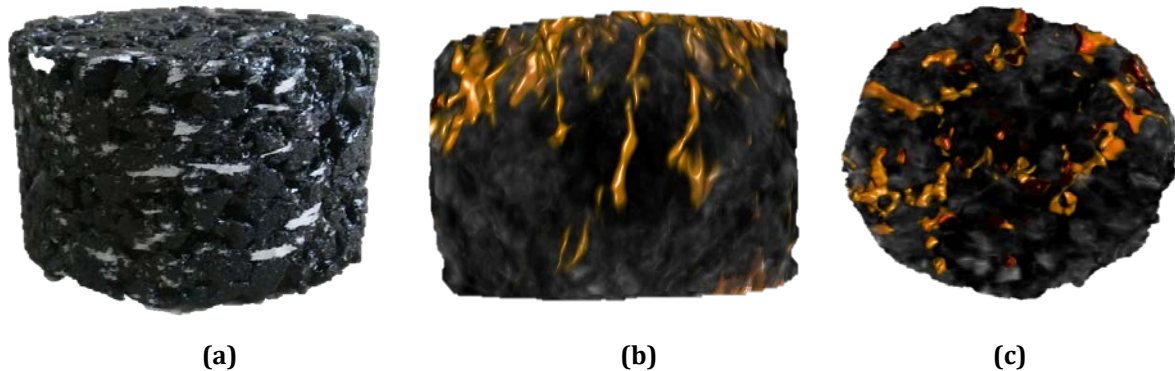


**Fig. 4-4.** [a] Sample compacted of PAM. [b] Sample PAM-115 including contrast (orange path). [c] Sample PAM-112 including contrast (orange path - plane view).

Fig. 4-4a shows the compacted OGFC sample. In it, all air voids around the diameter are shown that are discarded to calculate the AV content accessible to water, but only to calculate the total AV content. Fig. 4-4b shows the internal structure and flow path of the contrast agent almost along the entire height of the sample, after reconstruction in 3D images in the RCTA technique and also shows dispersed air voids. Finally, Fig. 4-4c shows the top plane of the surface where the contrast was injected and how many air voids were filled.

Since the X-ray RCTA contrast-enhanced procedure was performed in real-time (*i.e.* the contrast-agent injection and image-acquisition) the flow-path was more readily observed on-screen than in 2D images shown here. Nonetheless, this approach allowed displaying the AV connected structure (*i.e.* more air-voids connected along with the sample height) to provide more permeable OGFC than those samples that showed greater diameters. In the first case, the contrast-agent left the sample faster than in the second case.

## 4.6 Summary and conclusions

Permeability flow has been measured by means of the X-ray RCTA contrast-enhanced technique. Experimental measurements, as well as 2D image analyses, have shown a benchmark to assess the internal structure of PAM, related to the paths followed by contrast-agent in RCTA. In consequence, the results presented herein showed differences between total AV and water-accessible AV contents.

The flow-paths followed by the contrast agent in real-time led to the understanding that the anisotropy and AV distribution play an important role in the permeability rate of PAM and therefore, including this permeability parameter by means of proper laboratory tests and parameters, is another option to improve the mix design, behavior, and maintenance routines of OGFC.

Regarding the RCTA technique, it is important for future research to increase the acquisition-time in which the contrast-agent entirely crosses the sample to achieve more accurate time and flow fluid data. In addition, it is also necessary to ensure that the sample is in a saturated condition and to control the initial pressure at which the contrast-agent is liberated by the operator. The viscosity of contrast-agent should be also considered because it was a solution composed of 50% water and 50% iodine-based solution; to obtain an accurate measurement of permeability flow.

In terms of continuing research in this direction, a disadvantage found in this image-based RCTA technique is related to its high operating cost. Scanning of samples requires more exposure by the operator to X-rays as they must directly pour the contrast solution.

Finally, it is important to mention that the total AV content computed by dimensional analysis method includes the air voids in the surfaces around the diameter, and, in some cases, these are not essentially water-accessible air voids. The results showed a slight difference between these two parameters. Moreover, the technique presented provided a suitable method to verify the internal structure according to the AV content and distribution.

## References

- [1] L. A. Cooley Jr., R. C. Ahlrich, D. E. Watson, and P. S. Kandhal, "Improved Porous Friction Courses (PFC) on Asphalt Airfield Pavements," *Airf. Asph. Pavement Technol. Progr. Proj. 04-06*, vol. I, p. 157, 2007.
- [2] L. A. Cooley, "Construction and Maintenance practices for Permeable Friction Courses," *Natl. Coop. Res. Progr. Rep. 640 / Transp. Res. Board*, vol. 22, p. 162, 2009.
- [3] B. Huang, A. Raghavendra, and L. Mohammad, "Fundamentals of Permeability in Asphalt Mixtures," *Annu. Meet. Assoc. Asph. Paving Technol.*, no. 504, p. 17, 1999.
- [4] R. B. Mallick, P. S. Kandhal, L. A. Cooley Jr., and D. E. Watson, "Design, Construction, and Performance of New-Generation Open-Graded Friction Courses NCAT Report 00-01," *Annu. Meet. Assoc. Asph. Paving Technol.*, no. April, p. 26, 2000.
- [5] A. E. Alvarez, A. E. Martin, and C. Estakhri, "Internal structure of compacted permeable friction course mixtures," *Constr. Build. Mater.*, vol. 24, no. 6, pp. 1027–1035, 2010.
- [6] A. E. Alvarez, N. Macias, and L. G. Fuentes, "Analysis of connected air voids in warm mix asphalt," *DYNA*, vol. 172, no. 79, pp. 29–37, 2012.
- [7] V. Cnudde, B. Masschaele, M. Dierick, J. Vlassenbroeck, L. Van Hoorebeke, and P. Jacobs, "Recent progress in X-ray CT as a geosciences tool," *Appl. Geochemistry Elsevier*, vol. 21, no. 5, pp. 826–832, 2006.
- [8] V. Cnudde, A. Cwirzen, B. Masschaele, and P. J. S. Jacobs, "Porosity and microstructure characterization of building stones and concretes," *Eng. Geol.*, vol. 103, no. 3–4, pp. 76–83, 2009.
- [9] A. E. Alvarez, A. E. Martin, C. Estakhri, and R. Izzo, "Determination of Volumetric Properties for Permeable Friction Course Mixtures," *J. Test. Eval.*, vol. 37, no. 1, pp. 19–29, 2009.

- [10] A. E. Alvarez, A. E. Martin, and C. Estakhri, "Drainability of Permeable Friction Course Mixtures," *J. Mater. Civ. Eng.*, vol. 22, no. June, pp. 556–564, 2010.
- [11] A. E. Alvarez-lugo and J. S. Carvajal-muñoz, "Practical lessons learnt from the application of X-ray computed tomography to evaluate the internal structure of asphalt mixtures," *DYNA*, vol. 81, no. 188, pp. 52–59, 2014.
- [12] E. Masad, B. Birgisson, A. Al-Omari, and A. Cooley, "Analysis of permeability and fluid flow in asphalt mixes," *Proc. 82nd Annu. Transp. Res. Board*, pp. 1–33, 2003.
- [13] E. Masad, A. Al Omari, and H.-C. Chen, "Computations of permeability tensor coefficients and anisotropy of asphalt concrete based on microstructure simulation of fluid flow," *Comput. Mater. Sci. Elsevier*, vol. 40, no. 4, pp. 449–459, 2007.
- [14] Instituto Nacional de Vías, *Especificaciones Generales de Construcción de carreteras: Mezcla drenante [Colombian Specifications for Road Construction: Permeable Asphalt Mixes]*. Artículo 453 (Item 453-13). Bogotá, Colombia, 2007 [In Spanish].
- [15] American Society for Testing and Materials, *Standard Practice for Open-Graded Friction Course (OGFC) Mix Design. ASTM D 7064*, ASTM International, West Conshohocken, PA, USA, 2013.
- [16] S. N. Suresha, G. Varghese, and A. U. R. Shankar, "Characterization of porous friction course mixes for different Marshall compaction efforts," *Constr. Build. Mater. Elsevier*, vol. 23, no. 8, pp. 2887–2893, 2009.
- [17] American Society for Testing and Materials, *Standard Test Method for Theoretical Maximum Specific Gravity and Density of Bituminous Paving Mixtures. ASTM D2041/D2041M-11*, ASTM International, West Conshohocken, PA, USA, 2013, pp. 1–4.
- [18] E. Arambula, "A Dissertation for the degree of Doctor of Philosophy: Influence of Fundamental Material Properties and Air Void Structure on Moisture Damage of Asphalt Mixes Influence of Fundamental Material Properties and Air Void," Texas A&M University, 2007.



## Chapter 5. Conclusions and future research

### 5.1 Conclusions

An experimental investigation on the rutting resistance of permeable asphalt mixes (PAM) was presented herein. The rutting mechanism of PFC was investigated through three laboratory tests: DM test, FN test, and HWTT. In addition, an image-based analysis was performed using X-ray computed tomography (X-ray CT) bidimensional images obtained before and after HWTT, and AV redistribution due to rutting formation was also analyzed.

Results demonstrated that AV content has a strong impact on both dynamic modulus (DM) and flow number (FN) parameters. With higher AV content, the DN and FN values decrease. In consequence, PFC with lower AV contents has a higher resistance to rutting. From the results, it was found that for PFC mixes with AV contents between 18% and 22% can exhibit an adequate rutting resistance. The conducted multiple comparison tests by Tukey's HSD revealed a highly significant difference in the response of  $FN$  and  $|E^*|$  when the AV content is varied.

The non-destructive X-ray CT technique was adequate to explore the internal distribution of air voids in PFC mixtures. Differences were clearly identified when the scanned samples underwent the HWTT tests under dry and wet conditions. A higher percentage of air voids (above 30%) was observed for samples analyzed under wet conditions beneath the rut developed. In field conditions, these observations may be extrapolated primarily whether the PFC is in the early-ages of service, the mixture temperature rises above 50 °C and it is poorly compacted (higher AV content). Simultaneous scenarios of overloads and vehicular slow- speeds can also contribute PFC

to exhibit deeper ruts, whose damage (greater AV distribution) would extend to approximately the sample's half-thickness.

Permeability flow has been measured by means of the X-ray RCTA contrast-enhanced technique. Experimental measurements, as well as 2D image analyses, have shown a benchmark to assess the internal structure of PAM, related to the paths followed by contrast-agent in RCTA. In consequence, the results presented herein showed differences between total AV and water-accessible AV contents.

The flow-paths followed by the contrast agent in real-time led to the understanding that the anisotropy and AV distribution play an important role in the permeability rate of PAM and therefore, including this permeability parameter by means of proper laboratory tests and parameters, is another option to improve the mix design, behavior, and maintenance routines of OGFC.

## **5.2 Recommendations for Further Research**

As mentioned in the above paragraphs, this experimental study led to the evaluation of rutting resistance in permeable asphalt mixes by performing a set of laboratory tests and analyses of AV distribution profiles plotted from X-ray CT bidimensional images. Nonetheless, limitations in the availability of software and time established the need to further cover the following studies:

- Conduct large-scale testing where AV content and PAM layer thickness varies, in order to validate the response of these mixes, including high temperatures as the coupled effect.
- Develop a numerical model to evaluate the rutting resistance of PAM using the available experimental data in the literature and owned from this study (required properties for PAM).
- Since vehicle traffic loads and temperature conditions are different for each place implementing these mixes, local studies are encouraged to be performed regarding these particular parameters.